Title
Inhibition of Protein Tyrosine Phosphatase-Sigma Promotes Hematopoietic Stem Cell Regeneration

Author
Zhang, Yurun

Publication Date
2019

Peer reviewed|Thesis/dissertation

UNIVERSITY OF CALIFORNIA

Los Angeles

Inhibition of Protein Tyrosine Phosphatase-Sigma Promotes Hematopoietic Stem Cell Regeneration

A dissertation submitted in partial satisfaction of the requirements for the degree

Doctor of Philosophy in Molecular Biology

by

Yurun Zhang

2019

ABSTRACT OF THE DISSERTATION

Inhibition of Protein Tyrosine Phosphatase-Sigma Promotes Hematopoietic Stem Cell Regeneration

by

Yurun Zhang

Doctor of Philosophy in Molecular Biology

University of California, Los Angeles, 2019

John P. Chute, Chair

Receptor tyrosine kinases, such as c-Kit, Flt-3, and Tie 2, regulate hematopoietic stem cell (HSC) proliferation, differentiation, and maintenance. Substantially less is known regarding the function of protein tyrosine phosphatases (PTPs) in regulating HSC fate. We recently discovered that receptor type protein tyrosine phosphatase-sigma (PTPσ) is highly expressed by murine and human HSCs. PTPσ was originally discovered in adult neurons and has shown to regulate neural regeneration. In the hematopoietic system, constitutive deletion of PTPσ in mouse bone marrow

(BM) cells significantly increased HSC repopulating capacity compared to the wildtype. Furthermore, negative selection of human cord blood (CB) HSCs for PTPσ surface expression conferred more than 10-fold increase in human CB hematopoietic engraftment through 20 weeks in transplanted NSG mice. Additionally, PTPσ-deficient mice displayed significantly augmented recovery of BM colony forming cells at day +10 following 600 cGy total body irradiation. Based on these observations, we hypothesized that PTPσ may function as a negative regulator of HSC self-renewal and regeneration. Here we describe novel small molecule inhibitors of PTPσ that promote hematopoietic stem cell (HSC) regeneration *in vivo*. Systemic administration of DJ001, a PTPσ inhibitor, or its analog to irradiated mice promotes HSC regeneration, accelerates hematologic recovery, and improves survival. Similarly, following chemotherapy, DJ001 administration accelerates hematologic recovery in mice. DJ001 displays high specificity for PTPσ and antagonizes PTPσ via unique non-competitive, allosteric binding. Mechanistically, DJ001 suppresses radiation-induced HSC apoptosis via activation of the RhoGTPase, RAC1, and induction of BCL-X_L. Furthermore, treatment of irradiated human HSCs with DJ001 promotes the regeneration of human HSCs capable of multilineage *in vivo* repopulation. These studies demonstrate the therapeutic potential of selective, small-molecule PTPσ inhibitors for human hematopoietic regeneration.

The dissertation of Yurun Zhang is approved.

Gay M. Crooks

Steven M. Dubinett

Alexander Hoffmann

John M. Timmerman

John P. Chute, Committee Chair

University of California, Los Angeles

2019

To my parents, Xie Liu and Yubin Zhang.

TABLE OF CONTENTS

LIST OF FIGURES

LIST OF TABLES

ACKNOWLEDGMENTS

I would like to begin my acknowledgement by my expressing my deepest gratitude to Dr. John P. Chute for being my Ph.D. advisor during the past four years. I am forever grateful for Dr. Chute offering me the opportunity to explore and conduct research in the field of hematopoietic stem cell biology. I am also indebted to Dr. Chute's unparalleled support and insightful guidance, which has helped me tremendously to develop as an independent scientist.

I am proud to have been a Chute lab member during the past four years and I would like to thank all my colleagues, both past and present, for your mentorship, friendship, and constructive scientific input. Most importantly, thank you for creating such a vibrant lab environment that allows me to learn and grow to become a better scientist. Many thanks to Dr. Martina Roos and Dr. Heather A. Himburg, for your contribution to some of the mechanistic work and in vivo hematopoietic studies that are covered in Chapter 2. I am also grateful to your scientific and technical mentorship since my first day joining the lab. To Dr. Vivian Y. Chang, thank you for being the most supportive and caring bench mate since my first day in the lab. To Tiancheng Fang and Xiao Yan, my amazing graduate colleagues, our shared laughs and memories are what I will miss dearly when I depart for my next adventure, and I sincerely wish you both very good luck with your future endeavors.

To my committee members Dr. Gay Crooks, Dr. Alexander Hoffmann, Dr. Steven Dubinett, and Dr. John Timmerman, I would like to express my sincere acknowledgements for your scientific input and assistance throughout my Ph.D. career. My dissertation work would not have been completed without the generous help and input from our collaborator, Dr. Michael Jung and his

postdoctoral fellows Dr. Emelyne Diers and Dr. Hyo Jin Gim. Their knowledge in medicinal chemistry and speciality in drug synthesis laid the foundation of the PTPσ inhibitor project. My gratitude also extends to Jessica Scholes, Felicia Codrea, and Jeffrey Calimlim from the UCLA BSCRC Flow Cytometry Core, Ashley TerHorst from the Molecular Biology Institute, and my undergraduate research mentor, Dr. M. Thomas Record, Jr., from the Department of Biochemistry at University of Wisconsin-Madison.

Furthermore, I would like to acknowledge the Molecular Biology Institute and the UCLA Broad Stem Cell Research Center for their generous financial support for the first half of my graduate studies. I am also indebted to Dr. William Lowry, Dr. Leanne Jones and Dr. Pamela Hurley, who welcomed me into the family of UCLA and helped me tremendously through the ups and downs of my first year in graduate school. I have been fortunate to share this adventure with my dearest friends and classmates: Dr. Min Chai, Shawn Tan, Dr. Ruyi Huang, Dr. Liangke Gou, Dr. Zijun Zhang, Dr. Huachun Liu, Fangtao Chi, Ying Lin, Xiaorui Fan, Weixian Deng, Jihui Sha, and Xinyuan Chen. It was my pleasure to have met you all in Los Angeles, and I wish you very good luck with your future career.

Finally, none of my achievements could ever happened without the love and support from my beloved parents. They introduced me to the world of science from a very young age and has encouraged me to follow my heart ever since then.

Chapter 2 and 3 are reformatted versions of our recent publication in the journal *Nature Communications* authored by Zhang, Y., Roos, M., Himburg, H.A., Termini, C.M., Quarmyne, M., Yan, X., Zhao, L., Kan, J., Fang, T., Li, M., Pohl, K., Diers, E., Gim, H.J., Damoiseaux, R., Whitelegge, J., McBride, W., Jung, M.E. and Chute, J.P.

CURRICULUM VITAE

Yurun Zhang

Graduate Student Researcher
University of California, Los Angeles

I. EDUCATION

2014 - Present	Ph.D. Candidate, Molecular Biology University of California, Los Angeles, Los Angeles, CA
2010 - 2014	B.S., Biochemistry University of Wisconsin-Madison, Madison, WI

II. RESEARCH EXPERIENCE

2014 – Present	Graduate Student Researcher Molecular Biology Institute, University of California, Los Angeles Mentor: John P. Chute, M.D.
2011 – 2014	Undergraduate Researcher Department of Biochemistry, University of Wisconsin-Madison Mentor: M. Thomas Record, Jr., Ph.D.
2013	Undergraduate Summer Intern Department of Clinical Cancer Prevention, UT MD Anderson Cancer Center Mentor: Powel H. Brown, M.D., Ph.D.

III. FUNDING

2017 – 2018	Eli & Edythe Broad Stem Cell Research Center Pre-Doctoral Fellowship
2013 – 2014	Hilldale Undergraduate Research Fellowship

IV. PUBLICATIONS

1. **Zhang, Y.**, Roos, M., Himburg, H.A., Termini, C.M., Quarmyne, M., Yan, X., Zhao, L., Kan, J., Fang, T., Li, M., Pohl, K., Diers, E., Gim, H.J., Damoiseaux, R., Whitelegge, J., McBride, W., Jung, M.E. & Chute, J.P. (2019). PTPσ Inhibitors Promote Hematopoietic Stem Cell Regeneration. ***Nature Communications***, *10*(1), 1-15.

2. Himburg, H.A., Roos, M., Fang, T., **Zhang, Y.**, Termini, C.M., Schlussel., L., Kim, M., Pang, A., Kan, J., Zhao, L., Suh, H., Sasine, J.P., Sapparapu, G., Bowers, P.M., Schiller, G., & Chute, J.P. (2019). Chronic Myelogenous Leukemia Stem Cells Require Cell-Autonomous Pleiotrophin Signaling. ***Journal of Clinical Investigation***.

3. Sasine, J.P., Himburg, H.A., Termini, C.M., Roos, M., Tran, E., Zhao, L., Kan, J., Li, M., **Zhang, Y.**, de Barros, S.C., Rao, D.S., Counter, C.M., & Chute, J.P. (2018). Wild-type Kras Expands and Exhausts Hematopoietic Stem Cells. ***JCI Insight***, *3*(11).

4. Yan, X., Himburg, H.A., Pohl, K., Quarmyne, M., Tran, E., **Zhang, Y.**, Fang, T., Kan, J., Chao, N.J., Zhao, L., Doan, P.L., & Chute, J.P. (2016). Deletion of the Imprinted Gene Grb10 Promotes Hematopoietic Stem Cell Self-Renewal and Regeneration. ***Cell Reports***, *17*(6), 1584-1594.
5. **Zhang, Y.**, Quarmyne, M., Himburg, H. A., Yan, X., McBride, W., Jung, M., & Chute, J. P. (2016). A Small Molecule Inhibitor of Protein Tyrosine Phosphatase-Sigma (PTPσ) Promotes Hematopoietic Stem Cell (HSC) Regeneration. ***Blood***, *128*(22), 822.

V. AWARDS AND HONORS

2017 – 2018	Eli & Edythe Broad Stem Cell Research Center Pre-doctoral Fellowship
2017	UCLA Department of Medicine Research Day Poster Award
2013 – 2014	Hilldale Undergraduate Research Fellowship
2013	Mabel Duthey Reiner Scholarship
2012	UW-Madison Biochemistry Undergraduate Summer Research Scholarship
2010-2014	College of Agricultural and Life Sciences Dean's Lists for 8 Semesters

VI. PRESENTATIONS

Oral Presentation:

2018	UCLA Center for Medical Countermeasures against Radiation Monthly Meeting, Los Angeles, CA
2016	58th American Society of Hematology Annual Meeting, San Diego, CA.

Poster Presentation:

2018	14th Broad Stem Cell Research Center Annual Stem Cell Symposium, Los Angeles, CA
2017	2017 UCLA Department of Medicine Research Day, Los Angeles, CA
2017	14th Annual Meeting of International Society for Stem Cell Research, Boston, MA
2016	13th Annual Meeting of International Society for Stem Cell Research, San Francisco, CA

VII. PROFESSIONAL MEMBERSHIP

2016 – Present	American Society of Hematology
2016 – Present	International Society for Stem Cell Research

VIII. TEACHING EXPERIENCE

University of California, Los Angeles

2016-2017	Teaching Assistant, MCDB 138, Developmental Biology

CHAPTER 1: Introduction

1.1 Hematopoietic Stem Cells

Hematopoietic stem cells (HSCs) possess lifelong abilities to self-renew and differentiate into mature cells in the hematopoietic and immune systems. HSCs are required to replenish hematopoietic progenitor cells throughout life due to the limited lifespan of mature blood cells[1]. The hematopoietic system is a well-organized hierarchical structure in which multi-potency is progressively restricted as HSCs differentiate[2]. HSC self-renewal and differentiation are tightly regulated by both intrinsic mechanisms and extrinsic signals from the bone marrow microenvironment[3,4]. The majority of the HSCs reside in the bone marrow niche with few circulating in the peripheral blood. So far, HSCs have been the most well characterized adult human stem cells, thus providing a research model for other types of adult stem cells[5]. Clinically, HSCs are widely used in adult and pediatric bone marrow, cord blood, and mobilized peripheral blood transplants. Despite the powerful ability of HSCs to reconstitute the entire hematopoietic system in lethally irradiated transplant recipients, the hematopoietic system itself can be very delicate and fragile when exposed to high dose of chemo- or radiation therapy. Apart from their abilities to shrink tumor and kill cancer cells, chemo- or radiotherapies can also induce hematopoietic cell death which further leads to acute or chronic BM myelosuppression, a scenario that results in longer hospitalization, prolonged treatment and increased risk of infections[6]. Therefore, our knowledge of HSC's both at homeostasis and post injury can be used as a means to develop novel therapeutics that potentially benefits the patients.

1.2 The Emergence of HSCs

During embryogenesis, hematopoietic development starts in the yolk sac and then migrate to multiple anatomical sites. Hematopoietic progenitor cells are first found in the yolk sac blood

islands close to the endothelial cells at E8.0-8.5, followed by colonization of other developing hematopoietic organs once the circulation is established[7]. At E10.5, the aorta-gonad mesonephros (AGM), placenta, umbilical and vitelline arteries promote the generation of blood precursor cells[7]. Later in gestation, blood precursor cells migrate to and colonize the fetal liver, which is the major site for hematopoietic expansion and maturation[8]. Subsequently, the expanded blood precursor cells migrate to the bone marrow, a location that becomes the lifelong niche for hematopoietic stem cells[9]. Development of hematopoietic cells in the vertebrate embryo occurs in sequential waves. The primitive wave of hematopoiesis is the first wave of blood production which gives rise to unipotent blood cells that oxygenate all the developing tissues[9,10]. The primitive wave is transient and is replaced by pro-definitive and definitive hematopoiesis that generates multipotent hematopoietic progenitor cells. The cellular origin of definitive HSCs remains a controversial topic in the hematopoietic field[7]. Early development of hematopoietic progenitor cells in the yolk sac suggested a proximity between hematopoietic and endothelial cells. Further studies in different model organisms identified a single precursor cell, hemangioblast, which is capable of differentiating into both lineages[8]. However, lineage tracing in chimeric mice failed to detect the location of hemangioblast due to its rarity and transiency. Hemogenic endothelium, a vascular endothelium in the AGM, has been proposed as another cellular source of HSCs during definitive hematopoiesis[11]. The hemogenic endothelium is a type of endothelial cells which possesses the ability differentiating into HSCs.

1.3 HSC Hierarchy

The hematopoietic system is consisted of a wide-ranging of cells from stem cells with unlimited self-renewal ability to highly differentiated cells in the immune and blood systems. The classical

hematopoietic hierarchy is portrayed as a tree branch-like roadmap that depicts the differentiation of HSCs to mature blood and immune cells[12]. In this roadmap, differentiation of HSCs occurs in an asymmetrical process from multipotent, to oligopotent, to unipotent progenitor cells and to mature hematopoietic cells. Long-term HSCs (LT-HSCs) are rare and only represent 0.0001-0.00001% of the bone marrow (BM) cells in both murine and human[13]. LT-HSCs sit on top of the hematopoietic hierarchy and possess life-long ability to self-renew and to differentiate into hematopoietic lineage restricted progenitor cells which further differentiate into functional mature hematopoietic cells[14]. Short-term HSCs (ST-HSCs) possess short-term reconstitution capacity with limited self-renewal ability following transplantation into lethally irradiated recipients[12]. Multipotent progenitor (MPPs) cells that are differentiated from ST-HSCs demonstrate increased differentiation capacity but various degrees of self-renewal capacity from long-term to undetectable within the population[12,15]. Further downstream on the HSC hierarchy, MPPs give rise to common myeloid progenitors (CMPs) and common lymphoid progenitors (CLPs): the CMPs differentiate into megakaryocyte/erythrocyte progenitors (MEPs) and granulocyte/macrophage progenitors (GMPs) whereas the CLPs differentiate into mature lymphoid cells including T cell, B cell and nature killer (NK) cell[16].

Recent studies utilizing novel experimental techniques suggest that the tree branch-like hematopoietic hierarchy does not fully capture the complexity of the hematopoietic development process. A novel type of hematopoietic population, the intermediate-term HSCs (IT-HSCs), was recently identified as a transitory population between LT-HSCs and ST-HSCs with a clonal lifespan of 6-8 months before extinction[17]. Furthermore, multipotent progenitors (MPPs) were characterized into four distinct subpopulations: MPP1, MPP2, MPP3, and MPP4. At homeostasis,

MPP1 shares similar characteristics as ST-HSCs, whereas MPP2 and MPP3 are more myeloid-biased and MPP4 is lymphoid-biased[18]. Advances in single-cell methodologies provided more evidence that favors a continuous hematopoietic differentiation process with no obvious boundaries rather than the previous hierarchical pattern[19]. The revised continuous differentiation model suggests that lineage segregation occurs early at HSC stage with evidence of megakaryocytes differentiation directly from HSCs instead of MPPs or CMPs[20,21].

1.4 Microenvironment for HSCs

Stem cell niches are consisted of local tissue microenvironments and long-range signaling cues produced by other tissues[22,23]. As discussed in *1.3 HSC Hierarchy*, multiple tissues and organs are involved in HSC development at the embryonic stage. Therefore, the microenvironments that support early HSC maintenance is a complicated scenario in which diverse tissues are involved[24]. However, postnatally, HSCs primarily reside in the bone marrow which makes it the most extensively studied microenvironment in hematology research. The bone marrow microenvironment is tightly regulated through signals from surrounding cells within the niche and physical cues such as oxygen tension, stress, and temperature[1]. Clinically, high dose chemotherapy or radiation therapy can damage the BM microenvironment, thus disrupting hematopoiesis and causing prolonged hematopoietic recovery following injuries[25]. Therefore, our understanding of the regulatory role of BM niche can form basis for developing novel therapeutics that can accelerate hematopoietic regeneration in patients receiving chemo/radiotherapy or bone marrow transplant.

Earlier microscopic studies suggested osteoblasts resided closely to hematopoietic progenitor cells. Conditional manipulation of parathyroid hormone (PTH), bone morphogenetic protein (BMP), or thymidine kinase (TK) signaling pathways demonstrated that osteoblasts influenced hematopoietic stem and progenitor cells (HSPCs) *in vivo*[26–28]. However, the regulatory role of osteoblasts in HSC maintenance were challenged by later studies questioning the effects might not be direct. With the advancements in functional genetic deletion of critical niche factors and imaging techniques, investigators found that few HSCs were in close proximity to the osteoblasts and neither depletion nor augmentation of osteoblasts affected HSC frequency[29–32].

In recent years, the focus of key cellular players in HSC microenvironment has shifted from osteoblasts to perivascular cells, with HSCs located mainly adjacent to sinusoids throughout the BM[22,24]. Perivascular mesenchymal cells can be isolated based on surface expressions of *Cxcl12*-GFP, *Nes*-GFP, *Lepr*-Cre, and *Prx-1*-Cre, all of which were able to generate osteoblasts and maintain BM HSC pool by expressing chemokine ligand 12 (CXCL12) and stem cell factor (SCF)[29,31,33,34]. CXCL12 and its receptor chemokine receptor 4 (CXCR4) are essential for HSC maintenance, HSC migration, and B-cell development in the adult BM[34]. By knocking in a GFP reporter into the *Cxcl12* gene, the Nagasawa lab was the first to demonstrate that CXCL12-abundant reticular (CAR) cells co-localize with BM HSCs and function as a major producer of SCF and CXCL12 in adult BM[34,35]. Functionally, deletion of CXCL12-expressing BM cells fully ablates HSCs which leads to decreased osteogenic and adipogenic ability of BM cells[35]. Subsequent studies using a *Scf*-GFP knock in reporter mouse revealed that endothelial cells and perivascular cells also express adipo-osteogenic regulator *Lepr*, which overlaps with 90% of the CAR cells and 80% of the *Nes*-GFP$^+$ stromal cells in the adult BM[4]. Human skeletal stem cells

that express high levels of CD146 not only reside in close proximity to sinusoids in adult human BM, but also possess the ability to produce high levels of human SCF and CXCL12[36].

The human BM is a highly vascularized tissue consisted of arteries, arterioles, capillaries and sinusoids[37]. Endothelial cells line the inner layer of blood vessels and enable HSCs to enter or leave the bloodstream[4]. Approximately 60% of the murine HSCs characterized by SLAM markers ($CD150^{+}CD41^{-}CD48^{-}lineage^{-}$) are localized in close proximity to the sinusoidal endothelium[22,38]. Various secreted factors produced by endothelial cells have been reported to regulate HSC retention at homeostasis or to regulate HSC regeneration after myelosuppressive injuries, such as SCF, CXCL12, angiopoietin 1 (ANGPT1), pleiotrophin (PTN), E-selectin, and epidermal growth factor (EGF)[29,31,39–43]. Apart from the cellular types mentioned above, adipocytes, megakaryocytes, granulocytes, sympathetic nerves and macrophages have all been identified as cellular constituents in the BM microenvironment and implicated in HSC regulation, suggesting the complexity of HSC niche maintenance[4,22,44].

1.5 Hematopoietic Injury

Chemotherapy and radiation therapy have been widely used in cancer treatment because of their ability to shrink tumors and to kill cancer cells. Unfortunately, high dose of chemotherapy or ionizing radiation can alter the composition of BM microenvironment and induce cell apoptosis in highly proliferating hematopoietic progenitor cells[6]. A compromised hematopoietic and immune systems in cancer patients result in dose reductions and delays in curative treatments, which affects the overall survival of patients involved. Available treatments for acute myelosuppression include biologics erythropoietin (EPO), granulocyte – colony stimulating factor (G-CSF), and granulocyte

macrophage - colony stimulating factor (GM-CSF) to stimulate the repopulation of hematopoietic progenitor cells and to accelerate BM recovery in cancer patients[45]. However, there has been a growing awareness regarding long-term BM (LT-BM) injury in cancer survivors due to increasing rates of complete remission post cancer treatment. As of January 2019, there are more than sixteen million cancer survivors in the United States, and the number is estimated to reach twenty-two million by 2030[46]. Patients with LT-BM injury has normal complete blood cell counts and BM cellularity but diminishing self-renewal capacity of HSCs at homeostasis[47]. Treatment of G-CSF or GM-CSF in patients with acute myelosuppression not only stimulates HSC proliferation and differentiation into mature hematopoietic cells but also accelerates HSC exhaustion. Therefore, LT-BM injury although latent, its effect can be lifelong with no effective treatment to reverse its progression. In some cancer patients, BM injury increases the incidence of developing secondary cancer such as myelodysplastic syndrome after repeated cycles of consolidation treatments which brings additional stress to the hematopoietic system[25].

In history, nuclear disasters and radioactive accidents such as the Fukushima nuclear disaster (2011) and the Chernobyl disaster (1986), both served as alarming signs of the potential hazards of total body irradiation (TBI), causing severe injuries even death to the affected people[48,49]. The acute radiation syndrome (ARS), which involves damages to the hematopoietic, cutaneous, gastrointestinal and neurovascular systems, often occurs a few hours or days after total or partial body irradiation at a dose of more than 1 Gy[50]. The severity of ARS is proportionally associated with the radiation dosage that a person is exposed to. Among all the tissues and organs, the hematopoietic system is the most sensitive when expose to TBI. 2-7.5 Gy radiation dose in human can cause depletion of the hematopoietic progenitor cells and mature blood cells, leading to acute

and LT-BM suppressions[51,25]. Mechanistically, irradiation directly ionizes the water which makes up approximately 75% of adult human body mass. Ionization of water generates free radicals and reactive oxygen species (ROS) in the tissue that can damage DNA through base damage, double-stranded breaks (DSB), single-stranded breaks, and DNA cross linking[52]. Disruption of DNA in the hematopoietic cells can trigger DNA damage response (DDR) which leads to cellular apoptosis or senescence in order to protect overall genome stability. Other mechanisms that have been proposed to explain irradiation induced bone marrow injury include increased differentiation of BM HSCs and disruption of other cellular players in the BM microenvironment. A recent study by Wang et al. demonstrated that radiation-induced DNA damage in HSCs can promote lymphoid differentiation of HSCs through G-CSF/STAT3 pathway, thus leading to myeloid skewing in irradiated mice[53]. Radiation injury also disrupts the intricate network of sinusoidal vessels in the BM microenvironment which are crucial for maintaining HSC self-renewal capacity through secretion of angiocrine factors such as PTN, EGF, and ANGPT1[40,43,44].

1.6 Hematopoietic Assays

1.6.1 Hematopoietic Markers

Due to the advancement in fluorescent-activated cell sorting (FACS) and antibody development, hematopoietic stem, progenitor and mature lineage cells can be isolated using a cocktail of cell surface markers through FACS. The first step to enrich murine HSCs is the lineage$^-$ selection, which identifies and removes differentiated lineage cells using eight cell surface markers for mature lineage blood cells[14]. Subsequently, positive selection for markers, such as c-Kit$^+$ and Sca-1$^+$ were applied to enrich for the HSPC population, which includes long-term HSCs, short-term HSCs and multi-potent progenitor cells[54,55]. At least 100 c-Kit$^+$Sca-1$^+$lineage$^-$ (KSL) cells are

required for hematopoietic reconstitution in lethally irradiated mice 20 weeks following transplantation[55]. However, the KSL population is very heterogenous and only 10% of the population represent HSCs *in vivo*[56]. Further enrichment for long-term HSCs include using signaling lymphocytic activation molecule (SLAM) family-based markers ($CD41^{-}CD48^{-}CD150^{+}$) or $CD34^{-}Flk\text{-}2^{-}$ cell surface markers in addition to KSL markers. The SLAM markers significantly improved the purity of HSCs in which one in every two SLAM KSL cells can reconstitute lethally irradiated mice *in vivo*[38].

While mouse model has been widely used to study human diseases and shares many similarities with human HSC biology, the isolation strategy for human HSCs is different from that of the mouse. Human LT-HSCs are characterized by cell surface markers as $lineage^{-}CD34^{+}CD38^{-}CD45RA^{-}CD90^{+}CD49f^{+}$ cells[16]. However, in clinic, $CD34^{+}CD38^{-}$ human hematopoietic progenitor cells are more commonly used for therapeutic purposes.

1.6.2 *In vitro* Hematopoietic Assays

Multiple *in vitro* assays have been developed to identify and measure hematopoietic cells. Flow cytometric hematopoietic analysis using cell surface markers is widely used to isolate and identify HSCs. Unfortunately, it provides no functional information regarding hematopoietic stem cell activity[57]. Colony forming cell assays (CFCs) is a classic *in vitro* assay to determine the frequencies of hematopoietic progenitor cells. Input cells are plated in methylcellulose, a semisolid medium, supplemented with a cocktail of cytokines including SCF, thrombopoietin (TPO), interlukin-3 (IL-3) and EPO. Ten to fourteen days post seeding, hematopoietic progenitor cells can form three different types of colonies, which are blast-forming unit-erythroid (CFU-E), colony-

forming unit-granulocyte and monocyte (CFU-GM), and colony-forming unit-granulocyte, erythrocyte, monocyte and megakaryocyte (CFU-GEMM)[57]. Cobblestone area-forming cells (CAFC) and long-term culture initiating cells (LTC-IC) are two co-culture assays frequently used to measure short-term HSCs *in vitro*[58,59]. In both assays, a mesenchymal stromal cell (MSC) layer is required to support the colony forming capacity of seeded HSCs. However, there have been controversies regarding the CAFC and LTC-IC assays as they do not measure the true functional potential of HSCs to reconstitute an irradiated mouse and the quality of the MSC layers used in different labs varies which generates different outcomes[60].

The trans-endothelial migration assay was developed to mimic the migration process of HSCs from blood vessels into the BM niche. The assay utilizes a transwell plate in which the top chamber is coated with a confluent endothelial cell layer that mimic the blood vessel whereas the bottom chamber contains media supplemented with chemokine SDF-1. Isolated HSCs or BM cells are plated on top of the endothelial cells in the top chamber followed by migration towards the bottom chamber under SDF-1 gradient[61].

1.6.3 *In vivo* Hematopoietic Assays

Multi-lineage, long-term BM reconstitution assay, although time consuming and costly, is the gold standard to evaluate HSC functional capacity. Competitive repopulation unit (CRU) assay measures the functional capacity of HSCs by transplanting cells of interest with a competing cell dose into lethally irradiated recipient mice[56,57]. Engraftment rate of the donor cells are monitored every four weeks up to twenty week following transplantation. To measure long-term repopulation capacity, bone marrow cells from primary recipient are harvested and transplanted into secondary

and tertiary lethally irradiated recipients. Assessment of the functional capacity of human hematopoietic cells are performed in a xenotransplantation assay, in which cells are transplanted into immune deficient NSG mice without a competing dose and the engraftment rate is monitored every four weeks up to sixteen weeks. Furthermore, to calculate the frequency of HSCs in a given cellular source, limiting dilution assay is performed by serially diluting donor cells and transplanting them against a competing dose into lethally irradiated mice. The frequency of HSCs is estimated by Poisson statistics based on the number of transplanted mice that survives the transplant[62,63].

1.7 Protein Tyrosine Phosphatases (PTPs)

1.7.1 The complexity of the PTP family

Protein tyrosine phosphatases are a superfamily of enzymes that regulate signaling transductions and cellular activities through dephosphorylating the tyrosine residues on intracellular proteins. Although 98% of the phosphorylation activities occurred on serine/threonine residues, tyrosine phosphorylation by tyrosine kinase plays an important role in many physiological processes[64]. Disruption of normal tyrosine phosphorylation has been shown as an underlying cause of many human diseases, especially in the progression of many types of cancer. PTPs counterbalances the effect of protein tyrosine kinases (PTKs) by controlling the rate and duration of the phosphorylation process[65]. Recent studies of PTPs in various systems demonstrate their functional roles in regulating cell survival, migration, differentiation, and metabolism, implying that PTPs can no longer be overlooked as passive housekeeping enzymes[66]. The PTPs are encoded by 100 human PTP superfamily genes, indicating the diversity and complexity of the PTP family[67]. There are 107 different PTPs and they can be categorized into four different groups: the receptor-like

PTPs (RPTPs), the non-receptor PTPs (NR-PTPs), the dual specificity phosphatases (DSPs), and the pseudophosphatase PTPs[67,68].

The RPTPs is consisted of extracellular, transmembrane and intracellular domains. The extracellular domain contains several immunoglobulin-like or fibronectin type III-like domains which facilitate cell-cell or cell-matrix interactions. In the intracellular side, the membrane-proximal domain (D1) possesses phosphatase activity of RPTPs whereas the membrane-distal domain (D2) strengthens protein specificity and stability[67]. NR-PTPs are located in cytosol, plasma membrane and endoplasmic reticulum, directly or indirectly modulate cell signaling. Both RPTPs and NR-PTPs possess conserved sequence $(H/V)C(X)_5R(S/T)$ at the active site, in which the cysteine is essential for nucleophilic attack on the phosphoryl group of the substrate for subsequent dephosphorylation[65,68]. Interestingly, in some PTPs, alternative splicing or alternative promoters of the PTP gene can give rise to both receptor-like or non-receptor like PTP forms, such as PTPε or GLEPP1[67]. The DSPs are less conserved in sequences and possess less phosphatase activity due to the fact that its catalytic domain dephosphorylates not only tyrosine residues but also serine and threonine residues[69].

1.7.2 The role of PTPs in hematopoietic development and malignancy

Although less is known regarding the function of PTPs compared to receptor tyrosine kinases (RTKs) in hematopoiesis, multiple laboratories reported the roles of PTPs in hematopoiesis and hematologic malignancies. CD45, also known as protein tyrosine phosphatase C (PTPRC), is highly expressed on nucleated cells in the hematopoietic system, with the exception of mature erythrocytes and platelets[70]. CD45 plays a major role in activating T cell receptor (TCR) and B

cell receptor (BCR) mediated pathways through dephosphorylating the negative regulatory sites of FYN or LCK tyrosine sites of the SRC kinases[68,71]. Constitutive deletion of CD45 in mice showed severe combined immunodeficiency as a result of T- and B-cell dysfunctions. Lymphocytes in *CD45*$^{-/-}$ mice presented increased apoptosis compared to the wild-type, the mechanism of which was due to the ligation of CD45 with galectin[72]. Additionally, CD45 can also regulate cytokine productions and cytokine responses in various immunologic activities. For example, CD45 is involved in histamine degranulation after IgE crosslinking in mast cells, secretion of IL-6 in neutrophils, and cytokine generation by stimulated NK cells[72–75].

Protein tyrosine phosphatase non-receptor 11, commonly known as SHP2, regulates hematopoietic maintenance and differentiation. Deletion of SHP2 in mice depletes all the HSCs and hematopoietic progenitors which leads to eventual death at six to eight weeks after birth[76]. In human CD34^{+} hematopoietic cells, gain of function of SHP2 promotes differentiation and over-proliferation of the HSCs[77]. SHP2 mutation is associated with multiple human diseases, such as the Noonan syndrome (NS) and Noonan syndrome with multiple lentigines (NS-ML)[78]. Mutation that leads to gain-of-function of SHP2 has been shown in juvenile myelomonocytic leukemia (JMML), which is a serious chronic leukemia with a five-year survival rates of only 50% in children[79].

In 2014, our laboratory demonstrated that PTPσ is highly expressed in both murine and human HSCs compared to more differentiated BM progenitor cells. Constitutive deletion of PTPσ caused a marked increase in HSC repopulating capacity as measured in both primary and secondary competitive repopulation assays[80]. Negative selection of human cord blood HSCs for PTPσ surface

conferred more than 10-fold increase in human cord blood hematopoietic engraftment in NSG mice[80]. Mechanistically, PTPσ signals through RAC1 protein that regulates cell proliferation, cell survival, cell migration, and cytoskeletal dynamics. Deletion of PTPσ activates RAC1-GTP which leads to increased trans-endothelial migration of BM cells compared to the wild-type[80,81].

Recently, Ni et al. discovered that protein tyrosine phosphatase non-receptor 21 (Ptpn21) is also highly expressed in HSCs[82]. Deletion of *Ptpn21* stimulated stem cell mobilization out of the bone marrow microenvironment into the circulation, thus decreasing HSC retention at homeostasis. *Ptpn21*$^{-/-}$ HSCs also demonstrated increased cell death, decreased cellular stiffness and impaired long-term reconstitution ability *in vivo* compared to the wildtype[82]. The mechanistic explanation of *Ptpn21*$^{-/-}$ phenotype is intriguing since deletion of *Ptpn21* did not affect the activities of Rho guanosine triphosphatases. However, loss of *Ptpn21* significantly increased the phosphorylation of Septin1, which is an important component of the cytoskeleton organization and mechanics[82,83]. Septin1 is also highly expressed in the hematopoietic system and the central nervous system, hyperphosphorylation of which in *Ptpn21*$^{-/-}$ HSCs resulted in defective actin polymerization which explained decreased cell stiffness in *Ptpn21* knockout mice.

1.7.3 Protein Tyrosine Phosphatase-Sigma (PTPσ)

PTPσ belongs to the type 2A subclass of protein tyrosine phosphatases (PTPs) along with PTPf (LAR) and PTPδ[84]. All of them are receptor-like protein tyrosine phosphatases and are consisted of an extracellular domain, a single trans-membrane domain and two intracellular PTP domains. LAR and PTPσ are expressed in nervous system, lung, kidney, bone marrow, and thymus, whereas PTPδ is only expressed in the nervous system[85]. As a receptor protein, PTPσ interacts with the

extracellular matrix through binding with extracellular ligands such as heparan sulfate proteoglycans (HSPGs) and chondroitin proteoglycans (CSPGs). HSPGs and CSPGs have opposing roles regulating the growth and guidance of CNS neurons[86]. Treatment of HSPGs inactivates PTPσ by inducing oligomerization whereas CSPGs prevents PTPσ dimerization that activates PTPσ signaling pathway.

PTPσ was first extensively studied in mouse central and peripheral nervous system. The expression level of PTPσ significantly decreases in most of the brain after birth but maintains high level of expression in the hippocampus[85]. PTPσ modulates neuronal plasticity, learning and memory in adult central nervous system (CNS). Deletion of PTPσ in mice displays neuroendocrine abnormalities, growth retardation, and neonatal mortality[87]. PTPσ$^{-/-}$ mice increases the frequency of post-synaptic currents, indicating increased synapse density but decreased efficiency. PTPσ null mice displayed less long-term potentiation in hippocampal synapses and improved recognition ability of new object in the memory test[88]. Interestingly, post CNS injury, high levels of CSPGs are generated by astrocytes which inhibit axon extension into the injured sites. The mechanism of action of CSPG mediated axon growth inhibition was through binding with receptor PTPσ and LAR. Accordingly, deletion of PTPσ in mice demonstrated axon extension into the lesion area after spinal cord injury. PTPσ$^{-/-}$ mice also exhibit increased functional recovery of optic and peripheral nerve following facial nerve crush[89]. Therapeutically, treatment with a peptide mimetic of the PTPσ wedge domain restores serotonergic innervation and promotes locomotor and urinary recovery in rats with spinal cord injury[90].

The hematopoietic function of PTPσ is discussed in the previous section *1.7.2 The role of PTPs in hematopoietic development and malignancy*. Furthermore, PTPσ also acts as an inhibitory regulator on plasmacytoid dendritic cells (pDCs) in the immune system. Although PTPσ is highly expressed on plasmacytoid dendritic cells (pDCs), its expression is downregulated after pDC activation[91]. Conditional deletion of PTPσ in pDCs with a LAR null mouse causes IFN-α production, leukocyte infiltration in the intestine and mild colitis[91].

1.7.4 PTPs as therapeutic targets

As previously discussed, PTPs demonstrates regulatory roles in multiple physiological processes and human diseases, indicating its therapeutic potential. Unlike the class of PTKs which have more than 20 FDA approved small molecule inhibitors, the PTP family does not have any commercially available pharmacological modulators[68]. The PTP family has been considered challenging and undruggable due to highly conserved phospho-tyrosine binding sites among closely related family members which increase the difficulty to design specific modulators[92]. Additionally, the positively charged active sites bind with negatively charged molecules which has poor membrane permeability and bioavailability[93]. To overcome the difficulties in developing orthosteric competitive PTP inhibitors, efforts have been made to develop various types of small molecule inhibitors such as reversible bidentate inhibitors, reversible uncompetitive inhibitors and irreversible inhibitors. Furthermore, growing interests in tyrosine phosphatases advance the development of alternative strategies such as allosteric inhibitors, oligomerization-inhibiting small molecules, and decoy biologics. Of the many small molecules or biologics developed to target protein tyrosine phosphatases, only inhibitors AKB-9778 and MSI-1436 are currently undergoing clinical trials[93]. AKB-9778 is a vascular endothelial-PTP (VE-PTP) inhibitor designed for diabetic

macular edema (DME) patients. Systemic treatment of AKB-9778 in mice increased the phosphorylation level of Tie2, a VE-PTP substrate, which led to reduced vascular leakage and ocular neovascularization[94]. Phase IIA of the clinical trial reveled that treatment of AKB-9778 in combination with ranibizumab significantly decreased macular edema compared to ranibizumab treated patients[95]. MSI-1436, though originally discovered as an appetite suppressant in mice, demonstrated promising results in shrinking tumor size and preventing HER2-positive breast cancer metastasis in Phase I trials[93,96]. MSI-1436 bind to the C terminus in the allosteric site and inhibit PTP1B catalytic activity through conformational changes.

The PTPσ-targeted therapeutics are under development at early stages in the laboratories. Multiple publications reported the design of PTPσ specific intracellular wedge peptide mimetic (ISP) and its applications in two different disease models. In rats with spinal cord injury, subcutaneous administration of ISP regenerated neurons in CSPG-rich scar region and restored innervation by promoting recovery of the locomotor and urinary systems[90]. ISP administration in mouse with myocardial infarction demonstrated increased cardiac innervation in the CSPG-rich cardiac scar region and reduced cardiac arrhythmias[97]. The Bottini Lab reported an alternative approach to inhibit PTPσ activation by administering a PTPσ extracellular immunoglobulin-like domains Ig1&2 decoy protein to reverse the symptoms of rheumatoid arthritis in mice by reducing the invasiveness of joint-lining cells[98]. The PTPσ-Ig1&2 protein acted through binding with syndecan-4, a HSPG that has been shown to inhibit PTPσ by oligomerization. Therefore, treatment with decoy PTPσ-Ig1&2 restored the phosphatase activity of PTPσ and decreased the migration and cartilage attachment capacities of joint-lining cells in rheumatoid arthritis[98]. Identification of small

molecules that specifically target PTPσ has been shown in a couple of papers, however none of the discovered potential compounds have been tested for efficacy in an *in vivo* disease model[99,100].

1.8 Rho guanosine triphosphatase in the hematopoietic system

1.8.1 Signaling pathway of PTPσ

As a receptor phosphatase, PTPσ requires interactions with specific substrates at its active site to carry out its phosphatase activity. Multiple molecules have been identified as specific substrates of PTPσ in different organ systems: E-cadherin and β-cadherin were identified as colonic substrates for PTPσ, ezrin was identified as intestinal substrate for PTPσ, and p250GAP was identified as neuronal substrate for PTPσ[101–103]. Both ezrin and p250GAP recruited RAC1 protein, a Rho guanosine triphosphatase, as their downstream effector protein. Studies from our laboratory demonstrated that constitutive deletion of PTPσ in bone marrow KSL cells increased the level of RAC1-GTP compared to wildtype KSL cells, indicating PTPσ's inhibitory role in RAC1 activation in the hematopoietic system[80,81]. RAC1 protein belongs to the RAC protein family, a subfamily of the Rho guanosine triphosphatases (Rho GTPases). The RAC protein also acts as a critical regulator in many important cellular functions such as migration and cell cycling[104,105]. Given their critical roles in regulating multiple cellular activities, the Rho GTPases have been extensively studied by the hematopoietic field during the past decades.

1.8.2 Regulation of Rho GTPases

Rho GTPases, members of the Ras superfamily, regulates multiple signaling transduction pathways that further affect critical cellular processes. The Rho GTPases can be categorized into six major families: RAC, RhoA-related proteins, Cdc42, TC10 and TCL, Rnd, the Rho BTB, and

the Miro subfamily[106,107]. Among them, Rho, RAC, and Cdc42 are the most well-studied Rho GTPases and they serve as important players in regulating cell motility and actin assembly. At the molecular level, the Rho GTPases function as molecular switches transforming between inactive guanosine diphosphate (GDP) state to active guanosine triphosphate (GTP) state. The GTPase activating proteins (GAPs) and guanine nucleotide exchange factors (GEFs) act as negative and positive regulators of the Rho GTPases[104]. The active states of Rho GTPases further activate downstream effector proteins which trigger a multitude of cellular reactions, such as cytoskeleton reorganization, cell cycling, apoptosis, and genomic stability[107,108].

1.8.3 Rho GTPases in hematopoiesis

Active Rho GTPases, such as RAC1, Rac2, Cdc42, RhoA, and RhoH, have been shown to regulate multiple cellular activities that are critical to hematopoietic stem and progenitor cells. In the RAC family, RAC1 and RAC3 are ubiquitously expressed in the mammalians, whereas RAC2 is only expressed in the hematopoietic system[109]. Deletion of RAC2 in mice displayed increased migration of HSCs into the circulating peripheral blood, which suggested the regulatory role of RAC2 in HSC retention. RAC1, on the other hand, is essential to HSC homing and engraftment into the BM. Constitutive knockout of RAC1 in transplanted HSCs led to impaired homing capacity of transplanted into wildtype BM endosteal space compared wildtype HSCs[61]. Combined deletion of both RAC1 and RAC2 protein destroyed the adhesion and retention of HSCs in the BM microenvironment, which contributed to increased mobilization of HSCs to the circulating blood[61]. Mechanistically, loss of RAC1 activity reduces cell proliferation whereas deletion of RAC2 increases cell apoptosis. RAC1 also controls cell cycle entry by modulating cyclin D1 and $p27^{kip1}$ activities[109]. A multitude of downstream effector proteins such as p21-activated kinase (PAK),

POR1, and WAVE have been shown as RAC effector proteins in the hematopoietic cells[110]. Furthermore, RAC also possesses the ability to regulate downstream kinases such as p38 extracellular signal regulated kinase (ERK), c-Jun-activated kinase (JNK), and AKT kinase, which are all involved in mediating cell proliferation and cell death[111–113]. Furthermore, studies have shown that in HSCs, RAC integrates signals from three different receptors that are important to HSC cellular activities: receptor tyrosine kinase c-Kit, receptor CXCR4, and integrin receptor $\alpha_4\beta_1$ to activate its role in HSC homing and retention[107].

RhoH is a subfamily of the Rho family of GTPases predominantly expressed in the hematopoietic tissues[114]. Unlike the RAC1 subfamily, RhoH does not possess GTPase activity due to distinct amino acid sequences in the GTPase active domain[104]. In hematopoiesis, deletion of *RhoH* gene enhanced RAC1 activity and facilitated its translocation to the cell membrane, which led to increased chemotaxis of HSCs toward chemoattractant CXCL12[110,115]. Enforcing RhoH expression prevented actin assembly and HSC's response to chemoattractant CXCL12, indicating its regulatory role in HSCs is opposite from RAC1 and RAC2[115]. Another type of Rho GTPase, Cdc42, has been demonstrated to play an interesting role in HSC aging. Deletion of Cdc42 in mice displayed increased numbers of HSCs in the circulation, defects in HSC adhesion in the BM, and hyperactive cell cycling. In aged HSCs, Xing et al. observed elevated Cdc42 activity and increased migration of HSPCs into the peripheral blood[116]. Researchers hypothesized that increased Cdc42 activity during aging contributed to granulocyte – colony stimulating factor induced HSC mobilization in aged mice[116].

1.8.4 Rho GTPases in hematopoietic malignancies

Increased expressions of Rho GTPases have been shown associated with different human cancers, and in some cases accompanied by increased invasiveness and poor prognosis[106]. In mutant KRas-driven mice, RAC protein is required in the development of skin, lung, and pancreas cancer[111,117,118]. In acute myeloid leukemia (AML) model that carries MLL-AF9 mutation, the activities of RAC1 and Cdc42 significantly increased in response to CXCL12, suggesting that RAC1 is a potential therapeutic target[119]. Pharmacologic inhibition or knockdown of RAC1 in *MLL-AF9*-expressing cells led to increased apoptosis[110]. Other studies suggested that deletion of RAC2 delayed initiation of AML and deletion of RAC3 resulted in increased survival of mice with acute lymphoblastic leukemia (ALL)[120]. Another common type of leukemia is the chronic myeloid leukemia (CML), which accounts for approximately ten percent of all leukemias. CML is caused by translocation of *ABL1* gene with *BCR* gene, which creates a constitutively active fusion BCR-ABL oncoprotein. The BCR-ABL tyrosine kinase activates a multitude of signaling pathways include Ras, ERK, Akt, JNK, STAT5, p38, and NFκB, which further triggers hematopoietic cell proliferation and migration[107]. Studies by Thomas et al. showed that both RAC1 and RAC2 are downstream of BCR-ABL1. Deficiency of RAC2 or RAC1/RAC2 in mice expressing BCR-ABL improved the median survival of diseased mice (43 days vs. 92 days)[121]. However, deletion of RAC1 alone did not improve the median survival of BCR-ABL mice (21 days). Mechanistically, other signaling pathways including ERK, JNK, p38, Akt, and CrkL were all attenuated in RAC2 deficient mice expressing BCR-ABL and close complete abrogation in RAC1/RAC2 deficient mice expressing BCR-ABL[121]. The survival benefit in RAC1/RAC2 deficient mice can also be explained by decreased cell proliferation in RAC1/RAC2 deficient HSPCs that were transduced with BCR-ABL[107].

1.9 Treatment for Hematopoietic Injury

Available treatments for short-term BM myelosuppression include biologic agents such as erythropoietin (EPO), granulocyte – colony stimulating factor (G-CSF), and granulocyte macrophage - colony stimulating factor (GM-CSF) to increase the repopulation of erythroid and myeloid progenitor cells[45]. Among them, G-CSF is the most pivotal of all given its ability to promote neutrophil production in patients following chemo or radiation therapy-induced neutropenia. Neutrophils takes up 60 to 70 percent of the white blood cells in mammals and they are critical components of the innate immune system[122]. Therefore, administration of G-CSF shortens the duration and reduces the severity of grade VI neutropenia, which leads to less hospitalization and decreased consumption of antibiotics[123]. However, none of the currently available treatments are acting on a hematopoietic stem cell level, therefore leaving hematopoietic stem cell transplant (HSCT) the only option to patients who have long-term BM injury or acute BM failure.

In 1968, an infant with severe combined immunodeficiency (SCID) was successfully transplanted with BM cells from a human leukocyte antigen (HLA)-matched sibling donor[124]. Since then, more than one million patients worldwide underwent HSCT for the treatment of hematopoietic and immune disorders. So far, HSCT has become a standard of care for many malignant and non-malignant hematopoietic diseases, using BM cells acquired from the posterior iliac crests[125]. However, this procedure is an invasive operating room practice which requires anesthesia, resulting pains in donors during recovery. Since late 1980s, advances in hematology field expanded the approaches of obtaining hematopoietic cells and offered alternatives such as

mobilized peripheral blood stem cells (PBSCs) and umbilical cord blood cells[124,126]. The application of G-CSF as a mobilizing agent allows BM cells migrating out of the BM niche into the peripheral blood, thus decreasing the intrusiveness of harvesting HSCs in patients[125]. PBSCs also tend to engraft faster than BM cells following transplantation, and gradually replaced BM cells as the major cellular source for HSCT. However, PBSCs present higher rick of graft-versus-host disease (GVHD) compared to BM or cord blood cells, and they require multiple days of collection to acquire enough cell dose[125]. The lack of matched HLA donor has been a limitation to many patients who requires allogeneic HSCTs. Cord blood transplantation provides an alternative option for patients without a suitable donor due to the immaturity of cord blood cells. These immunologically naïve cord blood cells only require a match of three to four HLA antigens instead of the regular six[126]. Clinically, cord blood transplantation reduces the risk of GVHD but prolongs hematopoietic recovery in transplanted patients.

In recent years, several secreted factors have been discovered and identified as potential mitigators to chemotherapy or radiation-induced bone marrow injury. Systemic treatments of pleiotrophin (PTN), dickkopf-related protein 1 (DKK1), angiogenin (ANG) and epidermal growth factor (EGF) all demonstrated increased hematopoietic recovery and improved survival through different cellular and molecular mechanisms[40,43,127,128]. Other factor such as angiopoietin 1 was shown to accelerate regeneration of both HSCs and niche endothelial cells post irradiation[39].

CHAPTER 2: Inhibition of PTPσ improves murine and human hematopoietic stem cell regeneration

2.1 Introduction

Hematopoietic stem cells are characterized by their unique ability to self-renew and differentiate into mature lineage cells in the blood and immune systems[129].At homeostasis, HSC self-renewal and differentiation are regulated by both intrinsic cellular mechanisms and extrinsic signals from the BM microenvironment[130]. Clinically, chemotherapy and radiation therapy are widely used in cancer treatment because of their ability to shrink tumors and to kill cancer cells[131]. However, high dose of chemotherapy or radiation can induce hematopoietic cell apoptosis that leads to acute and chronic bone marrow (BM) myelosuppression[6]. Since limiting numbers of hematopoietic stem cells (HSCs) can reconstitute the entire blood and immune systems, our knowledge of HSC's cellular response in a radiation setting can be used as a means to develop novel therapeutics to mitigate radiation damage.

Our laboratory previously discovered that pleiotrophin, a paracrine growth factor secreted by the BM perivascular and endothelial cells, promoted HSC self-renewal and regeneration via inhibition of receptor protein tyrosine phosphatase-zeta (PTPζ)[40]. Genetic deletion of PTPζ in mice led to increased BM hematopoiesis, myelopoiesis and enhanced HSC repopulation capacity[132]. PTPζ belongs to the superfamily of PTPs that can remove phosphate groups from phosphorylated tyrosine residues on intracellular proteins. The PTPs counterbalance the phosphorylation effect of protein tyrosine kinases (PTKs) as a means to control signaling pathways underlying fundamental cellular processes[133]. It has been demonstrated that HSCs express a multitude of receptor tyrosine kinases (RTKs) that are important in regulating HSC self-renewal, maintenance, and differentiation, such as receptors c-Kit, FMS-like tyrosine kinase 3 (Flt-3), and tyrosine-protein kinase receptor Tie2[134]. Previous studies demonstrated that somatic mutations of RTKs led to

uncontrolled phosphorylation process in many types of aggressive cancers, thus making RTKs a popular therapeutic target in drug development[135]. Small molecule inhibitors of RTK has been the center of cancer drug discovery in the past decade, leading to successful clinical applications of imatinib (BCR-Abl, c-Kit, and PDGFR inhibitor), gefitinib (EGFR inhibitor), erlotinib (EGFR inhibitor), and lapatinib (HER2 and EGFR inhibitor)[136]. However, compare to RTK/PTKs, PTPs have been less of a focus in the field of hematopoietic research and small molecule drug discovery.

According to the regulatory role of PTN-PTPζ signaling in hematopoiesis, we performed gene expression screenings of other protein tyrosine phosphatases and identified that PTPσ was highly expressed in more primitive HSPC population than mature hematopoietic cells in both murine and human systems[80]. Constitutive deletion of PTPσ in BM cells significantly enhanced HSC self-renewal and engraftment capacity compared to PTPσ wildtype BM cells via activation of the RAC1-GTP signaling pathway[80]. Translationally, negative selection of PTPσ expression in human CB HSCs ($CD34^+CD38^-CD45RA^-lin^-PTP\sigma^-$) demonstrated more than 10-fold increase in cord blood repopulation capacity following transplanting into NSG mice compared to PTPσ expressed human CB HSCs ($CD34^+CD38^-CD45RA^-lin^-PTP\sigma^+$)[80]. The superior engraftment capacity of PTPσ negatively expressed human CB HSCs suggested significant therapeutic potential of targeting receptor PTPσ as an approach to augment HSC functional capacity. Therefore, we hypothesized that pharmacologic inhibition of PTPσ could be an effective strategy to promote HSC regeneration and hematopoietic reconstitution in patients following myelosuppressive radio/chemotherapy or hematopoietic stem cell transplantation.

Compare to RTK therapeutics, development of PTP small molecule inhibitors has progressed slowly due to conserved active domain structures and poor membrane permeability and bioavailability[92,93]. Currently, there have been two reports of In 2012, using *in silico* modeling and *in vitro* phosphatase assay, Martin et al. identified compound 6545075, 1-(3,4-dichlorophenyl)-3-[(2-hydroxy-5-nitrophenyl)amino]-2-propen-1-one (also known as 6545075), as a competitive inhibitor of PTPσ with a half-maximal inhibitory concentration (IC_{50}) value of 10 μM[99]. However, the *in vivo* efficacy of compound 6545075 was not tested in the paper and little did we know how it would affect the hematopoietic system. Therefore, based on the chemical structure of compound 6545075, we sought to interrogate whether pharmacologic inhibition of PTPσ via compound 6546075 or its chemical analogues would be an effective option to promote HSC regeneration post radiation or chemotherapy-induced BM injury.

2.2 Methods and Materials

2.2.1 Synthesis of *(Z)*-3-((3-nitrophenyl)amino)-1-phenylprop-2-en-1-one (DJ001)

DJ001: A mixture of 1-phenylprop-2-yn-1-one* (0.303 g, 2.3 mmol), 3-nitroaniline (0.427 g, 3.0 mmol) and copper (I) iodide (0.078 g, 0.4 mmol) in DMF (6 mL) and water (60 µL) was stirred at 85 °C for 16 h. After 16 h, the reaction mixture was allowed to cool down to 21 °C and was diluted with water (50 mL) and extracted with ethyl acetate (3 x 50 mL). The combined organic layer was washed with NH_4Cl/NH_3 (1:1 v/v, 3 X 20 mL) and brine (30 mL), dried over $MgSO_4$, filtered and concentrated under reduced pressure. The crude residue was purified by column chromatography (n-hexane/ethyl acetate = 20:1) to obtain DJ001 (140 mg, 0.52 mmol, 23%) as a yellow powder. ^{1}H NMR (400 MHz, $CDCl_3$) δ 12.26 (d, NH, *J* = 11.6 Hz), 7.96-7.91 (m, 3H), 7.90 (ddd, 1H, *J* = 8.0, 2.0, 0.8 Hz), 7.56-7.46 (m, 5H), 7.37 (ddd, 1H, *J* = 8.0, 2.4, 0.8 Hz), 6.16 (d, 1H, *J* = 8.0 Hz) ; ^{13}C NMR (100 MHz, $CDCl_3$) δ 191.8, 149.4, 143.4, 141.6, 138.6, 132.2, 130.6, 128.6, 127.5, 122.3, 117.8, 110.0, 95.7. *1-Phenylprop-2-yn-1-one was prepared by oxidation of 1-phenylprop-2-yn-1-ol in a two-step procedure from benzaldehyde and trimethylsilylacetylene by a known method[137].

2.2.2 PhosphataseProfiler™ screen

Compound DJ001 was evaluated in a PhosphataseProfiler™ screen at 10 µM and 1 µM (2.7 µg/mL and 0.27 µg/mL) concentrations at Eurofins Pharma Discovery Services UK (Study number UK022-0004033) against a panel of 21 Phosphatases. In each experiment, the respective reference antagonist/agonist was tested directly with DJ001, and the data were compared with historical values determined at Eurofins. DJ001 compound inhibition was calculated as percentage inhibition of the enzymatic activity compared to control.

2.2.3 Phosphatase assay

The two intracellular catalytic domains (D1 and D2) of *Ptprs* were cloned into a pET28a vector and were overexpressed in E. coli BL21 and purified as described previously[138]. Enzymatic activity of PTPσ was assayed using a modified version of the Malachite Green Assay[139] and the Tyrosine Phosphatase Assay Kit (Promega Corporation). Unless stated otherwise, standard assays were carried out using 50 nM PTPσ protein in 1x Buffer (10 mM Tris, 5 mM MgCl2, 10mM NaCl, 0.02% Tween) and Tyr Phosphopeptide as substrate (200uM for Fig. 1B and C, 50 – 1200 μM in Figure 1C). Purified catalytic domain 1 and domain 2 of PTPσ were pre-incubated with test compounds 3071, 5205, 5075 or control for 15 min in a 96 well plate before the addition of Tyr Phosphopeptide (DADE(pY)LIPQQG). For IC_{50} determination, rates normalized relative to uninhibited controls (DMSO) were plotted against compound concentration and fitted using a four-parameter nonlinear regression curve fit $y = (A - D)/(1 + (x/C)^B) + D$ (Prism 6.0, Graphpad Software). For mechanism studies and determination of the enzyme's K_m and V_{max}, data were analyzed using a nonlinear regression fit according to the classical Michaelis-Menten kinetics model, $Y=V_{max}*X/(K_m+X)$ (Prism 6.0, Graphpad Software).

2.2.4 *In silico* molecular docking studies

Molecular docking of DJ001 *(Z)*-isomer to the protein tyrosine phosphatase-σ (PDB ID: 2FH7) was carried out by AutoDock Vina, in which the Iterated Local Search Globule Optimizer was applied as optimization algorithm[140]. Each structure of ligand was prepared in Maestro 10.5 (Schroedinger, LLC) and minimized with the OPLS_2005 force field. All hydrogen atoms were added to each protein and ligand to be docked and each coordinate file of protein and ligand was

generated as PDBQT file using AutoDockTools-1.5.6. A grid box for binding site was set as 18 Å in the three dimensions (x, y and z) that covered the catalytic site of the protein or 40 Å in the three dimensions for allosteric binding site. The box had 1.0 Å grid spacing and centered at the geometric center of the protein. In each docking experiment, the best binding mode was selected according to the binding affinity calculated by the scoring function in AutoDock Vina. Docking results were analyzed with PyMOL and visualized by VMD 1.9.2.

2.2.5 Animal models

All animal procedures were performed in accordance with animal use protocols approved by the UCLA animal care and use committee. *Ptprs*$^{-/-}$ mice were provided by Dr. Michel Tremblay (McGill University). *C57BL/6* mice, *B6.SJL* mice and *NOD.Cg-Prkdc*^{scid}*Il2rg*^{tm1Wjl}*/SzJ (NSG)* mice between 8 to 12 weeks old were obtained from the Jackson Laboratory.

2.2.6 Flow cytometric analysis

Femurs and tibiae were harvested from euthanized C57BL/6 or Ptprs$^{-/-}$ mice and flushed with IMDM containing 10% FBS and 1% penicillin-streptomycin for BM cells. PB was collected through sub-mandibular puncture. Cells were filtered through a 40 μM strainer and then treated with ACK lysis buffer (Sigma Aldrich) before antibody staining for flow cytometry. For KSL and CD150+CD48-KSL cell analysis, BM cells were stained with allophycocyanin (APC)-and Cy7-conjugated anti-mouse Sca-1 (BD Biosciences; 560654; 1:100), phycoerythrin (PE)-conjugated anti-mouse c-kit (BD Biosciences; 553355; 1:100), V450 lineage cocktail (BD Biosciences; 561301; 1:10), Alexa Fluor 488-conjugated anti-mouse CD48 (BioLegend; 103414; 1:100), and Alexa Fluor 647-conjugated anti-mouse CD150 (BioLegend; 115918; 1:100) antibodies. For MEP,

CMP, GMP, and CLP cell analysis, BM cells were stained with APC-Cy7-conjugated anti-mouse Sca1 (BD Biosciences; 560654; 1:100), PE-conjugated anti-mouse c-kit (BD Biosciences; 553355; 1:100), V450 lineage cocktail (BD Biosciences; 561301; 1:10), Alexa Fluor 488-conjugated anti-mouse CD127 (BD Biosciences; 561533; 1:100), Alexa Fluor 647-conjugated anti-mouse CD34 (BD Biosciences; 560230; 1:100), and BV605-conjugated anti-mouse CD16/32 (BD Biosciences; 563006; 1:100) antibodies. For donor engraftment analysis in transplanted mice, PB or BM cells were stained with BV605-conjugated anti-mouse CD45.2 (BioLegend; 109841; 1:100), FITC-conjugated anti-mouse CD45.1 (BD Biosciences; 553775; 1:100), PE-conjugated anti-mouse Mac-1 (BD Biosciences; 557397; 1:100) and Gr-1 (BD Biosciences; 553128; 1:100), V450-conjugated anti-mouse CD3 (BD Biosciences; 561389; 1:100), and APC-Cy7-conjugated anti-mouse B220 (BD Biosciences; 552094; 1:100) antibodies.

2.2.7 Survival studies

For survival studies, 10 week old female C57BL/6 mice were irradiated with 750 cGy TBI, which is lethal for approximately 50% of C57BL/6 mice by day +30 (LD50/30), using a Shepherd Cesium-137 irradiator. Twenty four hours post-irradiation, mice were administered daily subcutaneous injections of 5 mg/kg DJ001 or DJ009 or vehicle in a volume of 100 µL for 10 days. DJ001 or DJ009 injections were prepared in PBS, 0.5% Tween 80, and 10% DMSO. Corresponding vehicle injections contained PBS, 10% DMSO and 0.5% Tween 80. PB complete blood counts were measured using a Hemavet 950 instrument (Drew Scientific) at day +10 post-irradiation. For hematopoietic analysis, BM cells were collected at day +10 post-irradiation.

2.2.8 Chemotherapy model

Ten week old female C57BL/6 mice received a single tail-vein injection of 250 mg/kg 5-Fluorouracil (5-FU) in 100 µL PBS. Two hours post 5-FU injection, mice were administered daily subcutaneous injections of 5 mg/kg (100 µg per mouse) DJ001 or vehicle in a volume of 100 µL for 8 days. DJ001 injections were prepared in PBS, 50% PEG-400 and 10% DMSO. Corresponding vehicle injections contained PBS, 50% PEG-400 and 10% DMSO. Retro-orbital blood was collected on day +8, +11 and +14 after 5-FU treatment with capillary pipettes (Fisher Scientific). Complete blood counts were measured as described above using a Hemavet 950 instrument (Drew Scientific).

2.2.9 Isolation of BM HSCs

BM HSCs were collected from mice as previously described[127,141]. Briefly, BM cells were first treated with ACK lysis buffer (Sigma Aldrich) and lineage committed cells were removed using a Direct Lineage Cell Depletion Kit (Miltenyi Biotec; 130-110-470; 1:5). Lin- cells were stained with APC-Cy7-conjugated anti-Sca1 (BD Biosciences; 560654; 1:100), PE-conjugated anti-c-kit (BD Biosciences; 553355; 1:100), V450 lineage cocktail (BD Biosciences; 561301; 1:10), and FITC-conjugated anti-CD34 (BD Biosciences; 553733; 1:100) antibodies. Sterile cell sorting was conducted on a BD FACS-Aria cytometer. Purified KSL cells and $CD34^{-}c\text{-}kit^{+}sca\text{-}1^{+}lin^{-}$ ($CD34^{-}$ KSL) cells were collected into IMDM (Life Technologies) + 10% FBS + 1% penicillin-streptomycin.

2.2.10 CFC assays, HSC cultures and competitive repopulation assays

CFC assays (colony-forming unit-granulocyte monocyte (CFU-GM), burst-forming unit-erythroid (BFU-E), and colony-forming unit-granulocyte erythroid monocyte megakaryocyte (CFU-GEMM) were performed using MethoCult GF M3434 (Stemcell Technologies), as we have previously described6. For all *in vitro* assays, BM $CD34^{-}KSL$ cells, KSL cells, and lin^{-} cells were cultured in TSF media (IMDM, 10% FBS, 1% pen-strep, 20 ng/mL recombinant mouse Thrombopoietin (TPO), 125 ng/mL recombinant mouse Stem Cell Factor (SCF), 50 ng/mL recombinant mouse Flt3 ligand) and treated as described. Recombinant mouse SCF, Flt-3 ligand, and TPO were purchased from R&D Systems. For competitive repopulation assays, BM cells were isolated from donor 10-12 week old female $CD45.2^{+}$ mice. Recipient 10 week old female $CD45.1^{+}$ B6.SJL mice were irradiated with 950 cGy TBI using a Cs137 irradiator, and donor BM cells were administered via tail vein injection along with a competing dose of 1 x 10^5 non-irradiated host BM cells. Multilineage donor hematopoietic cell engraftment was measured in the PB by flow cytometry, as previously described[142].

2.2.11 Cytokine analysis

For *in vitro* cytokine measurements, 3.5 x 10^4 BM KSL cells were irradiated with 300 cGy and cultured in TSF media with and without 1 µg/mL DJ001. Non-irradiated KSL cells were cultured in TSF media with and without 1 µg/mL DJ001. At 12 hours of culture, culture supernatants were collected for analysis. For *in vivo* cytokine measurements, adult C57BL/6 mice were irradiated with 750 cGy TBI and then treated with 5 mg/kg of DJ001 or vehicle, subcutaneously, from day +1 to day +5. Non-irradiated mice received the identical regimen of 5 mg/kg DJ001 or vehicle for 5 days. Mice were euthanized and BM cells were collected into IMDM. Cells were pelleted and

the BM supernatant was collected and sent to the UCLA Immune Assessment Core (IAC) for cytokine analysis. All samples were tested on a mouse 32-plex Cytokine/Chemokine panel platform from EMD Milipore using Luminex's xMAP® immunoassay technology (Luminex Inc). In addition, the following cytokine levels were assessed by solid phase enzyme-linked immunosorbent assays (ELISA) according to manufacturer's description: CXCL12 (R&D Systems), SCF (R&D Systems), TPO (R&D Systems), PTN (Biomatik), DKK1 (R&D Systems), and EGF (R&D Systems).

2.2.12 Synthesis of (Z)-3-((3,5-difluorophenyl)amino)-1-phenylprop-2-en-1-one (DJ009)

DJ009 (117.9 mg, 0.455 mmol, 59%, yellow powder) was prepared from 1-phenylprop-2-yn-1-one (100 mg, 0.768 mmol), 3, 5-difluoroaniline (108.5 mg, 0.840 mmol) and copper (I) iodide (29.3 mg, 0.154 mmol) in DMF (1 mL) using same procedure described for DJ001. ^{1}H NMR ($CDCl_3$, 400 MHz) δ (ppm): 12.0 (d, J = 11.7 Hz, 1H), 7.94 (dt, J = 6.9, 1.6 Hz, 2H), 7.55–7.50 (m, 1), 7.48–7.45 (m, 2H), 7.38 (dd, J = 11.7, 8.2 Hz, 1H), 6.64–6.57 (m, 2H), 6.54–6.47 (m, 1H), 6.09 (d, J = 8.2 Hz, 1H); ^{13}C NMR ($CDCl_3$, 100 MHz) δ (ppm): 191.7, 164.0 (dd, J = 249, 15 Hz), 143.5, 142.8 (t, J = 13 Hz), 138.7, 132.1, 128.6, 127.5, 99.3 (dd, J = 20, 8 Hz), 98.5 (t, J = 26 Hz), 95.3; ^{19}F NMR (CDCl3, 376 MHz) δ (ppm): - 107.9.

2.2.13 Pharmacokinetic study for DJ001

Pharmacokinetic (PK) studies for DJ001 were performed at Cyprotex (Study Number CYP1426-R1) under non-GLP conditions. Mice were subcutaneously injected with a single dose of 5 mg/kg DJ001 (in 10% DMSO, 40%PBS, 50% PEG) and plasma samples were collected at 0.08, 0.25, 0.5, 1, 2, 4, 8 and 24h. Samples were crashed with three volumes of methanol and analytical internal

standard (propranolol). Supernatant was subjected to liquid chromatography-mass spectrometry/mass spectrometry (LC-MS/MS) using an acetonitrile-water gradient system and ESI ionization in MRM mode for MS detection. All plasma samples were compared to an internal calibration curve prepared in mouse blank plasma.

2.2.14 Human BM cultures and human BM transplantation assays

Human BM mononuclear cells (MNCs) were purchased from AllCells. Cryopreserved human BM cells were recovered in IMDM + 10% FBS + 1% penicillin-streptomycin and then positively selected for $CD34^+$ stem/progenitor cells by using CD34 MicroBead Kit (Miltenyi Biotec; 130-046-702; 1:5). $CD34^+$ cells were cultured in human TSF media (IMDM, 10%FBS, 1% pen-strep, 20 ng/mL recombinant human Thrombopoietin (TPO), 125 ng/mL recombinant human Stem Cell Factor (SCF), 50 ng/mL recombinant human Flt3 ligand (R&D Systems). The progeny of 2 x 10^5 irradiated, human BM $CD34^+$ cultured for 36 hours and treated with DJ001 at 5 ug/mL, were transplanted via tail vein injection into 10-12 week old NSG mice preconditioned with 275 cGy TBI. Multilineage donor hematopoietic cell engraftment was monitored in the PB and BM by flow cytometry. The PB or BM cells were stained with BV605-conjugated anti-mouse CD45 (BioLegend; 103139; 1:100), AF647-conjugated anti-human CD34 (BioLegend; 343618; 1:100), FITC-conjugated anti-human CD33 (BD Biosciences; 555626; 1:100), V450-conjugated anti-human CD45 (BD Biosciences; 560368; 1:100), APC-conjugated anti-human CD3 (BD Biosciences; 555342; 1:100) and APC-Cy7-conjugated anti-human CD19 (BD Biosciences; 557791; 1:100) antibodies.

2.2.15 Statistical analysis

GraphPad Prism 6.0 was used for all statistical analyses. All data were checked for normal distribution and similar variance between groups. Data were derived from multiple independent experiments from distinct mice or cell culture plates. Sample sizes for *in vitro* studies were chosen based on observed effect sizes and standard errors from prior studies. For all animal studies, a power test was used to determine the sample size needed to observe a two-fold difference in means between groups with 0.8 power. A two-tailed Student's t test was utilized for all comparison excepts where otherwise noted in the Figure Legends. All animal studies were performed using sex- and age-matched animals, with wild-type littermates as controls. Animal studies were performed without blinding of the investigator. Values are reported as means ± SEM, unless stated otherwise. Results were considered significant when $P < 0.05$.

2.3 Results

2.3.1 Development of selective and allosteric PTPσ inhibitors

We hypothesized that PTPσ inhibition could promote HSC self-renewal and sought to develop a small molecule with specific inhibitory activity against PTPσ. We identified an organic compound, 6545075 (ChemBridge), which was reported to have binding and inhibitory activity against PTPσ's catalytic domain[99]. Structural comparison of 6545075 against a library of 80,000 small molecules yielded the identification of two additional compounds, 6515205 and 5483071 (ChemBridge), that were predicted to bind the catalytic domain of PTPσ (Figure 1a). We tested the inhibitory activity of these three molecules in a direct PTPσ enzymatic assay (Figure 1b). Compound 5483071 (3071) displayed stronger inhibitory activity against PTPσ, with a half-maximal inhibitory concentration (IC_{50}) of 1.5 μM compared to 33.01 μM of 6515205 and 2.33 μM of 6545075. We also tested the inhibitory activity of 3071 against protein LAR in the same direct enzymatic assay (Figure 1c). Compared to its strong inhibitory activity against PTPσ, 3071 demonstrated weak inhibitory with an IC_{50} value of 13.52 μM against protein LAR.

We then collaborated with Dr. Michael E. Jung's laboratory at Department of Chemistry and Biochemistry at UCLA. The Jung Laboratory synthesized a small molecule, DJ001, which had identical chemical structure of 3071 and confirmed the inhibitory effect of DJ001 in PTPσ enzymatic assay (IC50 = 1.43 μM) (Figure 2a and 2b). Importantly, DJ001 displayed no inhibitory activity against 20 other PTPs, with only modest inhibitory activity against Protein Phosphatase 5 (PP5) (Figure 3). These data suggested that DJ001 was a specific small molecule inhibitor that possessed strong inhibitory activity against PTPσ.

We next determined that DJ001 can exist in two different stereoisomeric forms, the *(Z)*- and *(E)*-isomers (Figure 2a). The *(Z)*-isomer showed significantly increased binding affinity to both PTPσ catalytic (active) and allosteric sites compared to the *(E)*-isomer (Figure 4a and 4b). The *(Z)*-isomer also demonstrated a 1.3 kcal/mol preference for binding to the allosteric site, located between domain 1 and 2 of PTPσ, over the catalytic site (-9.0 kcal/mol vs. -7.7 kcal/mol) (Figure 4c). Enzyme kinetic analysis via substrate titration studies demonstrated that DJ001 functions as a non-competitive inhibitor of PTPσ, consistent with its allosteric binding properties (Figure 5a and 5b). These studies revealed that DJ001 non-competitively inhibits PTPσ.

2.3.2 PTPσ inhibition promotes hematopoietic regeneration following myelosuppression

To determine the effect of PTPσ inhibition on HSC proliferation at homeostasis, we treated non-irradiated BM $CD34^{-}cKit^{+}Sca1^{+}lin^{-}$ ($CD34^{-}KSL$) in TSF media (containing 20 ng/mL Thrombopoietin, 100 ng/mL SCF, 50 ng/mL Flt3 ligand) with or without different concentrations of DJ001 (10 ng/mL to 1,000 ng/mL) for 7 days. Treatment of DJ001 increased the percentages and total cell numbers of KSL cells after 7-day culture compared with media only group (Figure 6a). DJ001 treatment of isolated BM KSL cells also significantly increased the colony formation capacity after 3 days of culture (Figure 6b). However, systemic treatment of DJ001 at 5 mg/kg in adult C57BL/6 mice for every Monday-Wednesday-Friday for four weeks did not alter their complete blood counts, BM KSLs, or BM CFCs compared with vehicle-treated controls (Figure 7 a, 7b, and 7c).

Based on previously described results at homeostasis, we next investigated the effects of DJ001-mediated PTPσ inhibition in BM HSCs post myelosuppressive injury. We irradiated BM KSL cells at 300 cGy and treated them in TSF media with or without 1 μg/mL DJ001. 3 days after culture, DJ001 treatment significantly increased the recovery of BM CFCs and multipotent colony-forming unit-granulocyte erythroid monocyte megakaryocyte (CFU-GEMM) colonies compare with non-treated control group (Figure 8a and 8b). Additionally, 600 cGy TBI of *Ptprs* knockout (*Ptprs*$^{-/-}$) mice demonstrated increased recovery of BM CFCs at day 10 post irradiation compared with irradiated *Ptprs* wild-type (*Ptprs*$^{+/+}$) mice (Figure 8c). These results suggested that deletion of *Ptprs* or inhibition of PTPσ promoted hematopoietic progenitor cell regeneration following irradiation.

In order to determine whether PTPσ inhibition could promote hematopoietic regeneration *in vivo*, we irradiated adult C57BL/6 mice with 750 cGy and treated subcutaneously with 5 mg/kg of DJ001 or vehicle for 10 days starting +24 hours post irradiation. At day 10 post irradiation, DJ001-treated mice displayed increased number of peripheral blood white blood cells, neutrophils, and lymphocytes by two-fold compared with vehicle-treated controls (Figure 9a). At the hematopoietic level, DJ001 treated mice demonstrated increased percentages and cell counts of BM cKit^{+}Sca1^{-} lin^{-} myeloid progenitor cells and BM KSL hematopoietic stem and progenitor cells, as well as SLAM KSL hematopoietic stem cells (Figure 9b and 9c). Isolated BM cells from DJ001 treated mice at day +10 post irradiation also enhanced the recovery of CFCs compared with vehicle-treated mice (Figure 9d). However, the percentages of BM megakaryocyte erythroid progenitors (MEPs), common myeloid progenitors (CMPs), granulocyte monocyte progenitors (GMPs), or PB myeloid, B-cell or T-cell populations in DJ001 treated mice did not demonstrate significant

differences post irradiation compared to the controls (Figure 10a and 10b). Percentage of BM common lymphoid progenitors (CLPs) showed a modest increase after DJ001 treatment versus the vehicle group (Figure 10a). Of note, pharmacokinetics (PK) study showed that one time treatment of 5 mg/kg DJ001 in adult C57BL/6 mice displayed 10–100 ng/mL DJ001 concentrations over 24 hours post injection, consistent with the concentration range that promoted BM hematopoietic progenitor cell recovery *in vitro* (Figure 11).

Radiation exposure is known to cause acute mortality via hematopoietic injuries. Here, we evaluated whether daily administration of 5 mg/kg DJ001 from day +1 to +10 could increase the survival of mice post sub-lethal irradiation dose. Following 750 cGy TBI, 41% of vehicle-treated C57BL/6 (12 out of 29 total) mice versus 93% of DJ001-treated C57BL/6 (27 out of 29 total) mice survived through day +40 (Figure 12). Therefore, systemic administration of DJ001, a PTPσ inhibitor, significantly improved survival following irradiation injury.

To determine whether DJ001 promoted the regeneration of long-term HSCs in mice receiving myelosuppressive irradiation, we performed competitive repopulation assays using B6.SJL ($CD45.1^+$) recipient mice and donor BM collected at day +10 from C57BL/6 ($CD45.2^+$) mice irradiated with 750 cGy TBI followed by daily treatment of 5 mg/kg DJ001or vehicle for 10 days. Recipient mice transplanted with 5 x 10^5 BM cells from irradiated control mice, along with 1 x 10^5 competitor $CD45.1^+$ BM cells, demonstrated decreased donor hematopoietic engraftment over time after transplantation (Figure 13a). This is consistent with our prior observations that high dose TBI depletes long-term HSCs therefore reducing their repopulation capacity in lethally irradiated recipients[43]. In contrast, mice transplanted with the same dose of BM cells from irradiated, DJ001-

treated mice displayed significantly increased donor hematopoietic reconstitution at 16 and 20 weeks of transplantation compare with irradiated controls (Figure 13a). Specifically, mice that were transplanted with BM cells from irradiated and DJ001-treated donor mice showed significantly increased percentages of donor $CD45.2^+Mac1^+/Gr1^+$ myeloid cells, $CD45.2^+B220^+$ B cells, and $CD45.2^+CD3^+$ T cells in the PB at 20 weeks post-transplant compared with recipients that received irradiated and vehicle-treated BM cells (Figure 13b).

In clinic, chemotherapy is widely used in cancer treatment for their ability to shrink tumors and to kill cancer cells[131]. However, high dose of chemotherapeutic agents can induce hematopoietic cell apoptosis that leads to acute and chronic BM myelosuppression[6]. Here, we treated adult C57BL/6 mice intravenously with 250 mg/kg 5-fluorouracil (5FU), an antimetabolite chemotherapeutic agent that causes depression of WBCs and neutrophils[143]. Control mice treated with 5FU demonstrated leukopenia and neutropenia from day +8 through day +14. Mice treated with 5FU followed by daily treatment of 5 mg/kg DJ001 subcutaneously significantly increased PB WBCs and neutrophils at day +14 (Figure 14).

In order to validate our hypothesis that small molecule inhibition of PTPσ could facilitate hematopoietic regeneration following myelotoxicity, we designed and synthesized more than 100 structural analogs of DJ001. One of them, DJ009, with a 3,5-difluorophenyl ring substituted for the 3-nitrophenyl unit of DJ001, strongly inhibited PTPσ activity *in vitro* (Figure 15a and 15b). When C57BL/6 mice were irradiated with 750 cGy TBI and subsequently treated daily with 5 mg/kg DJ009 for 10 days, we observed a significant increase in PB WBCs, neutrophils, lymphocytes, BM KSL cells, and CFCs in response to DJ009 treatment (Figure 15c, 15d, and 15e).

Consistent with these findings, DJ009 treatment also significantly increased survival of irradiated C57BL/6 mice through 30 days following 750 cGy sub-lethal irradiation (Figure 15f). These results provided further evidence that small molecule PTPσ inhibitors can promote hematopoietic regeneration *in vivo* following myelosuppression.

2.3.3 The effect of PTPσ inhibition on cytokine levels

Although our in vitro studies suggest that PTPσ inhibition directly promotes HSC regeneration, it is also possible that treatment with DJ001 may indirectly affect HSCs by altering cytokine production by hematopoietic progenitor cells or their bone marrow microenvironment. Hematopoietic progenitor cells have been shown to secrete several inflammatory cytokines in response to lipopolysaccharide and PAM3CSK4, a Toll-like receptor 2 ligand. To investigate the possible cytokine effect, we measured 38 cytokines in cultures of non-irradiated and irradiated BM KSL cells treated with and without DJ001, and also measured the identical cytokines in the BM of non-irradiated and irradiated C57BL/6 mice at day +5 following DJ001 or vehicle injections. At 12 hours following 300 cGy irradiation of BM KSL cells in vitro, we detected increased concentrations of LPS-induced CXC chemokine (LIX), macrophage inflammatory protein-1α (MIP-1α) and MIP-1β (Figure 16a and 16b). Following DJ001 treatment *in vitro*, concentration levels of the majority of the cytokines we measured remain the same with the exception of decreased level of LIX (Figure 15a). At day +5 post 750 cGy TBI, we detected decreased levels of LIX and CXCL12 but increased levels of SCF and PTN in the BM (Figure 17a and 17b). DJ001 treatment had no effects on cytokine levels in non-irradiated mice, but caused a modest increase in CXCL12 level and a decrease in PTN level in the BM of irradiated mice compared with vehicle-treated irradiated control mice (Figure 17b).

2.3.4 PTPσ inhibition promotes human HSC regeneration

Based on the regenerative effect of DJ001 in murine bone marrow hematopoietic cells following myelosuppression, we sought to determine whether DJ001 could also accelerate human HSC regeneration post injury. Irradiation of human BM $CD34^+$ cells with 300 cGy *in vitro* caused a significant loss of $CD34^+CD38^-$ human hematopoietic stem and progenitor cells at 36 hours post irradiation (Figure 18a). DJ001 also increased the recovery of multipotent CFU-GEMMs at 72 h following irradiation of human BM $CD34^+$ cells (Figure 18b).

In order to determine whether PTPσ inhibition could promote the recovery of human HSCs with *in vivo* repopulating capacity, we irradiated BM $CD34^+$ cells with 300 cGy and cultured in TSF media with or without DJ001 for 36 h, and transplanted the progeny into NSG mice to assess human hematopoietic engraftment over time (Figure 19a). Mice transplanted with irradiated, DJ001-treated BM $CD34^+$ cells displayed substantially increased engraftment of human $CD45^+$ cells, $CD34^+$ hematopoietic progenitor cells, $CD19^+$ B cells, $CD33^+$ myeloid cells, and $CD3^+$ T cells at 12 weeks post-transplant compared with mice transplanted with equal doses of irradiated, control BM $CD34^+$ cells (Figure 19b and 19c).

Therefore, PTPσ inhibition promoted the recovery of both murine and human HSCs with multilineage repopulating capacity following irradiation.

2.4 Discussions

PTPs have been recognized as important drug targets due to their involvement in the pathogenesis of numerous diseases. However, active site-directed PTP inhibitors frequently lack target specificity due to the high degree of homology between PTP active sites. Negative charged phosphor-tyrosine mimetics also have poor bioavailability, as they are typically cell impermeable. These barriers have hindered the development of PTP active site inhibitors for clinical use. A recent analysis of non-receptor and receptor PTPs for "druggability" suggested that the majority of PTPs were poor drug targets due to the hydrophilic or shallow nature of their catalytic pockets. As an alternative strategy, allosteric inhibitors have been described for specific PTPs, including selective inhibitors for dual specificity phosphatase 6 and the Src-homology-2-domain-containing phosphatase 2 (SHP2). A small molecule, allosteric inhibitor of SHP2 was recently shown to inhibit RTK-driven human cancer growth in xenograft models. Here, we describe a small molecule that non-competitively inhibits PTPσ via allosteric binding and is highly selective for PTPσ. Based on these unique properties, we propose that DJ001, and DJ001 structural analogues, are compelling candidates for therapeutic development.

The majority of the cancer patients undergo myelosuppressive chemotherapy and/or radiation therapy during the treatment of the disease. Hematopoietic toxicities occur commonly in such patients, resulting in hospitalizations, delays in curative therapy, and potentially life-threatening infections. Depletion of BM HSCs and progenitor cells, which occurs following repeated cycles of cytotoxic chemotherapy, contributes to prolonged myelosuppression in such patients. Therapies that promote HSC and progenitor cell regeneration could lessen the complications of myelosuppression and facilitate the timely completion of potentially curative chemotherapy.

However, the mechanisms that govern HSC regeneration are poorly understood and this gap in knowledge has impeded the development of targeted therapies to drive human hematopoietic regeneration. Here, we demonstrate that systemic administration of a small molecule inhibitor of PTPσ accelerated hematopoietic regeneration in mice following irradiation or chemotherapy. Furthermore, PTPσ inhibition strongly promoted the recovery of human hematopoiesis and human HSC long-term repopulation capacity in immune-deficient NSG mice following irradiation. Taken together, these results suggest the therapeutic potential for a small molecule PTPσ inhibitor to accelerate hematologic recovery in cancer patients receiving chemo- or radiotherapy.

Our *in vitro* studies of non-irradiated BM $CD34^-$ KSL cells also suggested the potential for DJ001 or its analogues to promote HSPC expansion; however, *in vivo* administration of DJ001 3 days a week for 4 weeks caused no expansions of HSCs, progenitors, or mature blood counts in non-irradiated mice. The absence of effect in non-irradiated mice may have occurred due to insufficient concentrations of DJ001 achieved in the BM of non-irradiated mice following that treatment schedule or possibly due to indirect effects of systemically administered DJ001 on cytokines or chemokines in the BM that counteracted direct effects on HSCs. Our analysis of the BM of non-irradiated mice revealed no significant changes in cytokine or chemokine levels in response to DJ001 treatment. Following irradiation, DJ001 treatment was associated with modest changes in concentrations of the HSC growth factors, CXCL12 and PTN, compared with control. Therefore, results from the cytokine array suggest that DJ001 promotes HSC regeneration primarily via direct effects on HSCs; however, indirect effects of DJ001 via undiscovered mechanisms excluded.

PTPσ and related receptors within the leukocyte antigen-related (LAR) subfamily of PTPs are expressed by neurons and act as receptors for heparan sulfate proteoglycans[86,93]. In the developing neuron system, PTPσ regulates axon guidance and synapse formation[144]. PTPσ also serves as a receptor for inhibitory glycosylated side chains of chondroitin sulfate proteoglycan (CSPGs)[144]. CSPGs, which are enriched in the extracellular matrix surrounding injured nerves, inhibit axon regeneration following spinal cord injury[67]. Genetic deletion of PTPσ promoted axon regeneration in a model of spinal cord injury, suggesting that PTPσ may be a therapeutic target to enhance nerve regeneration[144]. Subsequently, systemic delivery of a peptide-mimetic of the PTPσ wedge domain was reported to relieve CSPG-mediated inhibition and restore serotonergic innervation of the spinal cord in rats[90]. In a model of myocardial infarction, genetic deletion or administration of a PTPσ intracellular peptide beginning three days after injury promoted sympathetic innervation in the area of myocardial scar[97]. In our study, we demonstrate that systemic delivery of a small-molecule PTPσ inhibitor promotes HSC regeneration and long-term hematopoietic reconstitution *in vivo* following myelosuppressive irradiation or chemotherapy. The combined effects of PTPσ inhibition on hematopoietic and neural regeneration suggest an important role for PTPσ in regulating adult somatic cell regeneration.

2.5 Figures

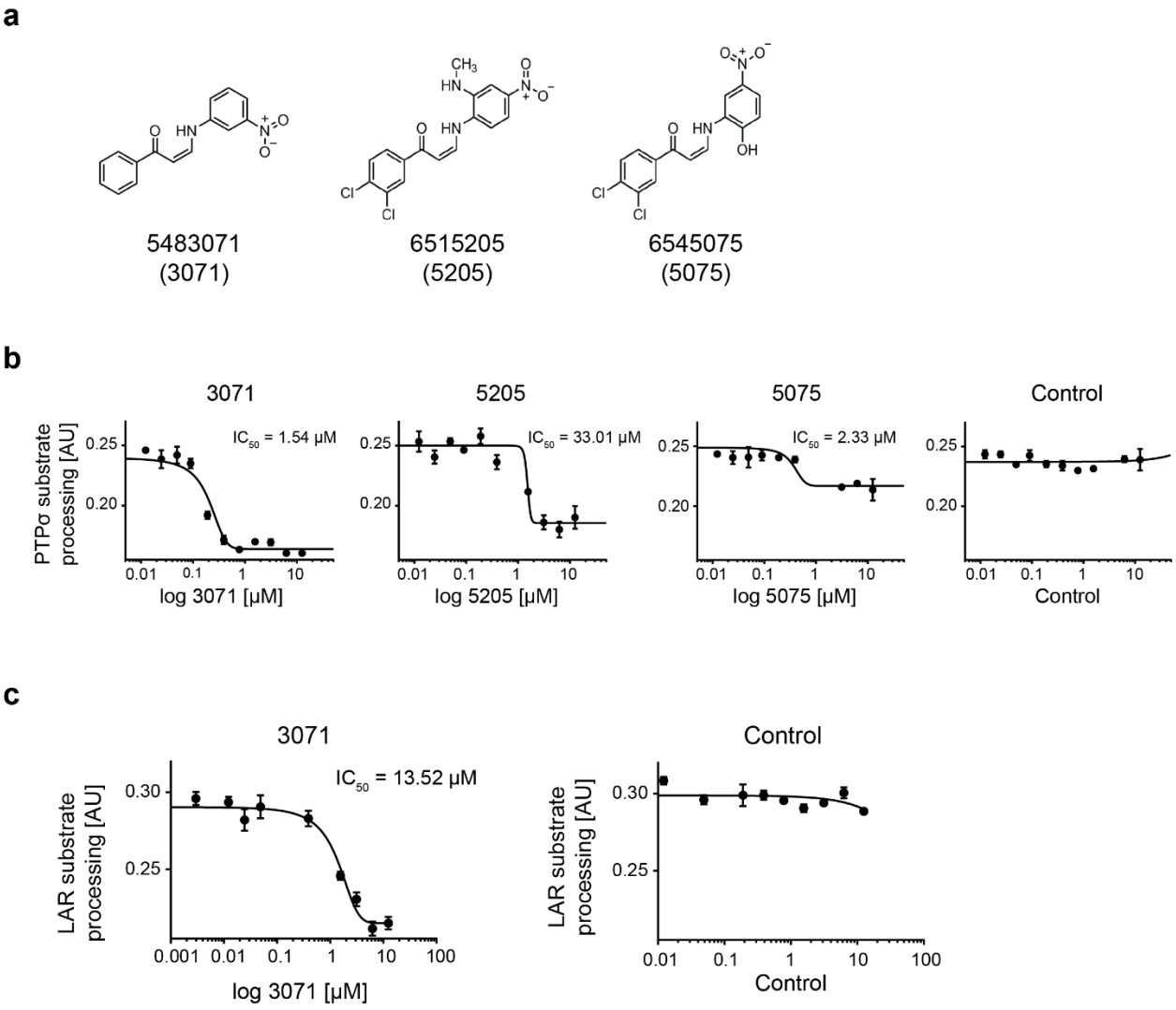

Figure 1 DJ001 has strong inhibitory activity against PTPσ.

a Chemical structure of compounds 3071, 5205, and 5075. **b** Concentration-inhibition curves and IC_{50} values for 3071, 5205, 5075, and control (DMSO) following incubation with PTPσ (n = 3). **c** Concentration-inhibition curves and IC_{50} values for 3071 and control following incubation with leukocyte common antigen-related (LAR) (n = 3). Error bars represent S.E.M.

a

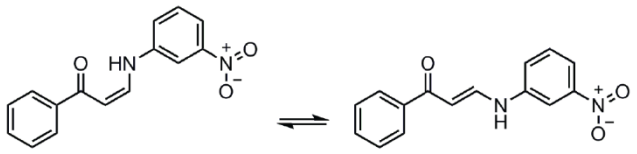

DJ001 (*Z*) DJ001 (*E*)

b

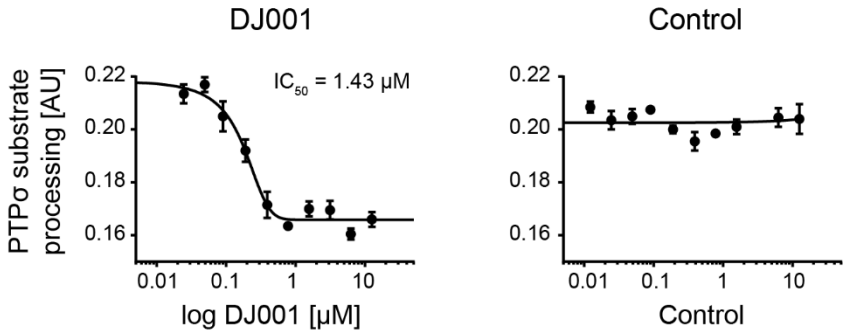

Figure 2 DJ001 exists in two stereoisomers in polar solvents.

a (*Z*) and (*E*)- stereoisomers of DJ001 are present in a 1:1 equilibrium in polar solvents such as DMSO. **b** Concentration-inhibition curves and IC_{50} values for 3071 and control following incubation with PTPσ (n = 3). Error bars represent S.E.M.

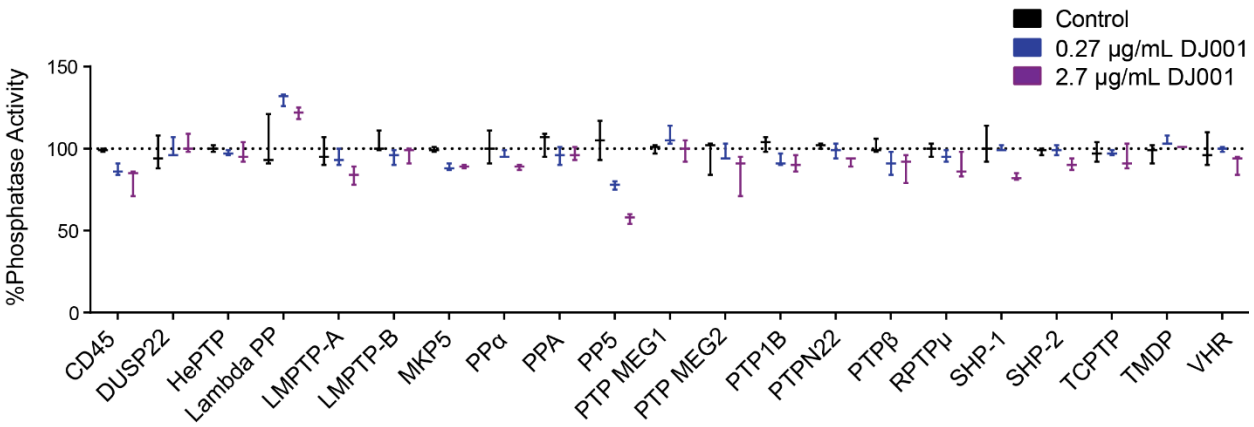

Figure 3 PTPσ does not inhibit other protein tyrosine phosphatases.

Percent phosphatase activity following exposure to DJ001. CD45: Protein Tyrosine Phosphatase, receptor type C; DUSP22: Dual Specificity Phosphatase 22; HePTP: Hematopoietic Protein Tyrosine Phosphatase; Lambda PP: Lambda Protein Phosphatase; LMPTP-A: Low Molecular Weight Protein Tyrosine Phosphatase A; LMPTP-B: Low Molecular Weight Protein Tyrosine Phosphatase B; MKP5: Mitogen-activated Protein Kinase Phosphatase 5; PPα: Protein Phosphatase 1 Catalytic Subunit alpha; PPA: Protein Phosphatase 1; PP5: Protein Phosphatase 5; PTPMEG1: Megakaryocyte Protein-Tyrosine Phosphatase; PTPMEG2: Protein Tyrosine Phosphatase Non-Receptor Type 9; PTP1B: Protein Tyrosine Phosphatase 1B; PTPN22: Protein Tyrosine Phosphatase Non-Receptor Type 22; PTPβ: Protein Tyrosine Phosphatase Receptor beta; RPTPμ: Receptor type Protein Tyrosine Phosphatase Mu; SHP-1: Protein-Tyrosine Phosphatase 1C; SHP-2: Protein-Tyrosine Phosphatase 2C; TCPTP: T-Cell Protein-Tyrosine Phosphatase; TMDP: Dual Specificity Phosphatase 13; VHR: Dual Specificity Phosphatase 3. Data represent minimum to maximum values (n = 3/group). Error bars represent S.E.M.

a

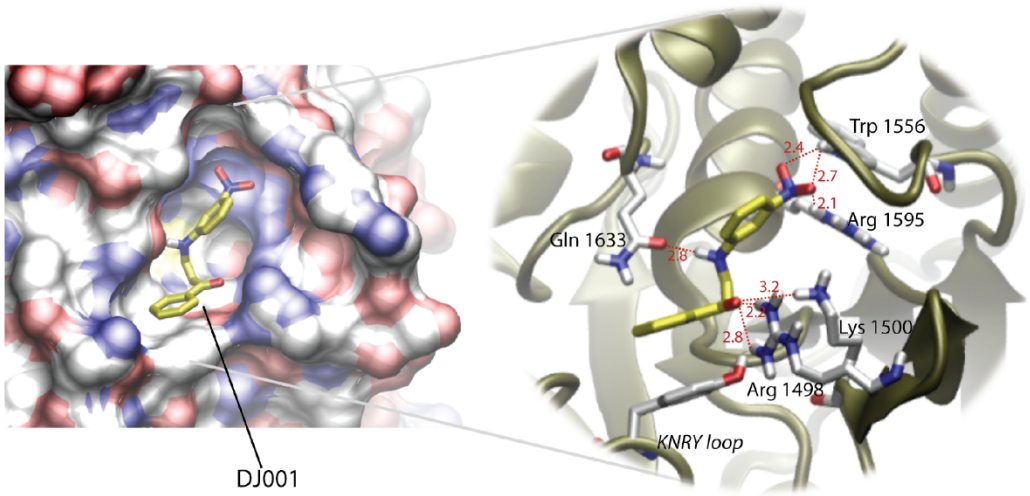
Trp 1556
2.4
2.7
2.1
Arg 1595
Gln 1633
2.8
3.2
2.2
2.8
Lys 1500
Arg 1498
KNRY loop
DJ001

b

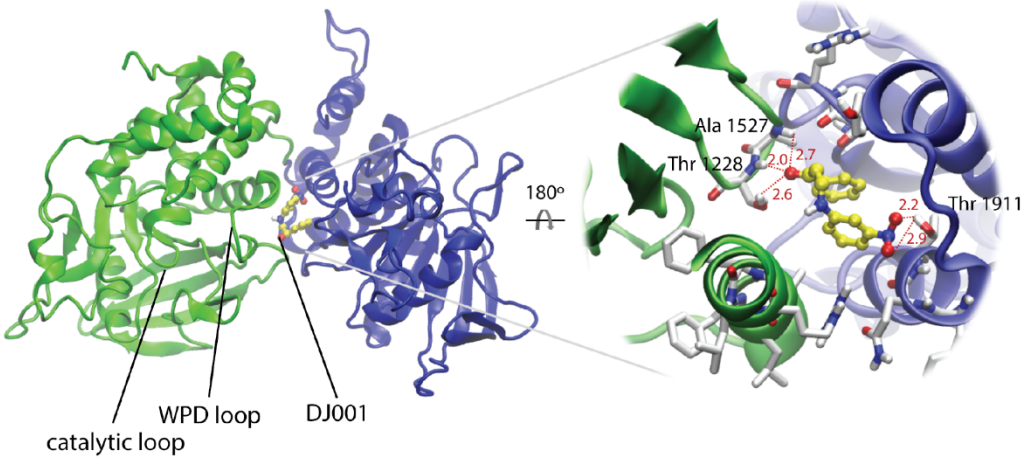
180°
Ala 1527
Thr 1228
2.0
2.7
2.6
2.2
2.9
Thr 1911
WPD loop
DJ001
catalytic loop

c

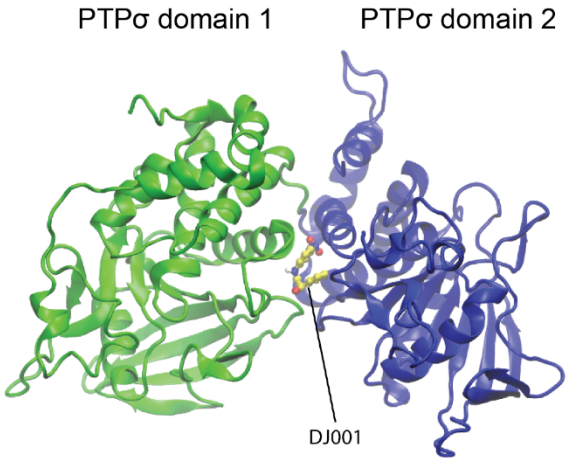
PTPσ domain 1
PTPσ domain 2
DJ001

Figure 4 DJ001 inhibits PTPσ primarily via allosteric binding.

a Details of three dimensional docking of DJ001 (Z) to the catalytic binding site of PTPσ (protein data base ID: 2FH7) which consists of the highly conserved phosphotyrosine recognition loop (KNRY loop: Lysine (K), Asparagine (N), Arginine (R) and Tyrosine (Y)) and important H-bonding interactions to the amino acids, Glutamine (Gln) 1633, L-Tryptophan (Trp) 1556, Arginine (Arg) 1595, Lysine (Lys) 1500 and Arginine (Arg) 1498, shown as red dashed lines with distances between two atoms. Structure of DJ001 (Z) represented as capped stick and yellow color. **b** Details of three dimensional docking of DJ001 (Z) to the allosteric binding site of human PTPσ (ID: 2FH7) showing important H-bonding interactions to Alanine (Ala) 1527, Threonine (Thr) 1228 and Threonine 1911 and close proximity to the highly conserved Tryptophan (W)/Proline (P)/Aspartate (D) protein loop (WPD loop). Structure of DJ001 (Z) is represented as ball and stick in yellow color. H-bonding interactions are shown as red dashed line with distances between two atoms and the catalytic loop as part of the catalytic binding site is indicated in domain 1. **c** *In silico* three-dimensional docking of DJ001 (*Z* isomer) (represented as ball and stick in yellow color) to the PTPσ allosteric binding site located between domain 1 (green) and domain 2 (blue) of PTPσ.

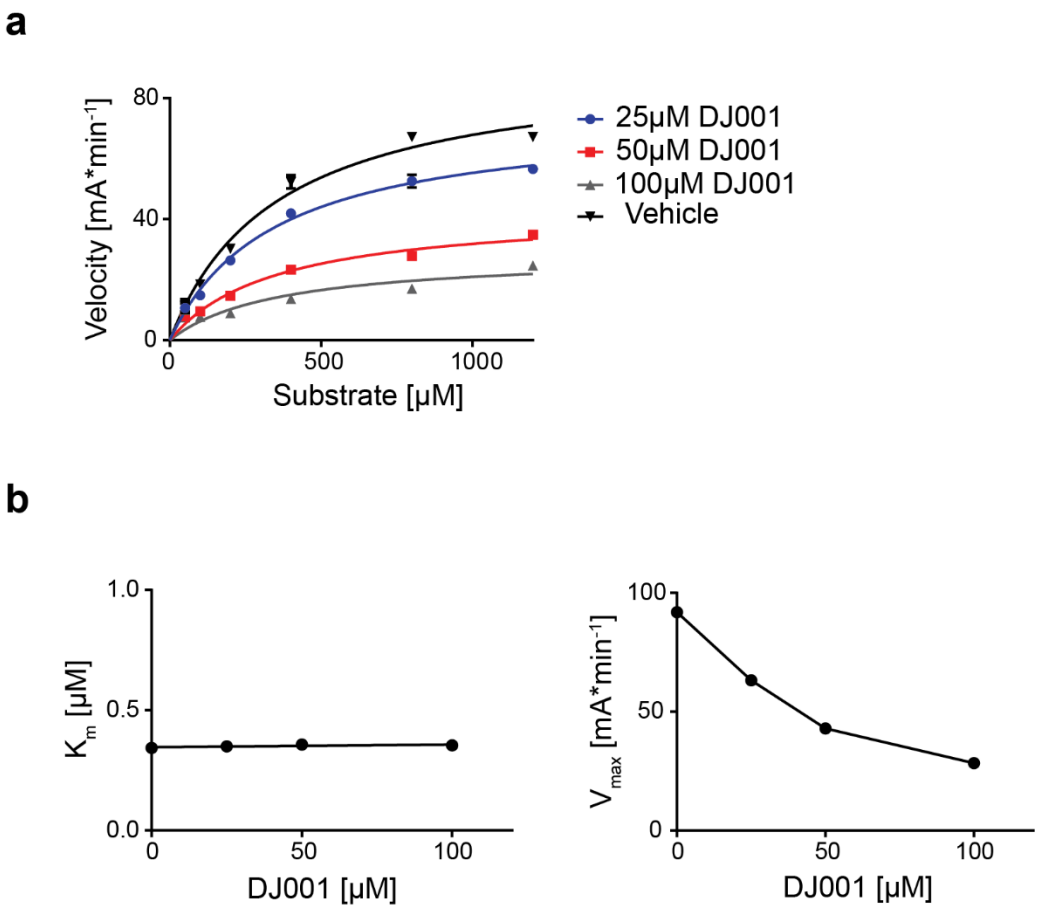

Figure 5 DJ001 is a non-competitive inhibitor of PTPσ.

a and **b** Substrate titration reveals DJ001 as a non-competitive inhibitor that inhibits substrate catalysis (V_{max}), but not substrate binding of PTPσ (constant K_m). **c** Plots of K_m and V_{max} as a function of compound concentration delivered from nonlinear regression in substrate titration. Error bars represent S.E.M.

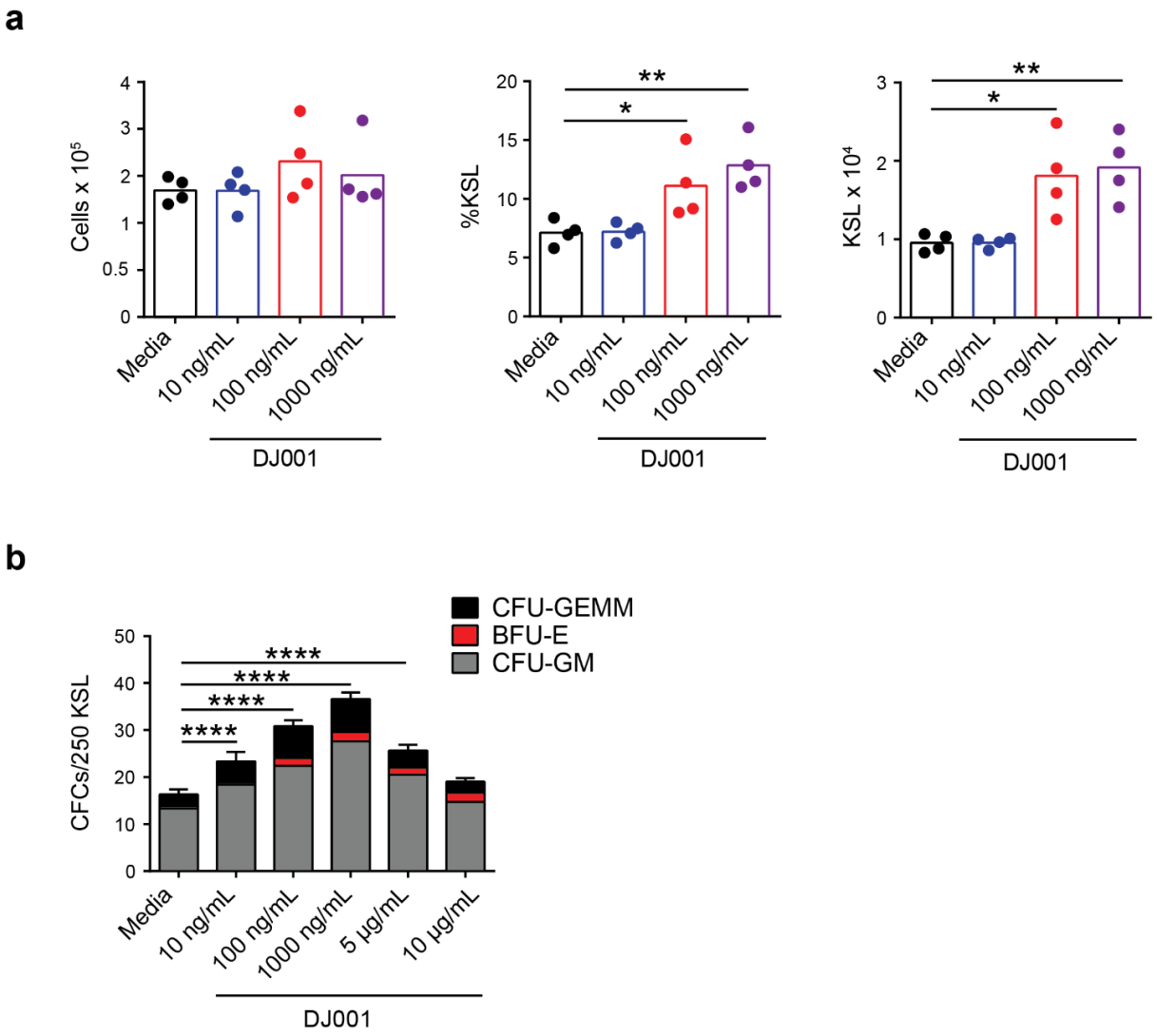

Figure 6 DJ001 expands murine BM hematopoietic stem/progenitor cells in culture.

DJ001 expands murine BM hematopoietic stem/progenitor cells in culture. **a** The numbers of cells, percentages of KSL cells and numbers of KSL cells are shown following culture of BM CD34$^-$ KSL cells for 7 days with TSF media (media) ± DJ001 (10, 100 or 1,000 ng/ml) (n = 4/group). **b** Mean numbers of CFCs at day +3 of culture of BM KSL cells with media ± DJ001 (10 ng/mL, 100 ng/mL, 1000 ng/mL, 5 µg/ml or 10 µg/ml) (n = 5 - 6/group). One-way ANOVA with Tukey's multiple comparison test for all comparisons. * $P < 0.05$, ** $P < 0.01$, **** $P < 0.0001$.

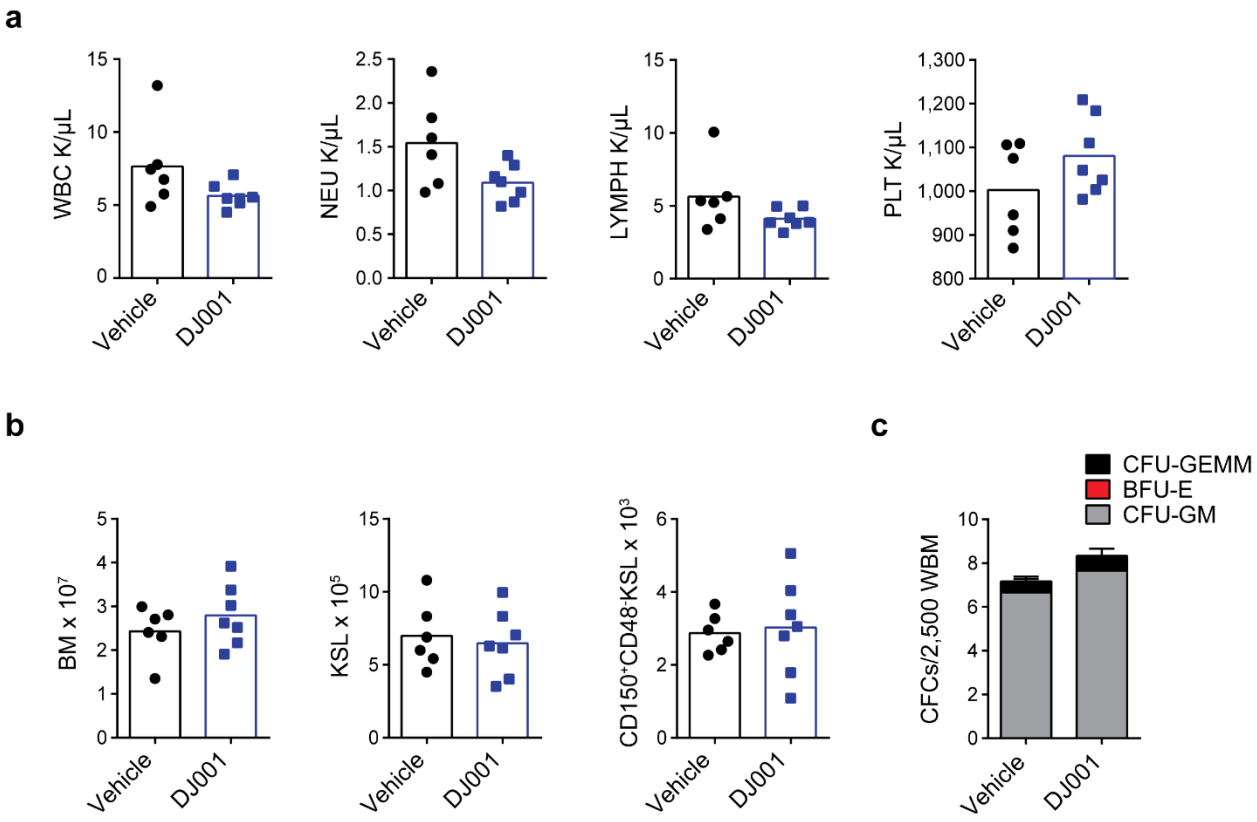

Figure 7 DJ001 does not affect BM hematopoiesis in vivo at homeostasis.

a Numbers of WBC, NEU, lymphocytes (LYMPH) and platelets (PLT) in the PB of mice treated subcutaneously every M-W-F with 5 mg/kg DJ001 or vehicle for 30 days (vehicle, $n = 6$; DJ001, $n = 7$). **b** BM cell counts and numbers of KSL cells and $CD150^{+}CD48^{-}$KSL HSCs in C57BL/6 mice at day +30 following treatment described in **c** (vehicle, $n = 6$; DJ001, $n = 7$). **c** Numbers of CFCs harvested from mice at day +30 following treatment described in **a** ($n = 6$ assays/group). Error bars represent S.E.M.

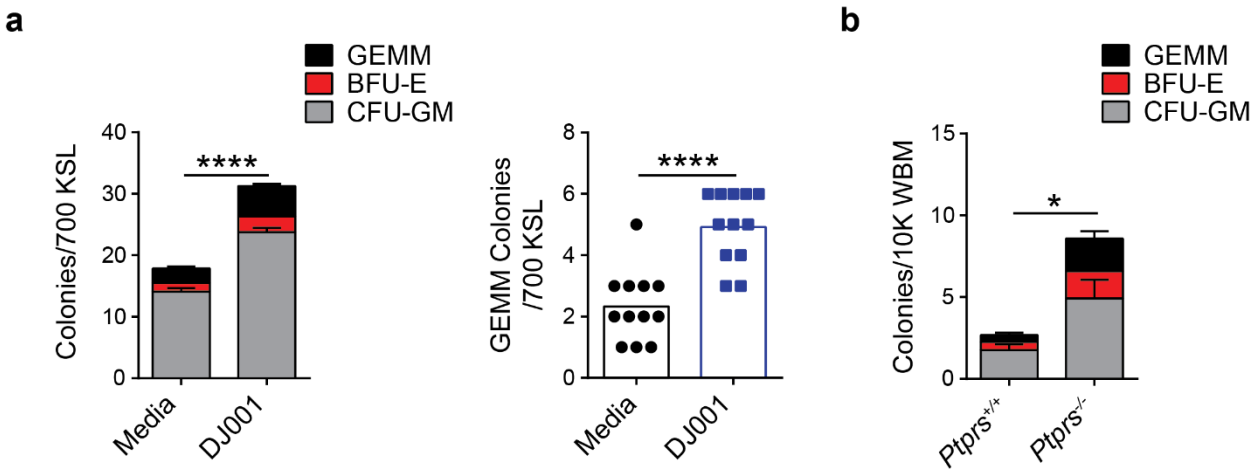

Figure 8 Pharmacologic inhibition of PTPσ or genetic deletion of *Ptprs* promotes bone marrow colony forming cell recovery post irradiation.

a Mean numbers of CFCs from BM KSL cells following 300 cGy irradiation and culture for 3 days in TSF media + DJ001 (n = 12). **b** Mean numbers of CFU-GEMMs within BM KSL cells at day +3 following 300 cGy irradiation and culture in media with or without DJ001 (n = 12/group). **c** Mean numbers of BM CFCs in Ptprs+/+ and Ptprs-/- mice at day +10 following 600 cGy TBI (n = 12). Error bars represent S.E.M. * $P < 0.05$, **** $P < 0.0001$.

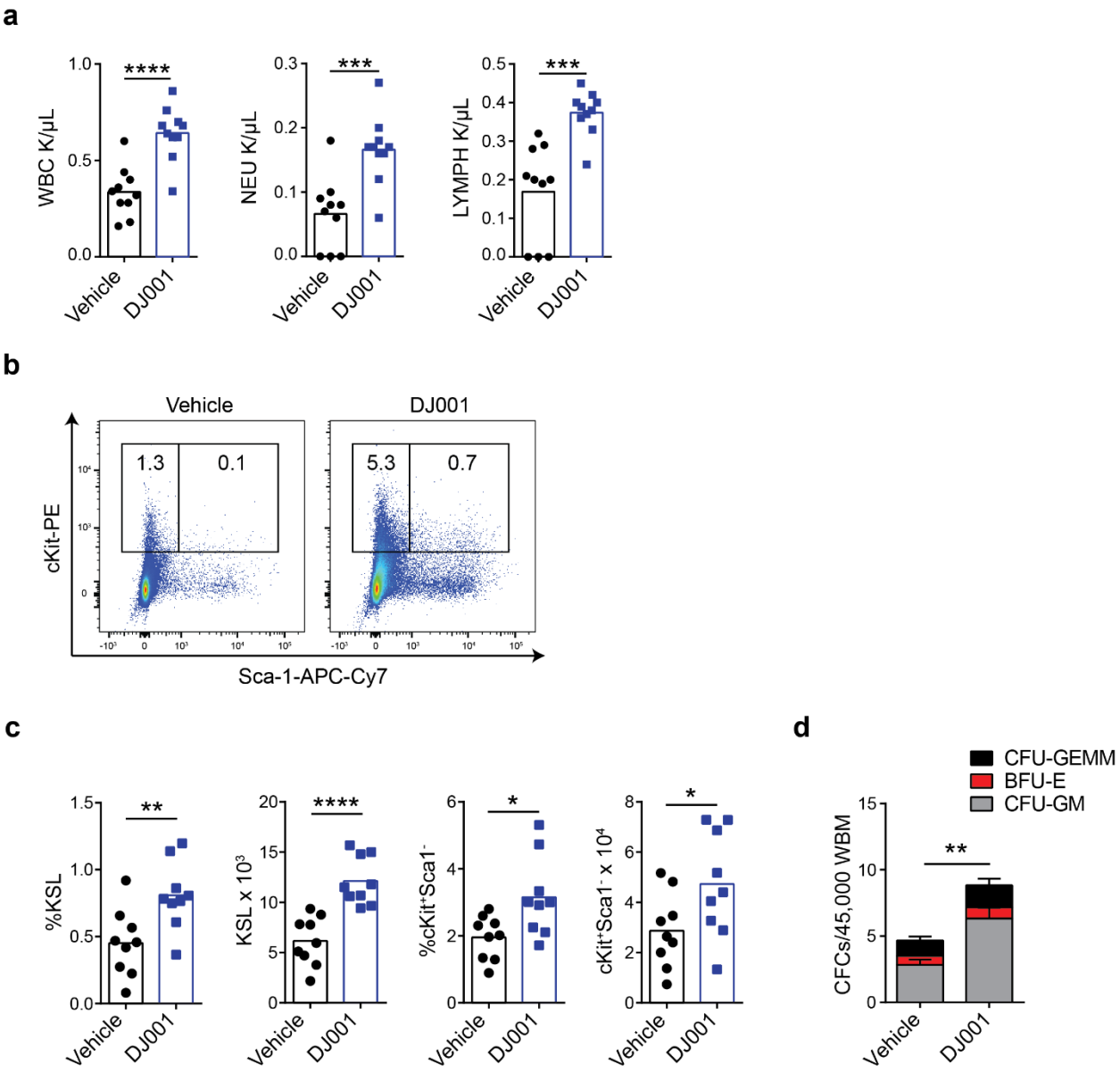

Figure 9 PTPσ inhibition promotes hematopoietic regeneration.

a Mean numbers of PB WBCs, neutrophils (NEU), and lymphocytes (LYMPH) in mice at day + 10 following 750 cGy and treatment with DJ001 or 10% DMSO (vehicle) (n = 10). **b** Representative flow cytometric analysis of percentages of KSL cells and $cKit^{+}Sca1^{-}$ progenitor cells at day + 10 post 750 cGy in the treatment groups shown. **c** Mean percentages and numbers of BM KSL cells and cKit+Sca1- cells and day + 10 post 750 cGy (n = 9). **d** Numbers of BM CFCs

at day +10 post 750 cGy TBI (n = 6). Error bars represent S.E.M. * $P < 0.05$, **$P < 0.01$, ***$P < 0.001$, **** $P < 0.0001$.

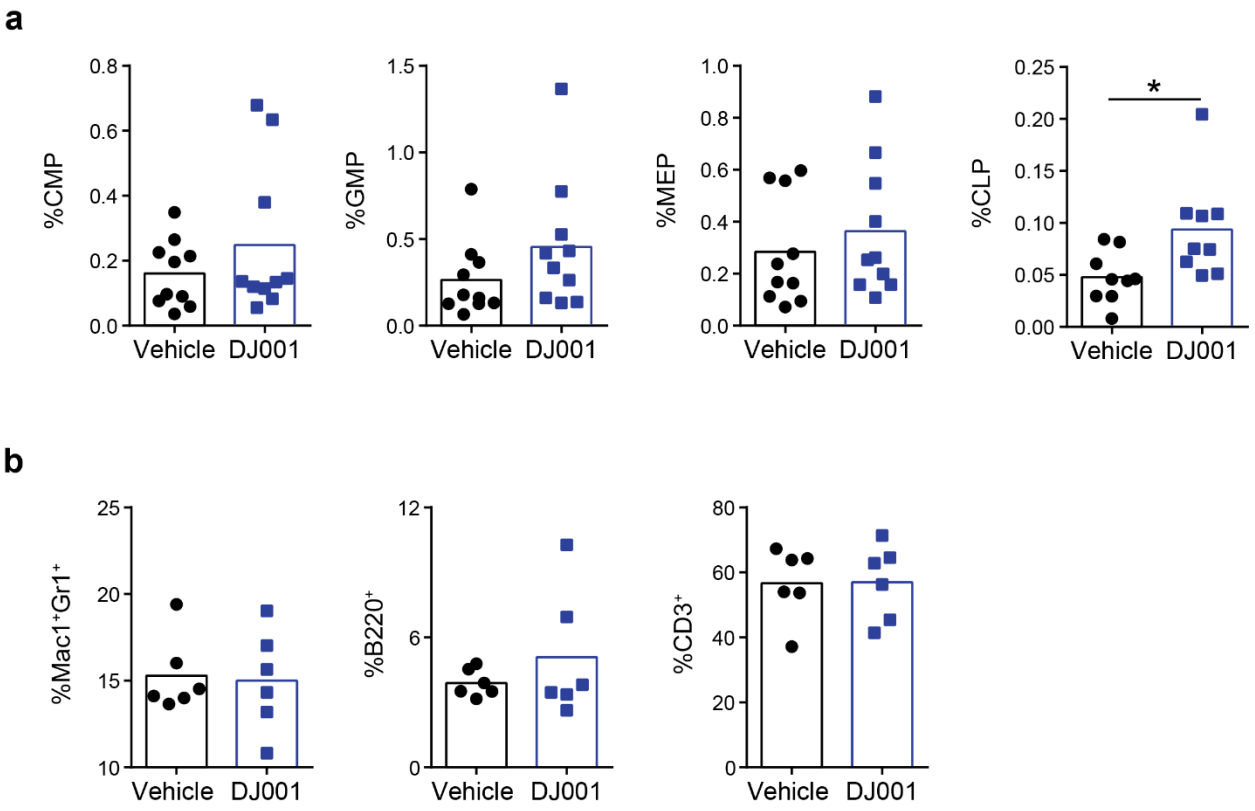

Figure 10 PTPσ inhibition does not affect recoveries of hematopoietic progenitor cells or hematopoietic mature cells.

a Mean percentages of megakaryocyte-erythrocyte progenitors (MEP), common myeloid progenitors (CMP), granulocyte-monocyte progenitors (GMP), and common lymphoid progenitors (CLP) in the BM at day +10 following 750 cGy irradiation and treatment with DJ001 or vehicle (n = 9 - 10). **b** Mean percentages of PB $Mac1^+Gr1^+$ cells, $B220^+$ cells and $CD3^+$ cells in mice at day +10 following 750 cGy TBI and treatment with DJ001 or vehicle (n = 6). * $P < 0.05$.

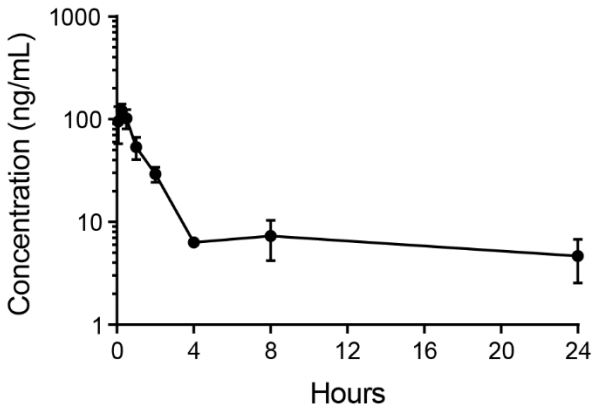

Figure 11 Pharmacokinetics of DJ001 in plasma.

Pharmacokinetics (PK) for mean plasma concentrations of DJ001 in adult C57BL/6 mice following subcutaneous administration of 5 mg/kg DJ001 (n = 3). Error bars represent S.E.M.

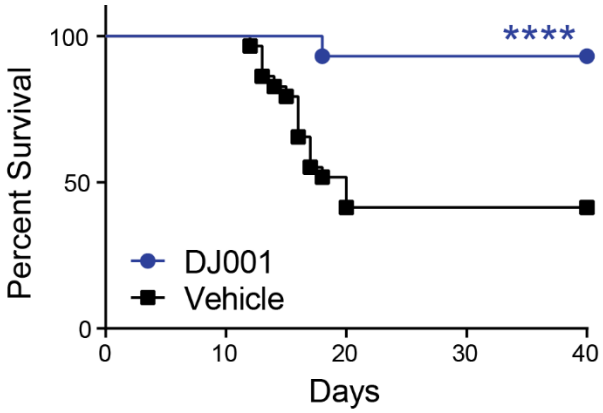

Figure 12 PTPσ inhibition improves survival in sub-lethally irradiated mice.

Percent survival of mice after 750 cGy and treatment with DJ001 (27/29 alive) or vehicle (12/29 alive). Log-rant test. **** $P < 0.0001$.

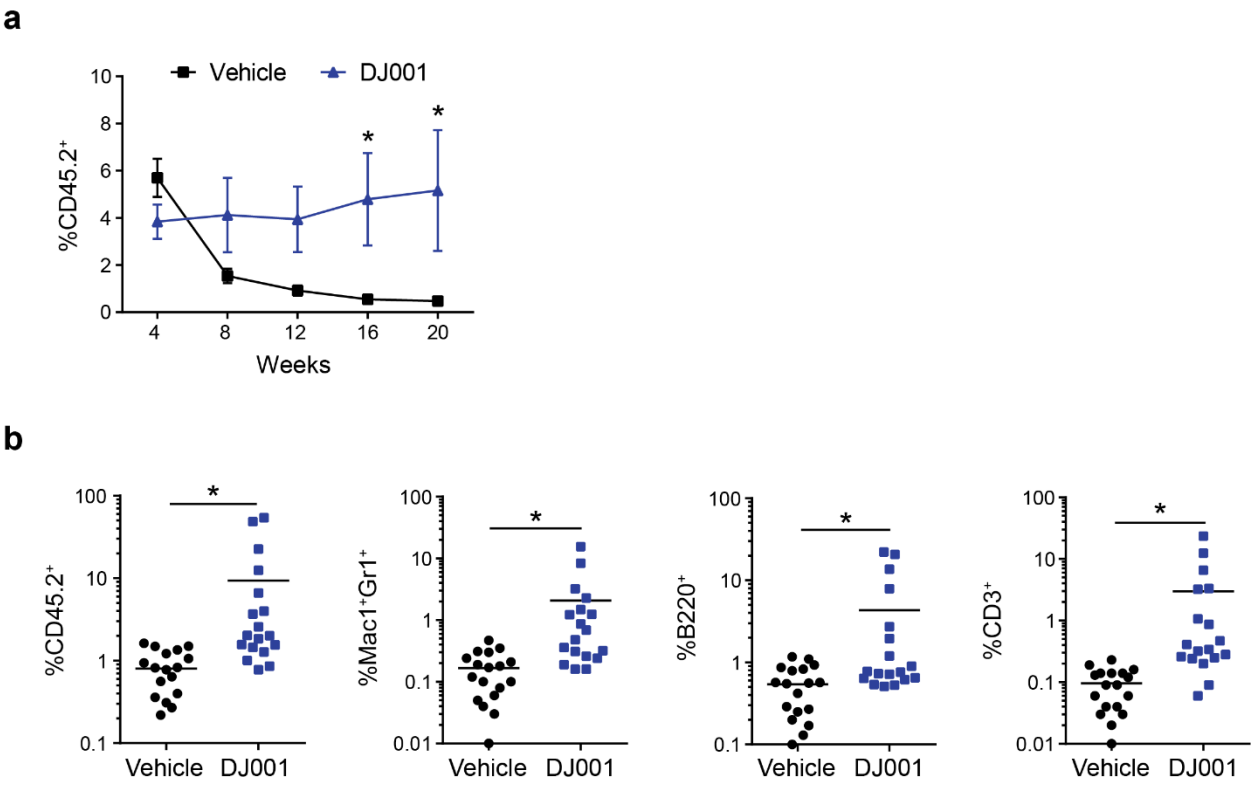

Figure 13 PTPσ inhibition enhances HSC repopulating capacity.

a Mean percentages of donor CD45.2$^+$ cells in the PB of CD45.1$^+$ recipient mice over time following transplantation of 5 x 10^5 BM cells from CD45.2$^+$ mice at day + 10 following 750 cGy TBI and treatment with DJ001 or vehicle, along with 1x 10^5 CD45.1$^+$ BM competitor cells (n = 18-21/group). **b** Mean percentages of total donor CD45.2$^+$ cells and CD45.2$^+$Mac1$^+$Gr1$^+$ myeloid cells, CD45.2$^+$B220$^+$ B cells, and CD45.2$^+$CD3$^+$ T cells in the PB of recipient mice at 20 weeks post transplantation (n = 18/group). Error bars represent S.E.M. * $P < 0.05$.

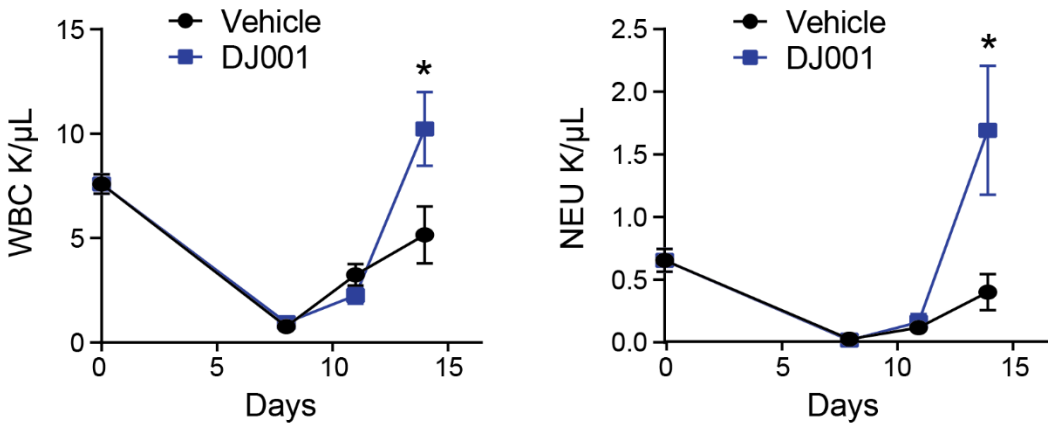

Figure 14 DJ001-mediated PTPσ inhibition promotes hematologic recovery post chemotherapy. Mean numbers of PB WBCs and NEU counts in mice at day + 0 (pre-5FU), + 8, + 11, and + 14 following 5FU treatment (n = 4-7/group). Error bars represent S.E.M. * $P < 0.05$.

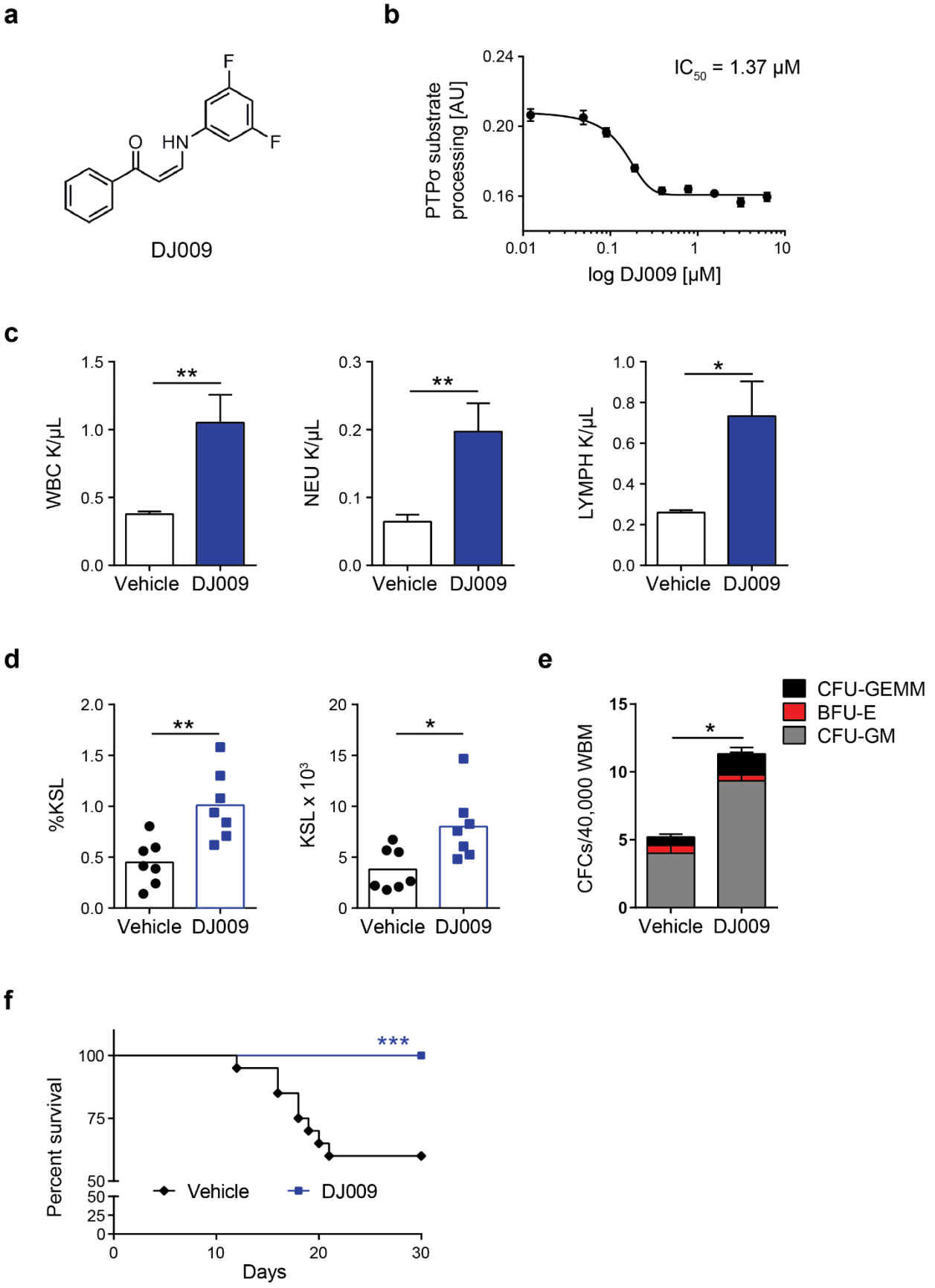
a
F
O
HN
F
DJ009
b
IC50 = 1.37 μM
PTPσ substrate processing [AU]
0.24
0.20
0.16
0.01
0.1
1
10
log DJ009 [μM]
c
WBC K/μL
NEU K/μL
LYMPH K/μL
**
**
*
Vehicle
DJ009
d
%KSL
KSL x 10³
**
*
Vehicle
DJ009
e
CFCs/40,000 WBM
CFU-GEMM
BFU-E
CFU-GM
*
Vehicle
DJ009
f
Percent survival
***
Vehicle
DJ009
Days

Figure 15 DJ009 inhibits PTPσ and promotes hematopoietic regeneration.

a Chemical structure for compound DJ009. **b** Concentration-inhibition curves and IC_{50} value for DJ009. Data points are means of absorption unit (n = 3). **c** Mean numbers of PB WBCs, NEU, and LYMPH in mice at day +10 following 750 cGy and treatment with 5 mg/kg DJ009 or vehicle (n = 7). **d** Mean percentages and numbers of BM KSL cells at day +10 post 750 cGy followed by treatment with DJ009 or vehicle (n = 7). **e** Mean numbers of BM CFCs at day +10 post 750 cGy TBI and treatment with DJ009 or vehicle (n = 9-10/group). **f** Survival of mice irradiated with 750 cGy and treated with 5 mg/kg DJ009 (24/24 mice) or vehicle (12/20 mice) daily for 10 d (*** P = 0.0006, log-rank test). Error bars represent S.E.M. * $P < 0.05$, ** $P < 0.01$, *** $P < 0.001$.

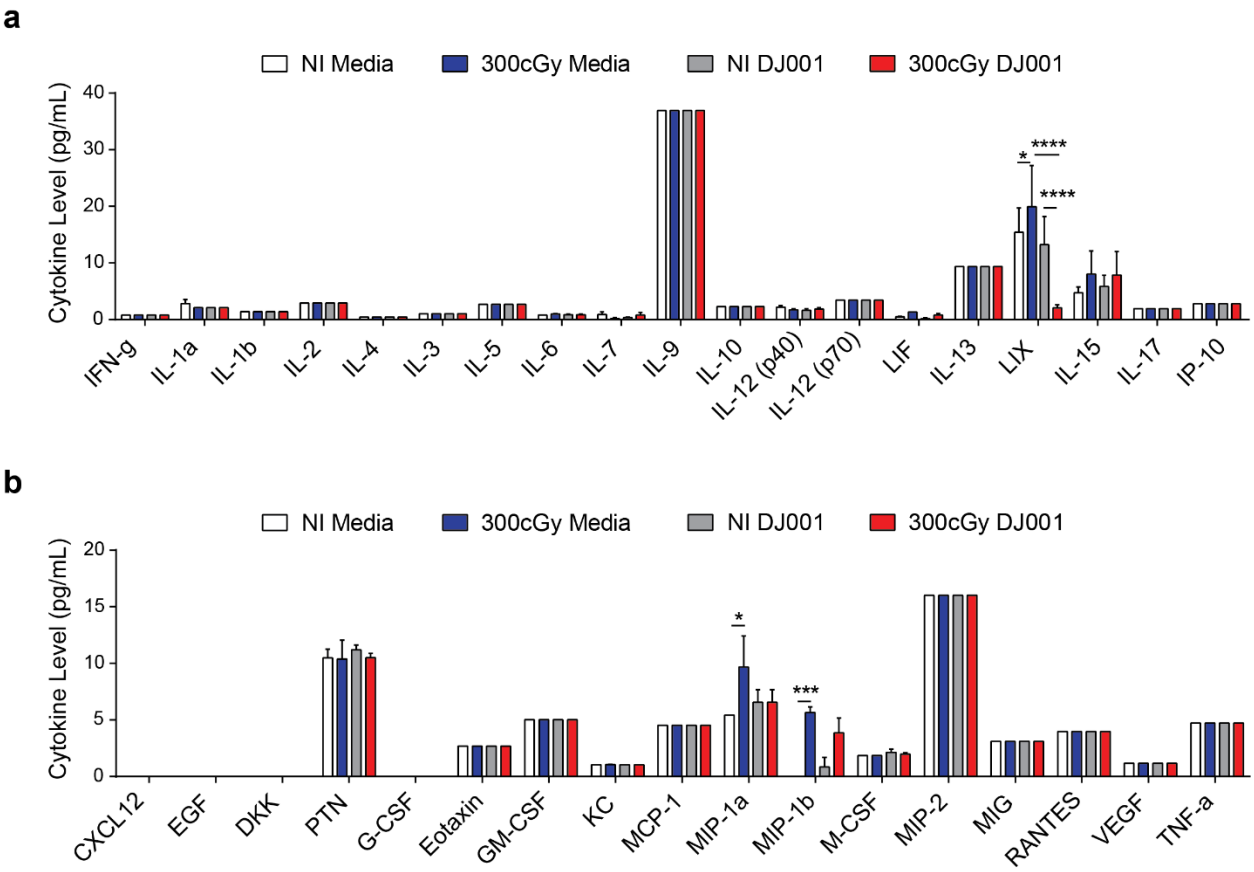

Figure 16 Effects of irradiation and DJ001 on cytokine levels *in vitro*.

a *In vitro* levels of interleukins and IFN-gamma at 12 hours of culture of non-irradiated and irradiated (300 cGy) KSL cells, treated with (gray bar and red bar) and without 1 μg/ml DJ001 (white bar and blue bar) (n = 3/group). **b** *In vitro* levels of HSC growth factors and other cytokines at 12 hours of culture of the populations described in a. SCF and TPO not shown since part of TSF media (n = 3/group). 2-way ANOVA with Sidak's multiple comparison test was performed for all comparisons. IFN-g, Interferon gamma; IL-1a, Interleukin 1 alpha; IL-1b, Interleukin 1 beta; IL-2, Interleukin 2; IL-3, Interleukin 3; IL-4, Interleukin 4; IL-5, Interleukin 5; IL-6, Interleukin 6; IL-7, Interleukin 7; IL-9, Interleukin 9; IL-10, Interleukin 10; IL-12 p40, Interleukin 12 subunit p40; IL-12 p70, Interleukin 12 subunit 70; LIF, Leukemia Inhibitory Factor; IL-13, Interleukin 13; LIX, LPS-induced C-X-C Chemokine; IL-15, Interleukin 15; IL-17, Interleukin 17; IP-10,

Interferon gamma induced protein 10; CXCL12, C-X-C Motif Chemokine Ligand 12; EGF, Epidermal Growth Factor; DKK1, Dickkopf 1; PTN, Pleiotrophin; G-CSF, Granulocyte Colony Stimulating Factor; GM-CSF, Granulocyte-Macrophage Colony Stimulating Factor; KC, C-X-C motif ligand 1; MCP-1a, Monocyte Chemoattractant Protein-1; MIP-1a, Macrophage Inflammatory Protein -1 alpha; MIP-1b, Macrophage Inflammatory Protein -1 beta; M-CSF, Macrophage Colony Stimulating Factor; MIP-2, Macrophage Inflammatory Protein - 2; MIG, Monokine induced by gamma interferon; RANTES, Regulated on Activation, Normal T cell Expressed and Secreted protein; VEGF, Vascular Endothelial Growth Factor; TNF-a, Tumor Necrosis Factor Alpha. Error bars represent S.E.M. * $P < 0.05$, *** $P < 0.001$, **** $P < 0.0001$.

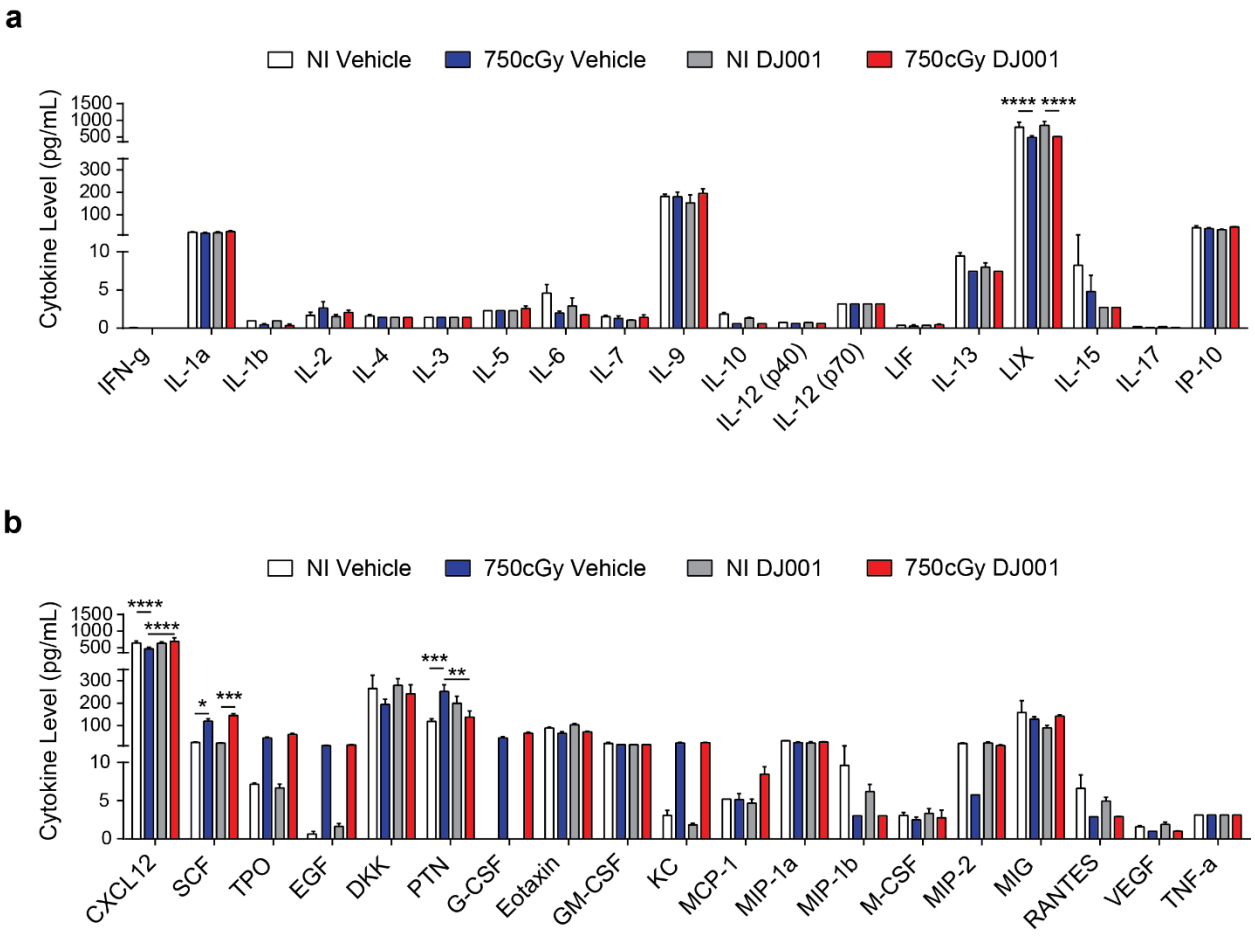

Figure 17 Effects of irradiation and DJ001 on cytokine levels *in vivo*.

a *In vivo* levels of interleukins and IFN-gamma in the BM of non-irradiated (white bar) and 750 cGy – irradiated mice (blue bar) at day + 5 of vehicle treatment; cytokine levels also shown in the same mice groups treated for 5 days with 5 mg/kg DJ001 (gray and red bar, respectively) (*n* = 3/group). **b** *In vivo* levels of HSC growth factors and other cytokines at day + 5 in the BM of the mice described in **a** (*n* = 3/group). 2-way ANOVA with Sidak's multiple comparison test was performed for all comparisons. IFN-g, Interferon gamma; IL-1a, Interleukin 1 alpha; IL-1b, Interleukin 1 beta; IL-2, Interleukin 2; IL-3, Interleukin 3; IL-4, Interleukin 4; IL-5, Interleukin 5; IL-6, Interleukin 6; IL-7, Interleukin 7; IL-9, Interleukin 9; IL-10, Interleukin 10; IL-12 p40, Interleukin 12 subunit p40; IL-12 p70, Interleukin 12 subunit 70; LIF, Leukemia Inhibitory Factor;

IL-13, Interleukin 13; LIX, LPS-induced C-X-C Chemokine; IL-15, Interleukin 15; IL-17, Interleukin 17; IP-10, Interferon gamma induced protein 10; CXCL12, C-X-C Motif Chemokine Ligand 12; EGF, Epidermal Growth Factor; DKK1, Dickkopf 1; PTN, Pleiotrophin; G-CSF, Granulocyte Colony Stimulating Factor; GM-CSF, Granulocyte-Macrophage Colony Stimulating Factor; KC, C-X-C motif ligand 1; MCP-1a, Monocyte Chemoattractant Protein-1; MIP-1a, Macrophage Inflammatory Protein -1 alpha; MIP-1b, Macrophage Inflammatory Protein -1 beta; M-CSF, Macrophage Colony Stimulating Factor; MIP-2, Macrophage Inflammatory Protein - 2; MIG, Monokine induced by gamma interferon; RANTES, Regulated on Activation, Normal T cell Expressed and Secreted protein; VEGF, Vascular Endothelial Growth Factor; TNF-a, Tumor Necrosis Factor Alpha. Error bars represent S.E.M. * $P < 0.05$, ** $P < 0.01$, *** $P < 0.001$, **** $P < 0.0001$.

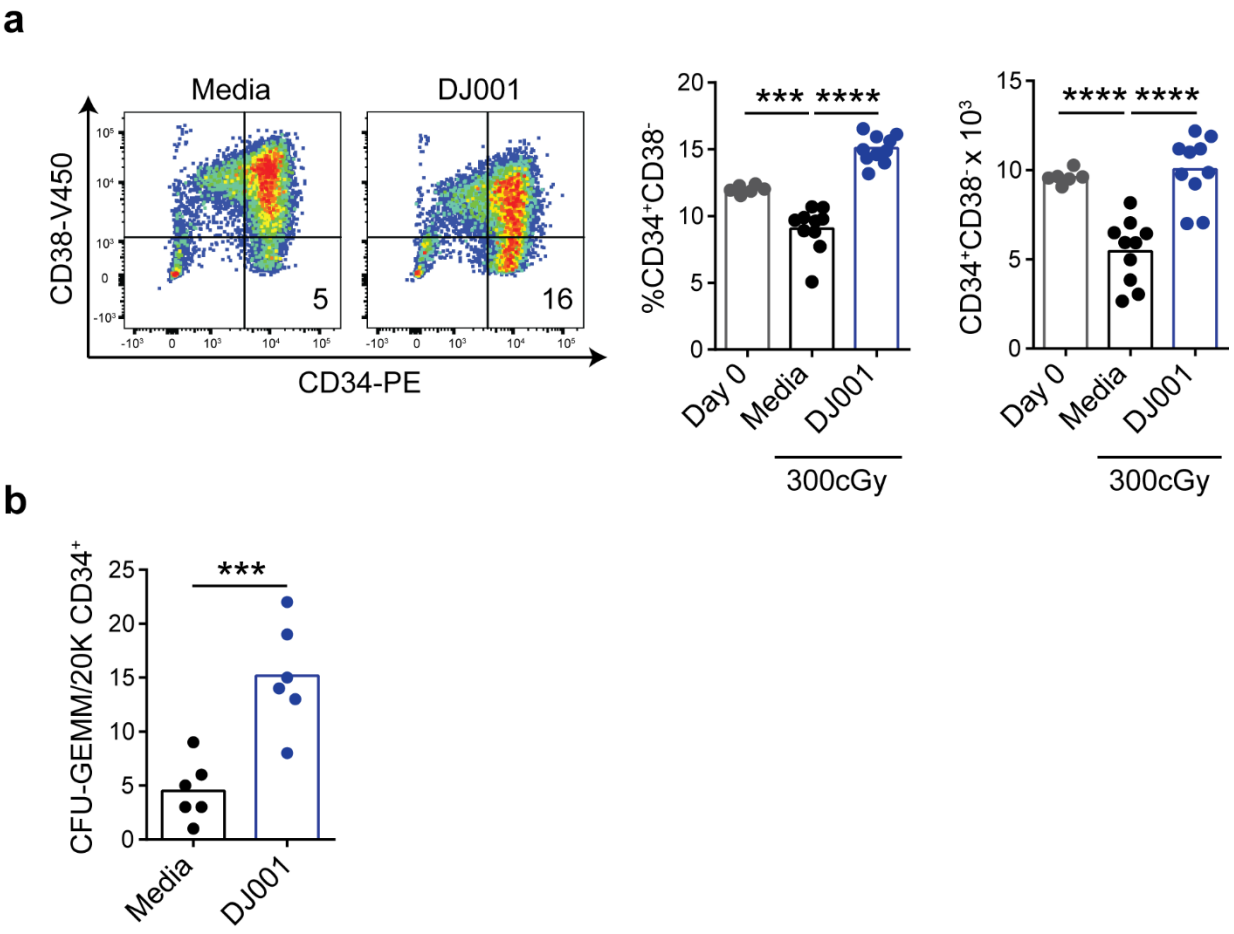

Figure 18 DJ001 promotes human hematopoietic cell recovery following irradiation.

a At left, representative flow cytometric analysis of $CD34^{+}CD38^{-}$ cells at 36 h after 300 cGy irradiation of BM $CD34^{+}$ cells and culture with media + 1 µg/mL DJ001. At right, mean percentages of numbers of CD34+CD38- cells in each group (Day 0, $n = 6$; media, DJ001, $n = 10$). One-way ANOVA with Tukey's multiple comparison test. **b** Numbers of CFU-GEMMs within cultures of $CD34^{+}$ cells at 72 h after 300 cGy and culture with media ± DJ001 ($n = 6$). *** $P < 0.001$, **** $P < 0.0001$.

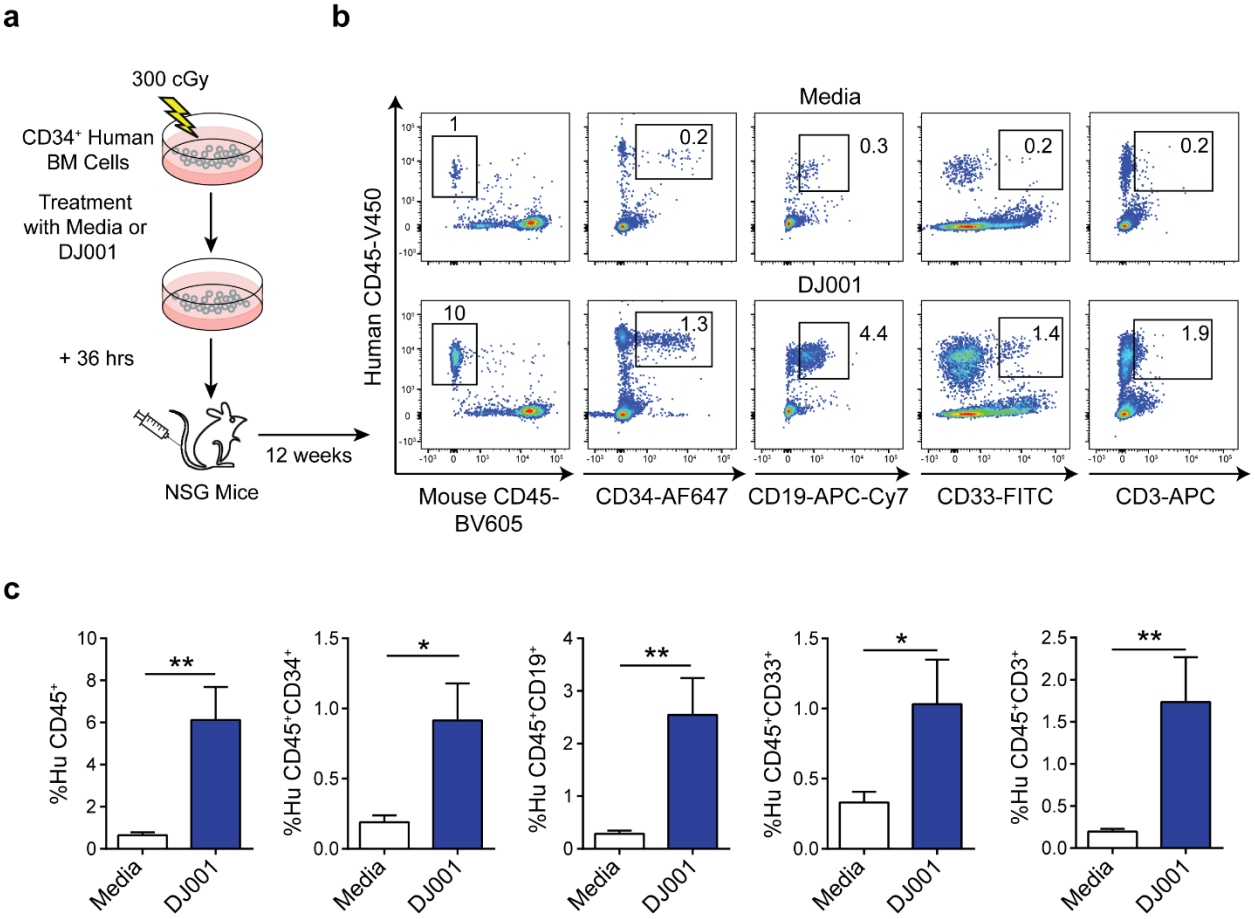

Figure 19 DJ001-mediated PTPσ inhibition promotes long-term HSC repopulation capacity.

a Schematic representation of NSG mice transplantation assay using the progeny of human BM $CD34^+$ cells irradiated with 300 cGy and treated with or without DJ001 for 36 h. **b** Representative flow cytometric analysis of human $CD45^+$ cells, human $CD34^+$ cells, human $CD19^+$ B cells, human $CD33^+$ myeloid cells, human $CD3^+$ T cells engraftment in the BM of NSG mice at 12 weeks post transplantation. **c** Percent engraftment of human hematopoietic cell subsets in the BM of NSG mice at 12 weeks post transplantation (n = 11-12/group). Error bars represent S.E.M. *P <0.05, **P < 0.01.

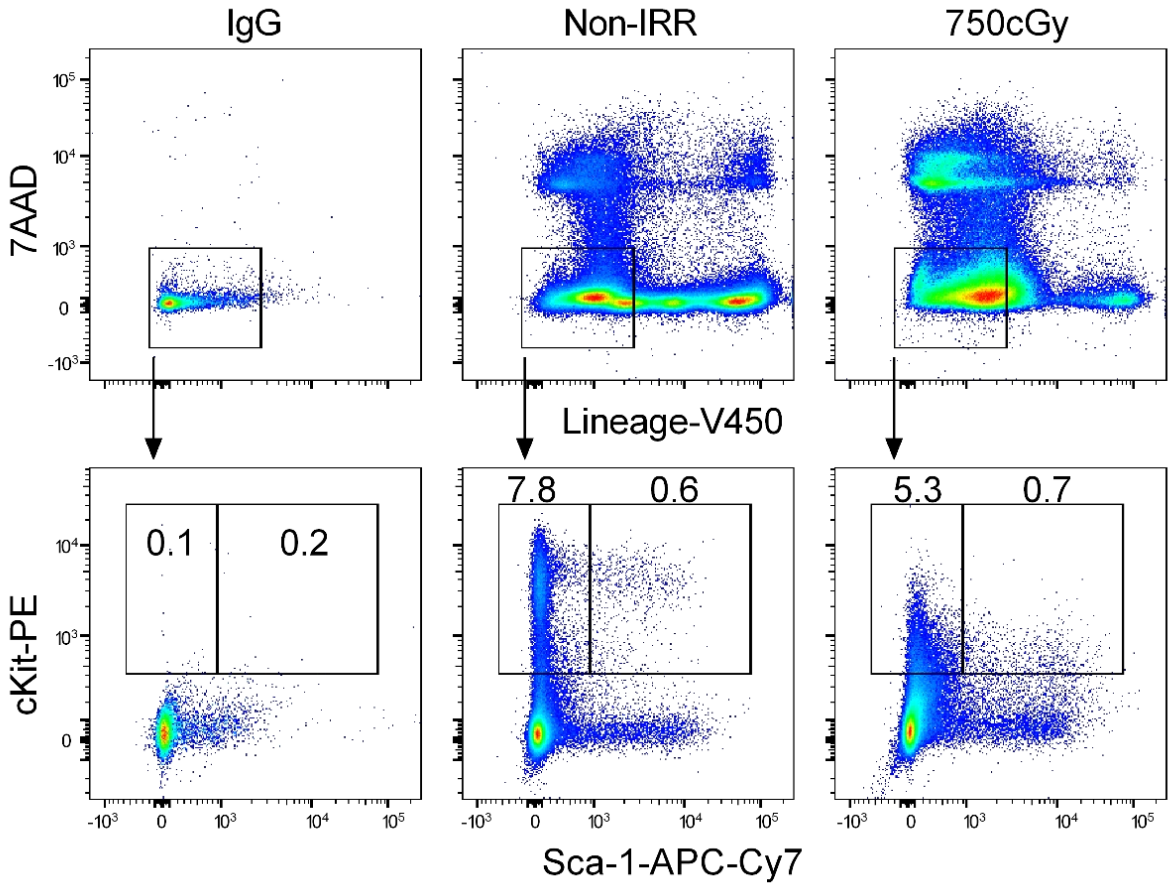

Figure 20 Gating strategy for hematopoietic stem and stem/progenitor cell populations. Representative gating strategy for BM ckit^{+}sca1^{-}lin^{-} cells and KSL cells in IgG stained mouse BM cells, non-irradiated (Non-IRR) mouse BM cells, and day +10 post 750 cGy irradiated mouse BM cells (750cGy).

CHAPTER 3: Mechanism of action of DJ001 mediated PTPσ inhibition

3.1 Introduction

Mechanistically, PTPσ deletion has been shown to increase RAC1-GTP activation in the neuronal system via dephosphorylating the p250GAP substrate protein[80,103]. In HSCs, enhanced RAC1-GTP activation in BM cells further led to increased transendothelial migration capacity at homeostasis. Treatment with a RAC inhibitor, EHT1864, abrogated the enhanced transendothelial migration effect of *Ptprs*$^{-/-}$ BM cells, suggesting the improved migration effect was in part RAC1 dependent. However at homeostasis, constitutive deletion of PTPσ does not cause alterations in BM homing, HSC cell cycling or HSC apoptosis compared to the wildtype[80]. Although we have delineated how PTPσ-RAC1 pathway regulates HSCs at homeostasis, the mechanisms of action of PTPσ in hematopoietic cells following myelosuppressive radiation are not well understood.

Exposure to irradiation leads to cell and tissue injuries due to direct ionization of the water, which makes up approximately 75% of cell and tissue mass[25]. Ionization of water generates free radicals and reactive oxygen species (ROS) that can damage multiple macromolecules in the cell or tissue, including DNA, lipids and proteins. Among them, DNA is the most critical regulator in cellular activities and irradiation induced double stranded breaks (DSB) can ultimately contribute to cell injury or cell death[52]. Mechanistically, DSB can be recognized by ataxia telangiectasia mutated (ATM). Increased activation of ATM leads to Chk2-mediated phosphorylation of p53[145], which further causes upregulation of p21 and Puma, two critical regulators in cellular apoptosis, senescence, and cell cycle arrest[47].

In HSCs, several mechanisms have been proposed to explain irradiation or chemotherapy induced BM injury, including HSC apoptosis, HSC senescence, BM microenvironment damage, and HSC

differentiation[25,43,53]. Multiple studies suggested that HSC apoptosis is primarily responsible for radiation induced ARS in the hematopoietic system. Domen et al. showed that overexpression of BCL-2 in the hematopoietic system increased the resistance of transgenic mice when exposed to lethal irradiation[146]. Multiple studies showed from a different angle in which p53 deficient mice were less sensitive to ionizing irradiation compared to the controls, and treatment with p53 inhibitor revealed radio-protective effect following radiation injury through inhibiting p53-dependent apoptotic pathway[147–149]. Secondly, HSC can undergo senescence following radiation exposure through similar signaling pathways (ATM-Chk2-p53-p21) activated by DNA double stranded breaks. Further, senescence in HSCs leads to decreased self-renewal and replication capacity, thus contributing to long-term HSC exhaustion[150]. Apart from HSC apoptosis and senescence, irradiation has been shown to promote HSC differentiation and abrogate HSC self-renewal. A recent study by Wang et al. demonstrated that radiation-induced DNA damage in HSCs can promote lymphoid differentiation through G-CSF/STAT3 pathway, thus leading to myeloid skewing in irradiated mice[53]. The same mechanism was also observed in melanocyte stem cells (MSCs) post irradiation, in which MSCs differentiate into hair follicle bulge thus resulting in hair greying and MSC depletion[151]. Lastly, radiation injury also contributes to apoptosis and senescence in different types of niche cells, including stromal cells, sinusoidal endothelial cells, and osteoblasts, which not only contributes to HSC injury but also delays hematopoietic recovery[152–154].

Results from Quarmyne et al. showed that RAC1 is an important molecular regulator downstream of PTPσ signaling in hematopoiesis[80]. RAC1 is one of the most extensively studied proteins of the Rho family of small GTPases and it functions as a molecular switch regulated by GTP/GDP

exchange[108]. Previous studies have shown that RAC1 regulates a number of cellular pathways including cell motility, cell cycling, cell survival, and cytoskeletal organization and adhesion[108,109,155]. p250GAP, a RAC1 GTPase- activating protein (GAP), has been shown as a neuronal substrate for PTPσ. Studies from other systems demonstrate that PTPσ can also interact with other proteins as its substrates, such as β-cadherin in the colon and ezrin in the intestine[101,102]. Therefore, the interactions between RAC1 and different substrates as well as its numerous effector proteins such as PAK1 and ERK1/2 contribute to the complexity of its functions[103,156]. Activation of ERK1/2 and AKT has been demonstrated in retinal ganglion cell axon regrowth in adult PTPσ$^{-/-}$ mice following spinal cord injury[86,157]. In breast cancer cell lines, the expression of RAC1 increases after ionizing radiation and further activates ERK1/2 phosphorylation, which contributes to increased radio-resistance[156]. Our results from Chapter 2 revealed that systemic administration of DJ001 was able to promote hematologic and hematopoietic regeneration in mice following radiation-induced BM suppression through inhibiting PTPσ activity. Therefore, we next sought to elucidate which pathway was DJ001 involved in promoting HSC regeneration following radiation injury.

3.2 Methods and Materials

3.2.1 Animal models

All animal procedures were performed in accordance with animal use protocols approved by the UCLA animal care and use committee. *Ptprs*$^{-/-}$ mice were provided by Dr. Michel Tremblay (McGill University). *C57BL/6* mice, *B6.SJL* mice and *NOD.Cg-Prkdc*^{scid}*Il2rg*^{tm1Wjl}*/SzJ (NSG)* mice between 8 to 12 weeks old were obtained from the Jackson Laboratory.

3.2.2 Proximity ligation assay

A proximity ligation assay (PLA) was performed by using the Duolink *In Situ* Red Starter Kit (Millipore Sigma) to detect the binding between PTPσ and p250GAP proteins. BM KSL cells from C57BL/6 mice were sorted by FACS and then plated onto fibronectin pre-coated chamber slides overnight. The next day, cells were treated with 1ug/mL DJ001 or vehicle (equal volume of DMSO) for 1 hour at 37°C. Cells were then fixed with 4% paraformaldehyde (PFA) for 20 minutes. The slides were blocked with Duolink blocking solution and incubated with rabbit anti-ARHGAP32 polyclonal antibody (Bioss Antibodies; bs-9296R; 1:50) and goat anti-PTPσ (K-19) polyclonal antibody (Santa Cruz Biotechnology; sc-10873; 1:50) overnight at 4°C. The PLA assay was performed as previously described5. Cells were imaged using a Leica SP8 Confocal Microscope equipped with a 63x objective lens. A white light laser set to 580 nm was used to excite dsRed and a UV laser was used to excite DAPI. Analysis was performed using the spots detection function in IMARIS 9.0.2 (Bitplane).

3.2.3 p250GAP phosphor-tyrosine sandwich ELISA

Clear, pre-blocked Protein A coated Microtiter wells (Fisher Scientific; 15132) were incubated with ARHGAP32 polyclonal antibody (Bioss Antibodies; bs-9296R; 1:500) in antibody dilution buffer (150 mM NaCl, 25 mM HEPES pH7.2, 0.5% BSA, 0.05% Tween 20) for 3 hours at room temperature (RT). Subsequently, the plate was washed three times and phosphorylated p250GAP from BM lin^- cell lysate was added to each well. BM lin^- cells were harvested in NP40 buffer (ThermoFisher Scientific; FNN0021) supplemented with 1x complete, Mini, EDTA-free Protease Inhibitor Cocktail (Sigma Aldrich; 4693159001) and 1x PhosSTOP (Sigma Aldrich; 4906845001). Following incubation for 2 hours at 4°C, the plate was completely emptied (without washing) and exposed to 50 µL of a fixation solution (0.5% formaldehyde in 300 mM NaCl, 20 mM sodium phosphate buffer, pH 7) for 10 minutes. The plate-bound, phosphorylated p250GAP was measured by a specific anti-phosphotyrosine peroxidase-coupled antibody (Sigma Aldrich; A5964-1VL; 1:500). Incubation was for 1 hour at RT. Peroxidase activity was measured by a Tecan Infinity plate reader using BM Chemiluminescence ELISA Substrate (POD) (Sigma Aldrich; 11582950001).

3.2.4 G-LISA activation assays

The RAC1-GTP, RHOA-GTP and CDC42-GTP activation levels in BM lin^- cells were measured using a colorimetric based RAC1-, RHOA- and CDC42 G-LISA Activation Assay Kit (Cytoskeleton Inc.). BM cells from femurs and tibias were isolated from 12 week old *Ptprs*$^{+/+}$ and *Ptprs*$^{-/-}$ mice. Cells were then depleted of lineage-committed cells with Direct Lineage Cell Depletion Kit (Miltenyi Biotec; 130-110-470; 1:5). The BM lin^- cell fraction was then serum starved in Iscove's modified Dulbecco's medium (IMDM) and treated with either vehicle (equal amount of DMSO) or 1 µg/mL DJ001 for 10 minutes at 37° C. After treatment, cells were washed

with ice-cold PBS and then placed in lysis buffer supplemented with protease inhibitor. Lysate concentrations were measured by Pierce™ BCA Protein Assay Kit (ThermoFisher Scientific). G-LISA was performed according to manufacturer's instructions. Briefly, 12.5 μg of lysates was added to a GTP-binding protein pre-coated plate and active RAC1-GTP, RHOA-GTP or CDC42-GTP levels were measured at 490nm using a PowerWave XS2 microplate reader (BioTek).

3.2.5 Lentivirus-mediated shRNA silencing

Rac1 CDS-targeting- and *Bcl2l1* CDS-targeting shRNA in lentiviral plasmid (TRCN0000310888 and TRCN0000004685) and control shRNA (SHC216V) were purchased from Sigma Aldrich. For viral production, 293T cells were transfected with lentiviral gag/pol and VSV-G (courtesy of Donald Kohn, UCLA) and the lentiviral plasmids, at a ratio of 2.2 : 1.2 : 3.3 (in [μg], gag/pol:VSVG:Plasmid) using Lipofectamine 3000 and P300 Enhancer. Viral particles were harvested after 24 hours and 48 hours. One milliliter of viral supernatant was used to infect 0.75 x 10^6 BM lin^- cells. Infected cells were harvested the next day and irradiated with 300 cGy followed by treatment with or without 1 μg/mL DJ001, prior to CFC assay.

3.2.6 Immunofluorescence microscopy

Lab-Tek chamber slides were coated with fibronectin at 25 ug/mL (Millipore Sigma; 341635). 1 x 10^4 sorted BM KSL cells were resuspended in 200 μL TSF media and added to each of the pre-coated wells and incubated overnight (37°C/5% CO_2). The next day, cells were serum starved for 30 minutes and then stimulated with DJ001 (1 μg/mL), EHT1864 (6 μg/mL) or equal volumes of DMSO for 5 minutes. Cells were washed once with PBS and fixed with 4% PFA for 10 minutes. Cells were permeabilized with 0.5% triton/PBS (PRM) for 30 minutes and then blocked with 5%

FBS/PRM for 1 hour. The slide was then incubated with a phospho-ERK1/2 primary antibody (Cell Signaling; 4377; 1:200) for 1 hour. The wells were washed three times and then incubated with a donkey anti-rabbit Alexa Fluor 488 secondary antibody (Thermo Fisher; A21206; 1:200) for 1 hour. The slide was washed three times and mounted with ProLong Gold Antifade Reagent with DAPI. Cells were imaged using a 63X objective on a Zeiss Axio Imager M2 widefield fluorescence microscope with all microscope settings derived from imaging a secondary only control. Data was analyzed using Fiji (ImageJ). Briefly, the cell outline was identified by threshold levels and the mean fluorescence intensity within the cell area was quantified.

3.2.7 Flow cytometric analysis

Intracellular flow cytometric analysis was performed on irradiated (300 cGy) or non-irradiated, sorted KSL cells after treatment with 1 μg/mL DJ001 or control (equal volumes of DMSO) for 24 hours. At 24 hours after irradiation, cells were fixed with 4% PFA for 10 min, followed by permeabilization using 0.25% saponin in PBS. Cells were washed again and stained with antibody at the recommended concentrations for 30 minutes at room temperature. Intracellular antibodies and phospho-flow antibodies used were: FITC-conjugated anti-BCL-X_L (Abcam; 26148; 1:100), active RAC1-GTP antibody (NewEast Biosciences; 26903; 1:100), anti-PAK1 (phospho S144) + PAK2 (phospho S141) + PAK3 (phospho S154) antibody (Abcam; ab40795; 1:100), and FITC-conjugated goat anti-rabbit IgG H&L (Abcam; ab97050; 1:200).

3.2.8 Gene expression analysis

For all studies, RNA was isolated using the Qiagen RNeasy micro kit (Qiagen). RNA was reverse transcribed using the High-Capacity cDNA Reverse Transcription Kit (ThermoFisher Scientific) and was then used for qPCR with SYBR Select Master Mix (Life Technologies). Values were

normalized to housekeeping gene *Gapdh/GAPDH and given as* ΔΔCt values normalized to media treated, non-irradiated BM KSL cells ($2^{-\Delta\Delta C(T)}$) method)[158].

Table 1 Primers used for mouse gene detection.

Target mRNA	**Sequence 5' – 3'**
Gapdh Fw	TGGATTTGGACGCATTGGTC
Gapdh Rv	TTGCACTGGTACGTGTTGAT
Bcl2l1 Fw	GACAAGGAGATGCAGGTATTGG
Bcl2l1 Rv	TCCCGTAGAGATCCACAAAAG
Bax Fw	TGAAGACAGGGGCCTTTTTG
Bax Rv	AATTCGCCGGAGACACTCG
Bcl2 Fw	TGAGTACCTGAACCGGCATCT
Bcl2 Rv	GCATCCCAGCCTCCGTTAT
Bim Fw	CGGATCGGAGACGAGTTCA
Bim Rv	TTCCAGCCTCGCGGTAATCA
Puma Fw	AGCAGCACTTAGAGTCGCC
Puma Rv	CCTGGGTAAGGGGAGGAGT
Mcl-1 Fw	AAAGGCGGCTGCATAAGTC
Mcl-1 Rv	TGGCGGTATAGGTCGTCCTC
Cdk2 Fw	CCTGCTTATCAATGCAGAGGG
Cdk2 Rv	TGCGGGTCACCATTTCAGC
Cdk4 Fw	ATGGCTGCCACTCGATATGAA
Cdk4 Rv	TCCTCCATTAGGAACTCTCACAC
Cdk6 Fw	GGCGTACCCACAGAAACCATA
Cdk6 Rv	AGGTAAGGGCCATCTGAAAACT
Cdkn1a Fw	CCTGGTGATGTCCGACCTG
Cdkn1a Rv	CCATGAGCGCATCGCAATC
Cdkn1b Fw	TCAAACGTGAGAGTGTCTAACG
Cdkn1b Rv	CCGGGCCGAAGAGATTTCTG
Cyclin E Fw	GCCAGCCTTGGGACAATAATG
Cyclin E Rv	CTTGCACGTTGAGTTTGGGT
Rac1 Fw	GAGACGGAGCTGTTGGTAAAA
Rac1 Rv	ATAGGCCCAGATTCACTGGTT
Cyclin D1 Fw	GCGTACCCTGACACCAATCTC
Cyclin D1 Rv	CTCCTCTTCGCACTTCTGCTC
Cyclin D2 Fw	GAGTGGGAACTGGTAGTGTTG
Cyclin D2 Rv	CGCACAGAGCGATGAAGGT

Table 2 Primers used for human gene detection.

Target mRNA	Sequence 5' – 3'
hGAPDH Fw	CCTGCACCACCAACTGCTTA
hGAPDH Rv	GGCCATCCACAGTCTTCTGAG
hBCL2L1 Fw	GACTGAATCGGAGATGGAGACC
hBCL2L1 Rv	GCAGTTCAAACTCGTCGCCT
hMCL-1 Fw	TGCTTCGGAAACTGGACATCA
hMCL-1 Rv	TAGCCACAAAGGCACCAAAAG

3.2.9 *In vivo* BrdU incorporation analysis

For BrdU incorporation analysis in BM KSL cells *in vivo*, adult C57Bl/6 mice were irradiated with 750 cGy TBI and treated with 5 mg/kg DJ001 or vehicle daily from day +1 to day +10. On day +10, mice were injected intraperitoneally with 2 mg BrdU (BD Biosciences). Sixteen hours later, BM cells were collected and stained with anti-BrdU FITC (BD Biosciences; 557891; 1:50), APC-Cy7-conjugated anti-Sca1 (BD Biosciences; 560654; 1:100), PE-conjugated anti-c-kit (BD Biosciences; 553355; 1:100), and V450 lineage cocktail (BD Biosciences; 561301; 1:10). We repeated this BrdU incorporation analysis on donor $CD45.2^+$ cells at day +7 and day +21 following competitive transplantation into recipient $CD45.1^+$ mice.

3.2.10 Apoptosis assay and cell cycle analysis

Eight to ten week old female C57BL/6 mice were irradiated with 500cGy TBI followed by subcutaneous injections of 5 mg/kg DJ001, or vehicle, or 5 mg/kg DJ001 plus 40 mg/kg EHT1864. Twenty four hours after irradiation, mice were euthanized to harvest BM cells for Annexin V apoptosis analysis. BM cells were stained with APC-Cy7-conjugated anti-Sca1 (BD Biosciences; 560654; 1:100), PE-conjugated anti-c-kit (BD Biosciences; 553355; 1:100), and V450 lineage cocktail (BD Biosciences; 561301; 1:10) antibodies for 30 minutes at 4°C. Cells were resuspended in 1X Annexin V binding buffer and then stained with FITC-conjugated anti-Annexin V antibody

(BD Biosciences; 556547; 1:50) and 7AAD antibody (BD Biosciences; 559925; 1:40). For *in vitro* human BM cell apoptosis assays, isolated human BM $CD34^+$ cells were plated into 96 well plates and then irradiated with 300 cGy. Immediately after irradiation, cells were treated with 5 μg/mL DJ001 or vehicle for 24 hours and then collected for Annexin V cell apoptosis analysis. For cell cycle analysis, sorted KSL cells were irradiated at 300 cGy and then treated with 1 μg/mL DJ001 or vehicle for 36 hours. Subsequently, cells were resuspended in 200 μL of PBS, fixed by adding 1 mL of ice-cold fixation solution (0.25% Saponin, 2.5% paraformaldehyde, 2% FCS in PBS) and incubated for 30 minutes on ice and in the dark. Cells were washed in ice-cold Saponin wash buffer (0.25% Saponin, 2% FCS in PBS) and resuspended in 200 μL of Saponin wash buffer containing 20 μL of FITC-conjugated anti-Ki67 antibody (BD Biosciences; 556026; 1:10) and 1 μL of RNase (Qiagen; 19101; 100 mg/mL). After 30 minutes of incubation, cells were washed in Saponin wash buffer and resuspended for flow analysis in 200 μL of Saponin wash buffer containing 5 μL of 7AAD (BD Biosciences; 559925; 1:40).

3.2.11 Survival studies

For survival studies, 10 week old female C57BL/6 mice were irradiated with 750 cGy TBI, which is lethal for approximately 50% of C57BL/6 mice by day +30 (LD50/30), using a Shepherd Cesium-137 irradiator. Twenty four hours post-irradiation, mice were administered daily subcutaneous injections of 5 mg/kg DJ001 or DJ009 or vehicle in a volume of 100 μL for 10 days. DJ001 or DJ009 injections were prepared in PBS, 0.5% Tween 80, and 10% DMSO. Corresponding vehicle injections contained PBS, 10% DMSO and 0.5% Tween 80. PB complete blood counts were measured using a Hemavet 950 instrument (Drew Scientific) at day +10 post-irradiation. For hematopoietic analysis, BM cells were collected at day +10 post-irradiation. To

study whether DJ001 increased survival rates through activation of RAC signaling, the RAC inhibitor, EHT1864 (Selleckchem), was dissolved in PBS and administered intraperitoneally, 40 mg/kg every other day, to 750 cGy irradiated mice until day +10.

3.2.12 Transendothelial migration assay

Transendothelial migration assay was performed as previously reported[141]. VeraVec™ mouse spleen endothelial cells (Angiocrine Biosciences) were cultured to confluence in 8μM pore transwells (Corning Incorporated). Transwells were then seeded with 50,000 sorted BM KSL cells in IMDM with 10% FBS, 1% pen-strep, 20 ng/mL TPO, 125 ng/mL SCF, and 50 ng/mL Flt3 ligand with or without 1 μg/mL of DJ001. SDF-1, 500 ng/mL (R&D Systems), was added to the bottom chamber of the transwell. At 18 hours post incubation, cells in the bottom chamber were collected and cell counts were performed.

3.2.13 Homing study

100,000 sorted BM sca-$1^{+}$$lin^{-}$ cells from $DsRed^{+}$ mice were transplanted into lethally irradiated (950 cGy) recipient C57BL/6 mice followed by subcutaneous treatment of 5 mg/kg DJ001 or vehicle x 1 dose. At 18 hours post transplantation, BM cells were harvested from the recipient mice and were analyzed for percentages of $DsRed^{+}$ cells in the BM, following a previously described method[80].

3.2.14 Statistical analyses

GraphPad Prism 6.0 was used for all statistical analyses. All data were checked for normal distribution and similar variance between groups. Data were derived from multiple independent

experiments from distinct mice or cell culture plates. Sample sizes for *in vitro* studies were chosen based on observed effect sizes and standard errors from prior studies. For all animal studies, a power test was used to determine the sample size needed to observe a two-fold difference in means between groups with 0.8 power. A two-tailed Student's t test was utilized for all comparison excepts where otherwise noted in the Figure Legends. All animal studies were performed using sex- and age-matched animals, with wild-type littermates as controls. Animal studies were performed without blinding of the investigator. Values are reported as means ± SEM, unless stated otherwise. Results were considered significant when $P < 0.05$.

3.3 Results

3.3.1 Inhibition of PTPσ promotes HSC survival via induction of RAC1

PTPσ has been shown to dephosphorylate substrate p250GAP as a means to activate p250GAP functions. Activated p250GAP in a yeast-two-hybrid system leads to decreased activation of RAC1 by converting RAC1-GTP to RAC1-GDP form[103]. Here, we tested whether DJ001-mediated PTPσ inhibition could alter the phosphorylation level of p250GAP and RAC1 in primary hematopoietic or hematopoietic progenitor cells. To measure the activation level of p250GAP, we developed an enzyme-linked immunosorbent assay (ELISA) using immunoglobulin A capture of p250GAP (Figure 21a). Treatment with 1 μg/mL DJ001 significantly increased phosphorylation level of p250GAP in BM lin^- cells. Furthermore, DJ001 treatment significantly decreased co-localization of PTPσ and p250GAP in BM KSL cells detected by proximity ligation assay (Figure 21b). DJ001 treatment also caused a rapid increase in RAC1-GTP levels in *Ptprs*$^{+/+}$ BM KSL cells; however, no alteration was observed in *Ptprs*$^{-/-}$ BM KSL cells with or without DJ001 treatment (Figure 22a). This result suggested that DJ001-mediated activation of RAC1 occurred specifically through PTPσ. Importantly, DJ001 treatment did not contribute to activation of other RhoGTPases such as CDC42 and RHOA in BM lin^- cells, suggesting that CDC42 and RHOA were not participated in DJ001-mediated regenerative effects in hematopoietic progenitor cells (Figure 22b). Therefore, PTPσ repressed RAC1 activation in HSPCs via regulation of p250GAP and DJ001 promoted RAC1 activation via inhibition of PTPσ and p250GAP functions. DJ009 also did not induce RAC1 activation in BM cells from *Ptprs*$^{-/-}$ mice, further suggesting similar specificity of DJ009 for PTPσ inhibition (Figure 22c). Treatment of BM KSL cells with DJ001 further led to increased phosphorylation level of p21-activated kinase 1 (PAK1), a substrate of RAC1. Co-

treatment of DJ001 with the RAC inhibitor, EHT1864, in BM KSL cells abrogated DJ001-mediated phosphorylation of PAK1 (Figure 22d).

Ionizing radiation has been known to cause hematopoietic cell death via DNA damage, upregulation of apoptotic genes, and disruption of the HSC niche[25]. DJ001 treatment significantly decreased the percentage of apoptotic BM KSL cells in C57BL/6 mice at 24 hours following 500 cGy TBI compared with vehicle-treated controls (Figure 23a). Administration of the RAC inhibitor, EHT1864, abrogated DJ001-mediated anti-apoptotic effects on BM KSL cells in irradiated mice (Figure 23a). Similarly, treatment with EHT1864 inhibited DJ001-mediated CFC generation from isolated BM KSL cells irradiated with 300 cGy *in vitro* (Figure 23b). Systemic administration of EHT1864 also completely abrogated DJ001-mediated survival benefits in sub-lethally irradiated C57BL/6 mice (Figure 23c). Therefore, DJ001-mediated anti-apoptotic effect on BM HSPCs was RAC1 signaling pathway dependent.

RhoGTPases such as RAC1 can affect multiple signaling pathways that regulate cell survival, so we next measured the effect of DJ001 treatment on gene expressions of pro- and anti-apoptotic regulators in irradiated KSL cells[156,159]. DJ001 treatment had no effect on the expression of pro-apoptotic regulators, *Bim, Bax, p53 upregulated modulator of apoptosis (Puma)*, or the anti-apoptotic genes, *Bcl2,* in BM KSL cells (Figure 24a). On the contrary, DJ001 treatment did increase the expressions of *Mcl-1* and *Bcl2 like 1 (Bcl2l1)*, which encodes the anti-apoptotic protein, BCL-X_L (Figure 24a). At protein levels, BCL-X_L expressions were significantly increased post 300 cGy irradiation in sorted BM KSL cells (Figure 24b). Treatment with DJ001 in 300 cGy irradiated KSL cells significantly enhanced the protein levels of BCL-X_L compared to non-treated

group (Figure 24b). Concomitant treatment with EHT1864 blocked the DJ001-mediated increase in BCL-X_L protein expressions in irradiated BM KSL cells (Figure 24b). These results indicate that DJ001 treatment upregulates anti-apoptotic gene expressions through RAC1 signaling pathway. To confirm that DJ001-mediated effects on irradiated HSPCs were dependent on RAC1 and BCL-X_L, we transduced isolated lin^- cells with lentiviral short hairpin RNAs (shRNAs) targeting *Rac1* and *Bcl2l1* separately and measured hematopoietic progenitor cell recovery following 300 cGy irradiation. Silencing of either *Rac1* or *Bcl2l1* blocked DJ001-mediated recovery effect of hematopoietic progenitor cells that were harvested 3 days after irradiation (Figure 25). In summary, DJ001-mediated HSPC recovery after irradiation was dependent on RAC1 activation induced BCL-X_L expression.

In human hematopoietic system, DJ001 treatment decreased radiation-induced apoptosis of $CD34^+CD38^-$ cells following irradiation (Figure 26a). RAC inhibition blocked DJ001-meiated survival of irradiated human $CD34^+CD38^-$ cells, suggesting that DJ001-mediated anti-apoptotic effects on human HSCs were RAC pathway dependent (Figure 26a). As we observed in our murine studies, DJ001 treatment also increased the expressions of the pro-survival genes *BCL2L1* and *MCL-1* in irradiated human $CD34^+$ cells (Figure 26b).

Additionally, RAC1 has been demonstrated to activate ERK1/2 signaling pathway through PAK1- and PAK2- mediated phosphorylation of MEK1 in order to facilitate the formation of Raf/MEK/ERK complex[160]. Here, we treated freshly isolated KSL cells with or without DJ001, or DJ001 + EHT1864 for 10 minutes and stained with phospho-ERK antibody for fluorescent microscopy. DJ001 treatment did induce ERK1/2 phosphorylation level in BM KSL cells (Figure

27a). Treatment of DJ001 together with EHT1864 in KSL cells suppressed the enhanced phosphorylation level of ERK compared with DJ001 treatment alone (Figure 27a). Additionally, treatment with ERK1/2 inhibitor, BVD523, blocked DJ001-mediated increase of BCL-X_L protein levels in 300 cGy irradiated BM KSL cells and abrogated hematopoietic progenitor cell recovery capacity following irradiation damage (Figure 27b and 27c). In conclusion, these data suggested that DJ001-mediated upregulation of BCL-X_L in HSPCs was ERK1/2 dependent and ERK1/2 is downstream of the RAC1 activation pathway.

3.3.2 Effect of DJ001-mediated PTPσ inhibition in HSPC proliferation

Hematologic recovery following myelosuppressive requires not only the survival of HSCs, but also the proliferation of live HSCs as well as progenitor cells to improve the regeneration of mature blood and immune cells. At homeostasis, DJ001 treatment did not affect cell cycling profile of non-irradiated KSL cells for 36 h in culture (Figure 28a). However, BM KSL cells that were irradiated at 300 cGy and then treated with 1 μg/mL DJ001 demonstrated significant increase in G_2/S/M phase compared with irradiated control cells (Figure 28b). Evaluation of the expression of cell cycle regulatory genes revealed that DJ001 treatment significantly increased the expressions of *cyclin-dependent kinase 2* (*Cdk2)* and *Cyclin E* in irradiated BM KSL cells (Figure 29a). However, expression levels of other cell cycle regulatory genes such as *Cdk4, Cdk6, Cdkn1a, Cdkn1b, Cyclin D1, and Cyclin D2* were not altered with DJ001 treatment post irradiation for 36 hours (Figure 29a). Transduction of BM lin^- cells with sh*Rac1* blocked DJ001-mediated transcription of *Cdk2* and *Cyclin E*, suggesting that upregulations of *Cdk2* and *Cyclin E* were RAC1 dependent (Figure 29b). Furthermore, treatment of irradiated BM KSL cells with CDK2 inhibitor SU9516, or RAC inhibitor EHT1864 together with DJ001 suppressed DJ001-mediated

cell cycle transition from G_1 to G_2/S/M phase (Figure 30a and 30b). *In vitro* study of cell cycling transition in irradiated BM KSL cells demonstrated DJ001-mediated HSC cell cycle progression was RAC1 pathway dependent which further upregulates *Cdk2.*

To determine whether systemic administration of DJ001 *in vivo* could alter BM hematopoietic proliferation following irradiation, we measured Bromodeoxyuridine (BrdU) incorporation at day +12 post 750 cGy irradiation in mice treated with or without DJ001. BM KSL cells from DJ001-treated mice displayed increased $BrdU^+$ percentage compared with vehicle-treated irradiated controls (Figure 31a). To determine whether DJ001 treatment could cause a long-term effect in HSC cell cycling, we measured BrdU incorporation in donor $CD45.2^+$ cells in recipient $CD45.1^+$ mice at day +7 and +21 following competitive BM transplantation. Donor $CD45.2^+$ cells were harvested from sub-lethally irradiated mice that were treated subcutaneously with vehicle or DJ001 (5 mg/kg) for 10 days. 5 x 10^5 donor $CD45.2^+$ cells were then transplanted competitively with 1 x 10^5 $CD45.1^+$ cells into lethally irradiated B6.SJL mice. However, at both time points, no differences in BrdU incorporation were shown in recipient mice that were transplanted donor $CD45.2^+$ cells from vehicle or DJ001 treated groups (Figure 31b).

Deletion of RAC1 has been shown to decrease homing, engraftment, and niche localization of HSPCs. Therefore, it is possible that systemic administration of mice with DJ001 can produce an effect on HSC migration that facilitates them homing to the supportive BM niche. We performed a homing assay by transplanting 100,000 $Sca\text{-}1^+lin^-DsRed^+$ cells into lethally irradiated recipient C57BL/6 mice followed by subcutaneous treatment of DJ001 or vehicle for one dose. 18 hours post transplantation, DJ001 treatment did not alter the homing of transplanted cells compared with

vehicle-treated controls (Figure 32b). Additionally, *in vitro* migration assay demonstrated no difference in BM KSL migration through EC monolayers after DJ001 treatment for 18 hours compared with the control group (Figure 32a). Therefore, DJ001-mediated inhibition of PTPσ did not facilitate BM HSC migration or homing.

3.4 Discussions

At the mechanistic level, we are able to demonstrate that PTPσ inhibition suppressed radiation-induced apoptosis in murine and human HSCs. Downregulation of leukocyte common antigen-related (LAR) protein has similarly been shown to have pro-survival effects on neurons in the setting of serum deprivation[161]. Our results suggest that PTPσ inhibition promotes HSC survival following irradiation via RAC pathway activation and induction of BCL-X_L in HSCs. Treatment with PTPσ inhibitor, DJ001, uncoupled PTPσ binding to p250GAP, causing RAC1 activation in primary BM HSCs, without affecting other RhoGTPases, CDC42 and RhoA. Deletion of *Rac1* in murine hematopoietic cells caused decreased HSPC engraftment, homing, and niche localization[61,107], whereas expression of a dominant-negative *Rac2* increased HSPC apoptosis[61,109]. RAC1 has also been shown to inhibit apoptosis of irradiated breast cancer cell lines, epithelial cells, and T cells via induction of BCL-X_L, MCL-1, and other BCL-2-like proteins[156,162,163]. Here, PTPσ inhibition increased the expression and protein levels of BCL-X_L in HSCs and suppressed HSC apoptosis following irradiation, dependent upon RAC pathway and RAC-mediated ERK1/2 activation. These results suggest that RAC pathway activation and induction of BCL-X_L regulate HSC survival in response to PTPσ inhibition.

In addition to DJ001-mediated effects on HSC survival, our results suggest that DJ001 promoted early HSPC proliferation compared with irradiated, control HSCs. Further, DJ001-mediated SHC cell cycle progression was dependent on RAC pathway activation and induction of CDK2. These findings are consistent with the observations by Gu et al.[109], who showed that *Rac1*$^{-/-}$ HSPCs displayed decreased entry into G_2/S/M phase in response to SCF. As PTPσ regulates phosphorylation of several kinases and the RAC pathway regulates multiple effector pathways,

PTPσ inhibition may have altered the expression of other effectors that regulate HSC proliferation beyond CDK2. However, we did not observe any durable effect of DJ001 treatment on the proliferation potential of HSCs or their progeny based on BrdU incorporation analysis of engrafted donor $CD45.2^+$ cells over time following transplantation into recipient $CD45.1^+$ mice. It is therefore perhaps more likely that the anti-apoptotic effects of systemic DJ001 treatment on HSCs in irradiated mice contributed to the increase in recovery of phenotypic HSPCs as well as HSCs with *in vivo* repopulating capacity. It is also possible that DJ001 treatment favorably affected HSC transcriptional programs that regulate myeloid and lymphoid cell differentiation and HSC repopulating potential.

The paucity of therapeutics capable of accelerating HSC regeneration and hematopoietic reconstitution in myelosuppressed patients highlights an unmet medical need. Our study demonstrates a novel class of selective, allosteric PTPσ inhibitors that can promote the regeneration of murine and human HSCs capable of long-term hematopoietic reconstitution. Our results provide the mechanistic foundation for the development of selective PTPσ inhibitors to promote hematopoietic regeneration in patients receiving myelosuppressive chemotherapy, radiotherapy, and those undergoing myeloablative hematopoietic cell transplantation.

3.5 Figures

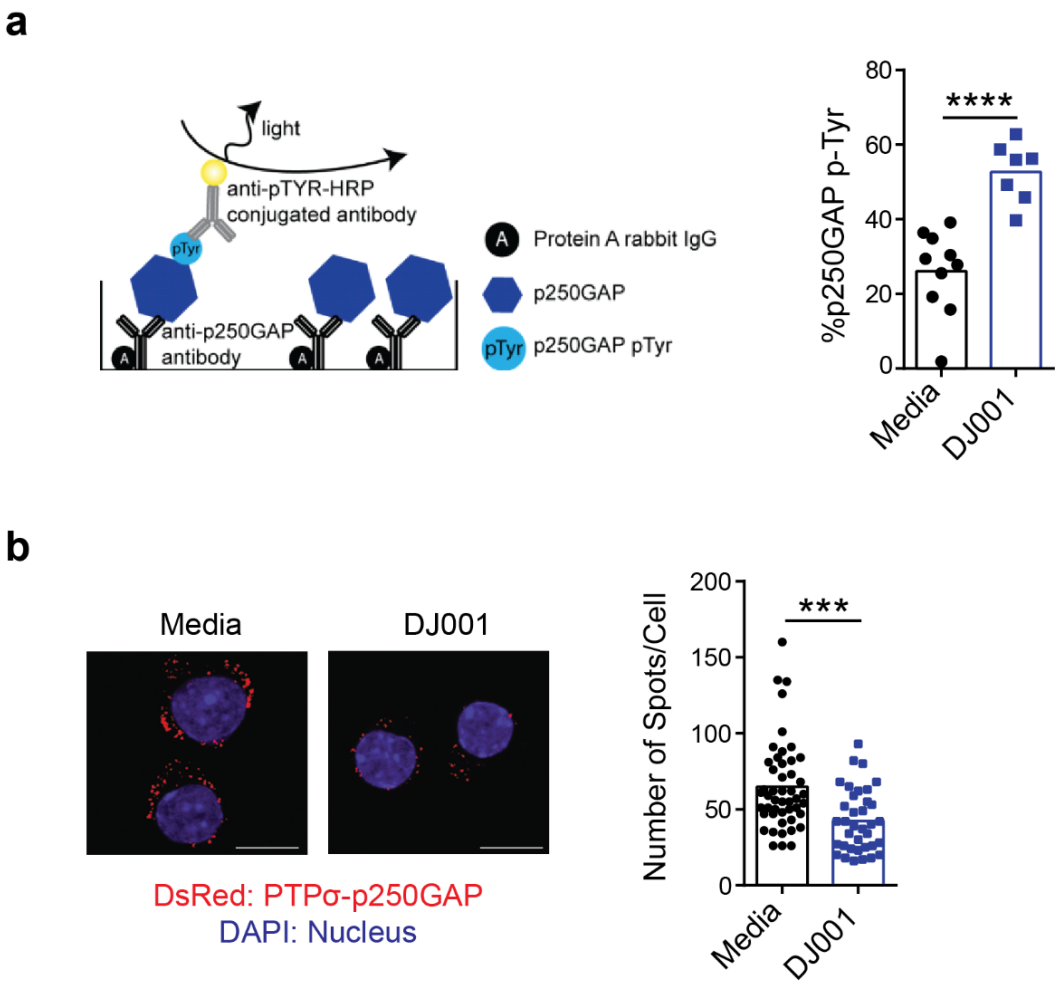

Figure 21 DJ001 treatment affects co-localization of PTPσ and its substrate p250GAP.

a At left, schematic of p250GAP phospho-tyrosine (pTyr) sandwich ELISA assay. At right, %p250GAP phospho-tyrosine (pTyr) in BM lin$^-$ cells cultured in media ± DJ001 (media, n = 10; DJ001, n = 7). **b** At left, representative images of PLA in BM KSL cells treated in media ± DJ001. Red = DsRed+, PTPσ-p250GAP complex; blue = DAPI, nucleus. Original magnification x63, scale bars = 10 μm. At right, numbers of DsRed$^+$ KSL cells in each condition (n = 48, control; n = 36, DJ001). *** $P < 0.001$, **** $P < 0.0001$.

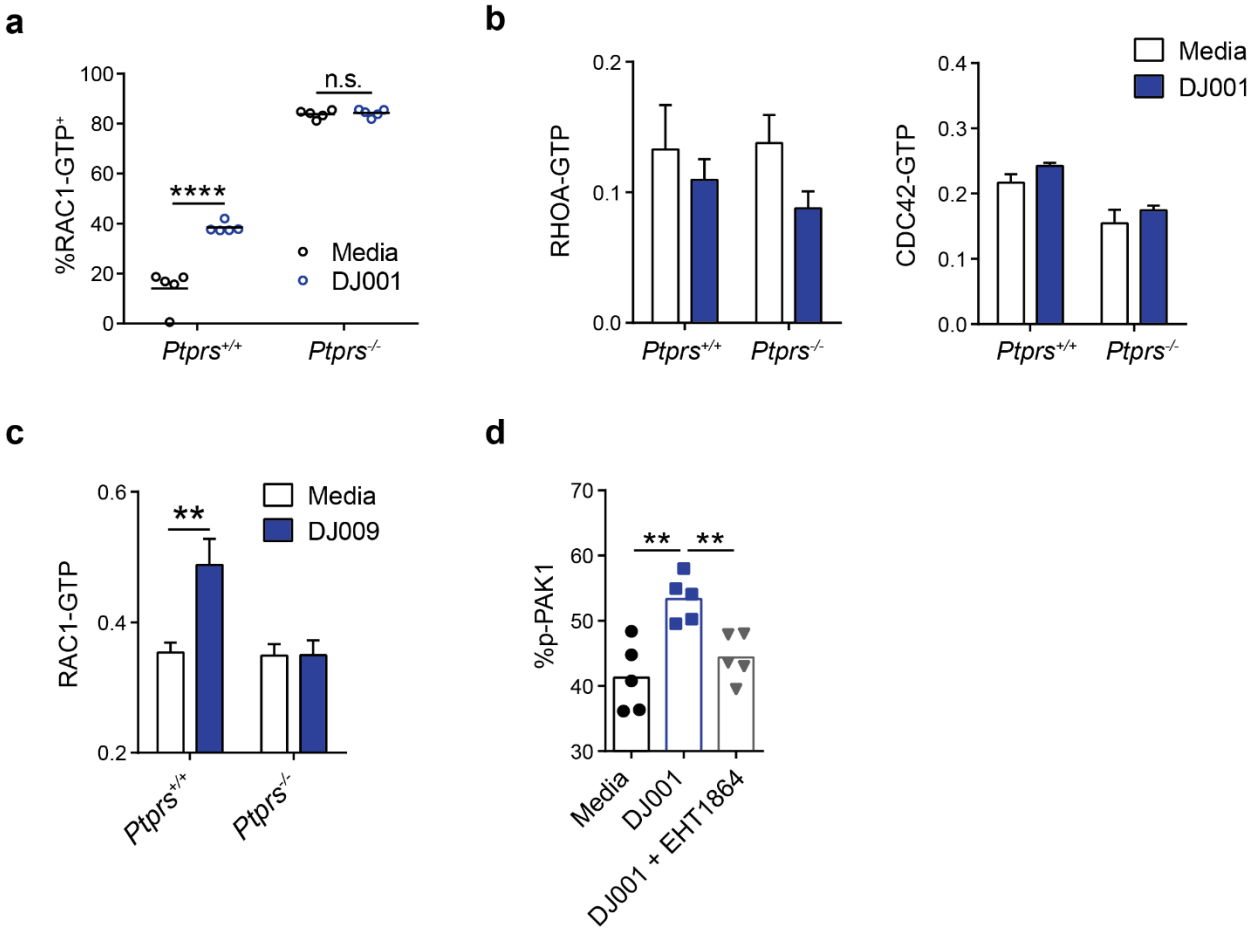

Figure 22 DJ001-mediated PTPσ inhibition activates RAC1-GTP signaling.

a %RAC1-GTP^{+} KSL cells from *Ptprs*$^{+/+}$ and *Ptprs*$^{-/-}$ mice treated with or without DJ001 in culturing media (n = 5). Two-way ANOVA with Sidak's multiple comparison test. **b** Mean RHOA-GTP and CDC42-GTP levels in BM lin^{-} cells from *Ptprs*$^{+/+}$ and *Ptprs*$^{-/-}$ mice that were pulse-treated in media ± 1 μg/ml DJ001 for 10 min (n = 3/group). **c** Mean RAC1-GTP levels in BM lin^{-} cells from *Ptprs*$^{+/+}$ mice and *Ptprs*$^{-/-}$ mice that were pulse-treated in media ± 1 μg/ml DJ009 for 10 min. Two-way ANOVA with Sidak's multiple comparison test (n = 3 - 4/group). d Percentages of p-PAK1^{+} KSL cells following treatment with media alone, 1 μg/mL DJ001, or DJ001 + 6 μg/mL EHT1864 (n = 5). One-way ANOVA with Tukey's multiple comparison test. Error bars represent S.E.M. ** $P < 0.01$, **** $P < 0.0001$.

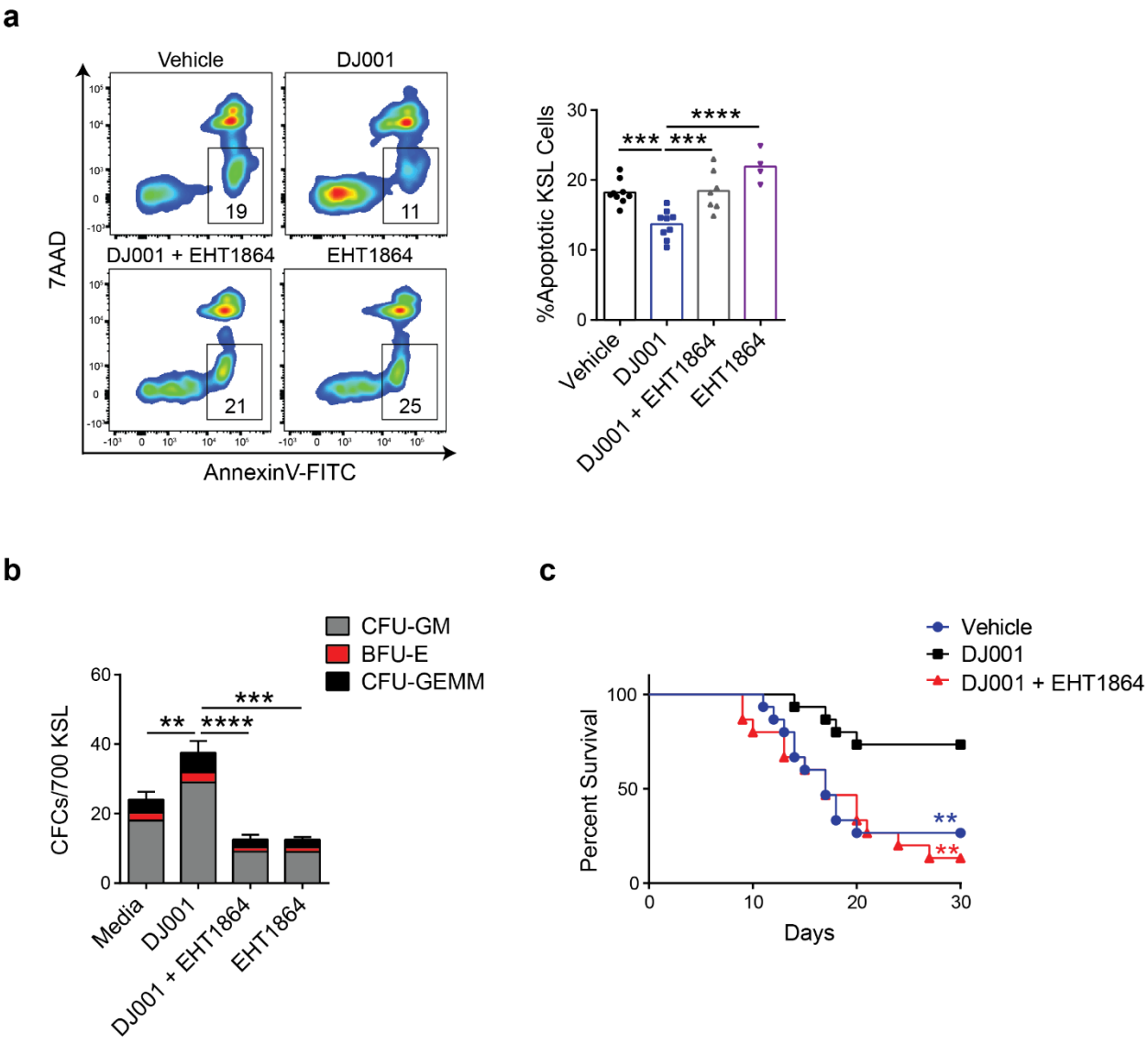

Figure 23 DJ001 promotes HSC regeneration via RAC1 dependent anti-apoptosis.

a At left, Annexin V/7AAD staining of BM KSL cells from mice at 24 h post 500 cGy and treatment with vehicle, 5 mg/kg DJ001, DJ001 + 40 mg/kg EHT1864, or EHT1864 alone. Numbers represent percentages in each gate. At right, %AnnexinV^{+}7AAD^{-} BM KSL cells (media and DJ001, $n = 9$; DJ001 + EHT1864, $n = 7$; EHT1864, $n = 4$). **b** Numbers of BM CFCs at day +3 from BM KSL cells irradiated with 300 cGy and cultured with media ± 1 µg/ml DJ001, DJ001 + 6 µg/ml EHT1864 and EHT1864 alone ($n = 6$-12/group). **c** Percent survival of mice following 750

cGy and 10-day treatment with DJ001 (11/15 alive), vehicle (4/15 alive), or DJ001 + EHT1864 (2/15 alive); log-rank test. Error bars represent S.E.M. ** $P < 0.01$, *** $P < 0.001$, **** $P < 0.0001$.

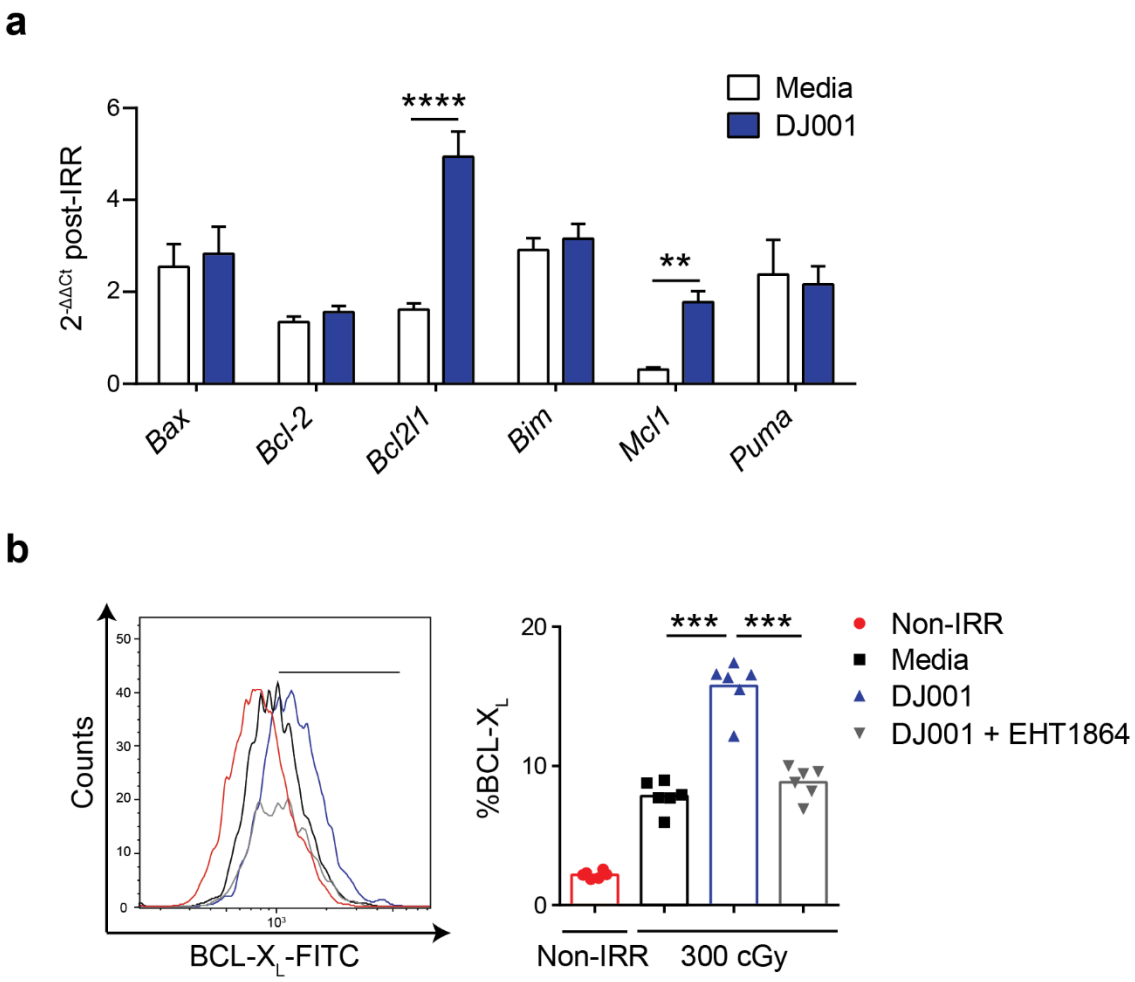

Figure 24 RAC1 activation leads to induction of downstream anti-apoptotic protein BCL-X_L.

a Fold changes ($2^{-\Delta\Delta Ct}$) of gene expression in BM KSL cells at 12 h post 300 cGy and treatment with or without DJ001 in culturing media (n = 3-6/group). Two-way ANOVA with Sidak's multiple comparison test. **b** At left, BCL-X_L protein levels in non-irradiated BM KSL cells (red), 300 cGy-irradiated KSL cells in media alone (black) or treated with DJ001 (blue) or DJ001 + EHT1864 (gray). At right, %BCL-X_L^+ KSL cells (n = 6). One-way ANOVA with Tukey's multiple comparison test. Error bars represent S.E.M. ** $P < 0.01$, *** $P < 0.001$, **** $P < 0.0001$.

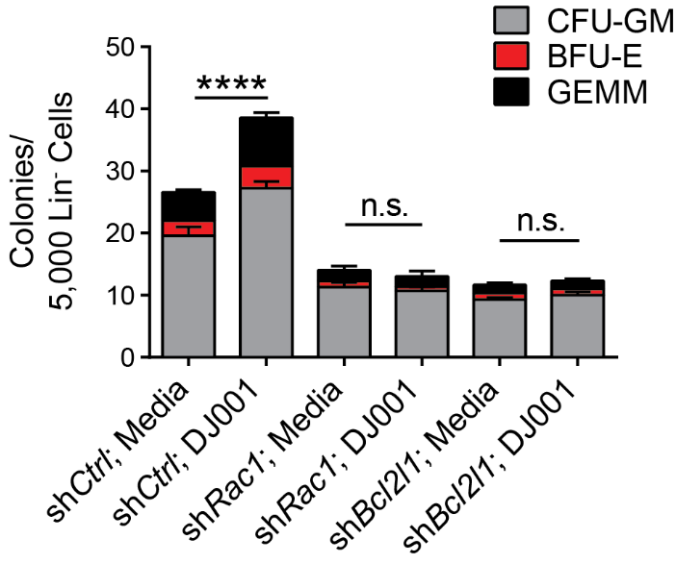

Figure 25 shRNA-mediated knockouts of *Rac1* and *Bcl2l1* abrogate DJ001-mediated hematopoietic regeneration effects.

CFCs from BM KSL cells at 48 h following 300 cGy and culture with or without DJ001, and with or without sh*RAC1* or sh*Bcl2l1* (n = 3-9/group). Two-way ANOVA with Sidak's multiple comparison test. Error bars represent S.E.M. **** $P < 0.0001$.

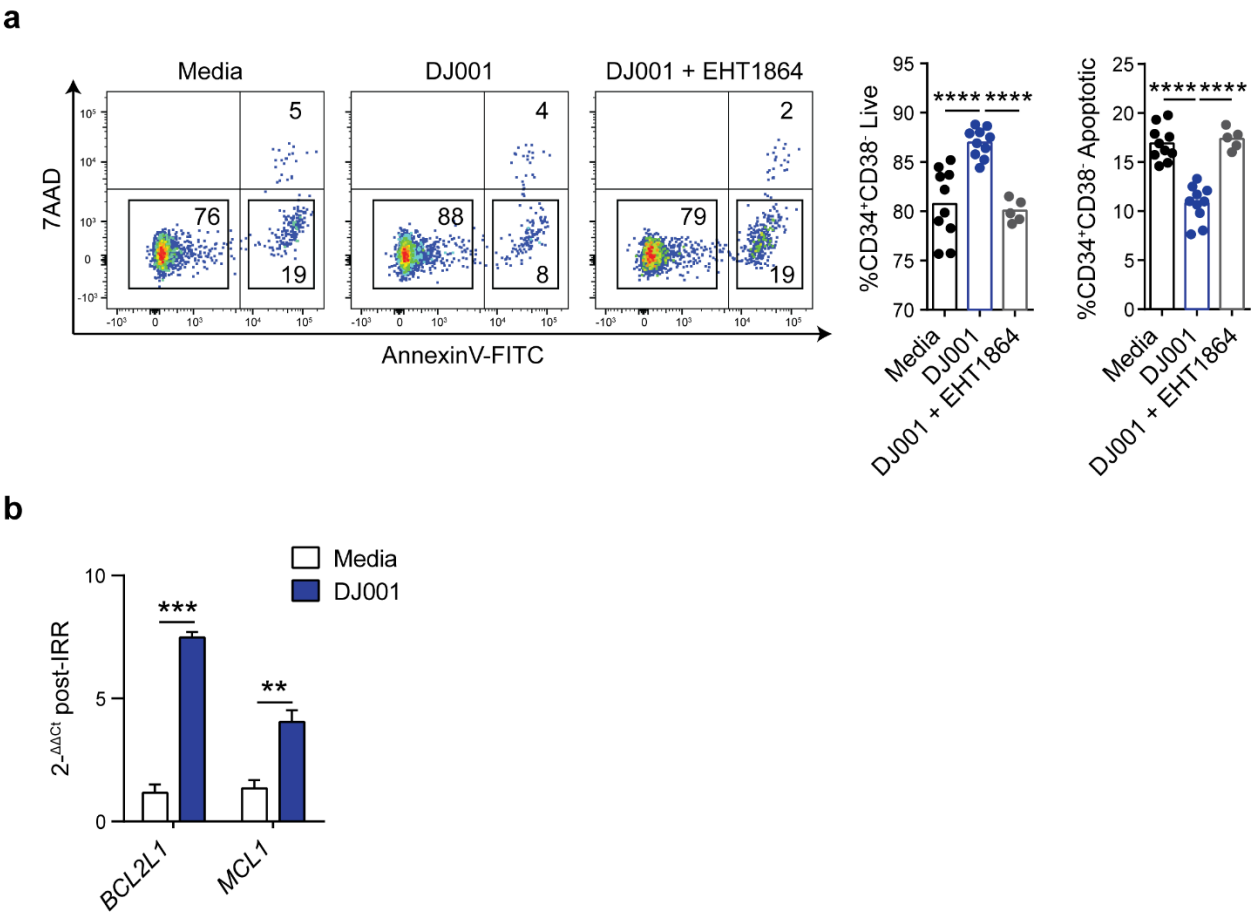

Figure 26 DJ001 accelerates human HSC regeneration through anti-apoptosis.

a At left, representative flow cytometric analysis of Annexin V/7AAD staining of $CD34^+$ cells at 24 h after 300 cGy and culture with media + DJ001 + EHT1864. At right, percentages of live and apoptotic $CD34^+CD38^-$ cells in each condition (media and DJ001, $n = 10$; DJ001 + EHT1864, $n = 5$). One-way ANOVA with Tukey's multiple comparison test. **b** Fold changes ($2^{-\Delta\Delta Ct}$) in *BCL2L1* and *MCL-1* gene expressions in $CD34^+CD38^-$ cells at 12 h after 300 cGy in media ± DJ001 ($n = 3$). Gene transcripts were normalized to *GAPDH* and media treatment. Error bars represent S.E.M. ** $P < 0.01$, *** $P < 0.001$, **** $P < 0.0001$.

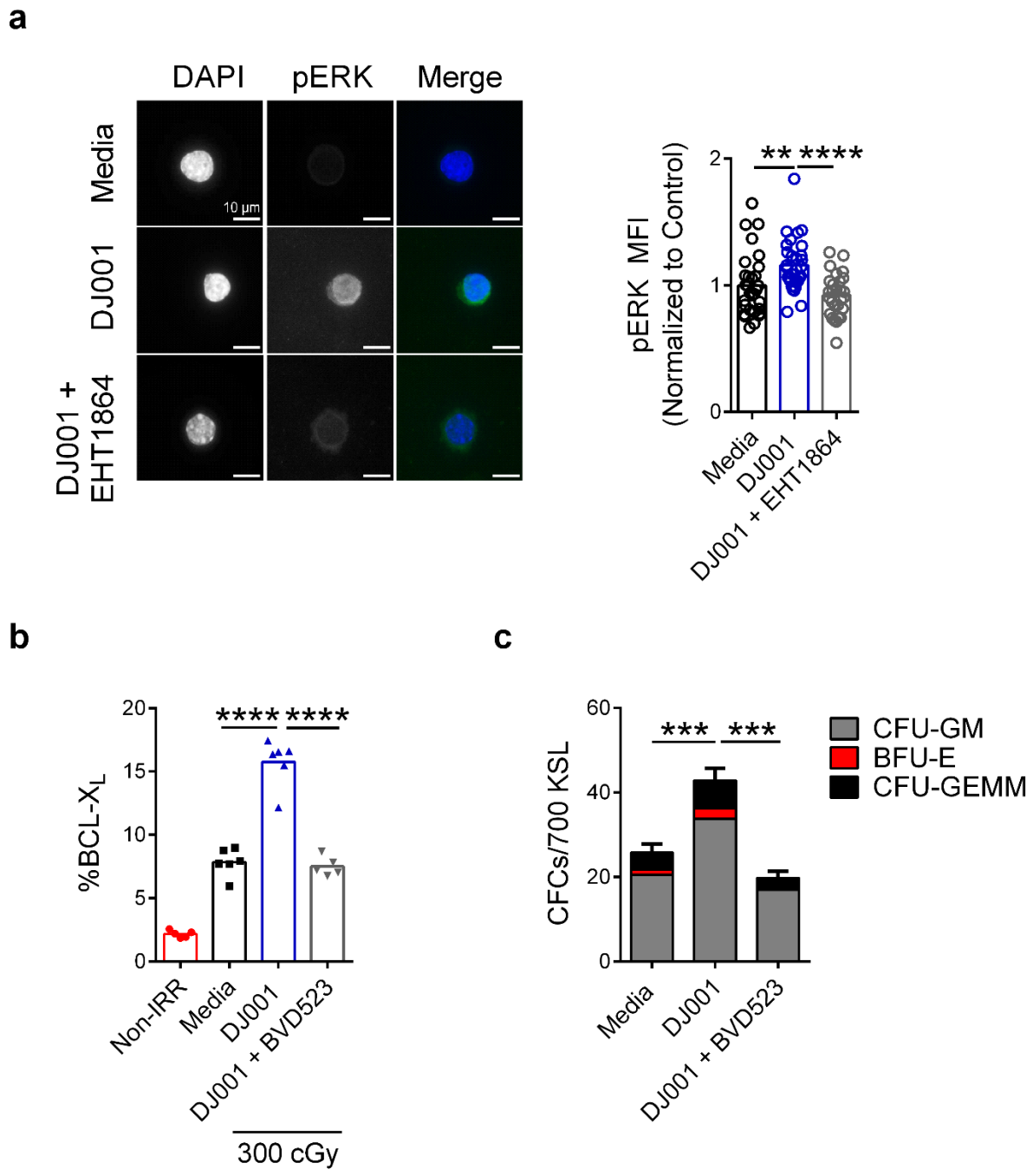

Figure 27 DJ001-mediated RAC1 activation increases downstream ERK phosphorylation.

a At left, microscopic images of BM KSL cells cultured in media ± DJ001, or DJ001 + 6 μg/ml EHT1864 for 10 minutes, and stained for pERK and DAPI (scale bar = 10 μm). At right, MFI of

pERK. One-way ANOVA with Tukey's multiple comparison test. **b** Percentages of BCL-X_L protein in non-irradiated (Non-IRR) BM KSL cells and at 24 hours following 300 cGy and culture with media ± DJ001, or media ± DJ001 + 43 ng/ml BVD523 (n = 5 - 6/group). One-way ANOVA with Tukey's multiple comparison test. **c** Numbers of BM CFCs at day +3 of culture of BM KSL cells following 300 cGy and treatment with media ± DJ001, or DJ001 + 43 ng/mL BVD523 (n = 5 - 12 assays/group). One-way ANOVA with Tukey's multiple comparison test. Error bars represent S.E.M. ** $P < 0.01$, *** $P < 0.001$, **** $P < 0.0001$.

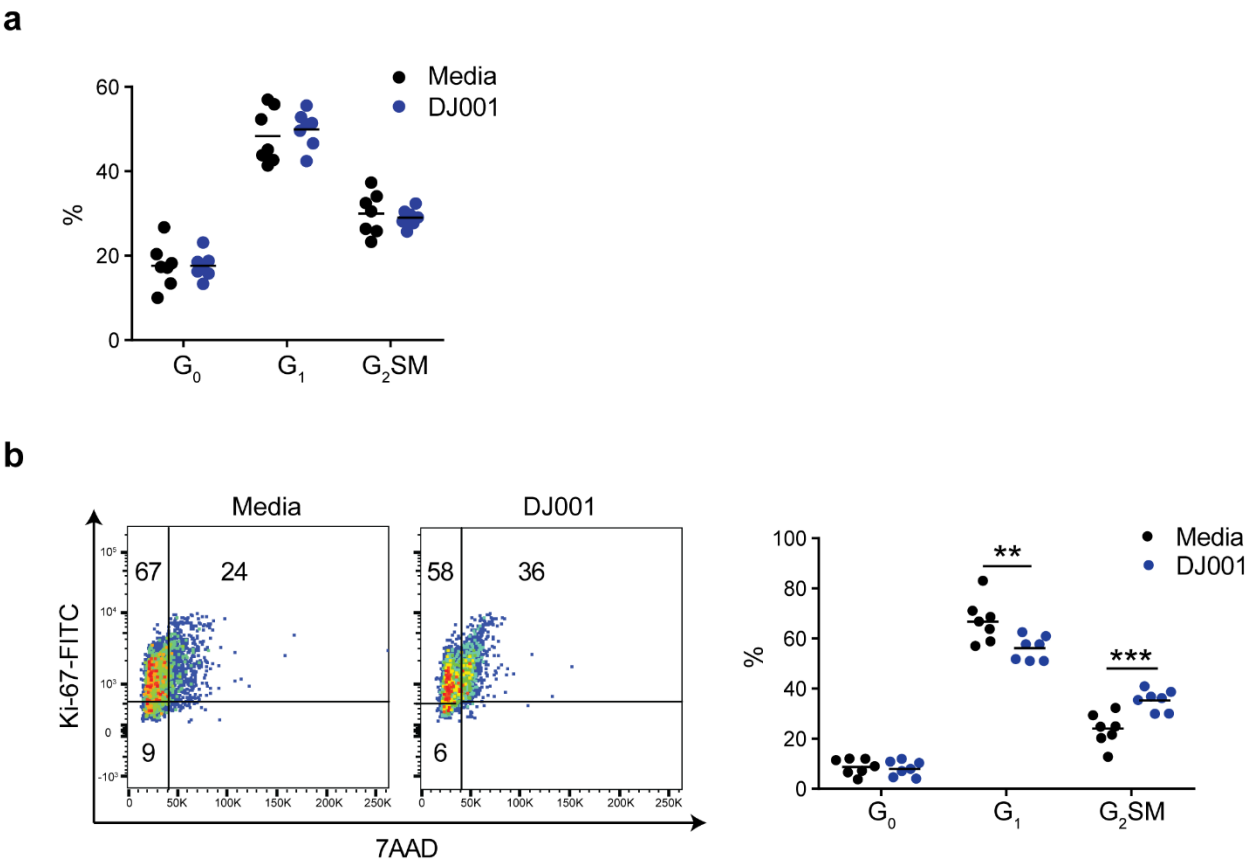

Figure 28 DJ001 promotes HSC proliferation following radiation injury.

a Percentages of BM KSL cells in G_0, G_1, and G_2/S/M phases after 36 hours of culture in media ± DJ001 ($n = 7$/group). **b** At left, representative cell cycle analysis of BM KSL cells at 36 h following 300 cGy and culture with media ± 1 μg/mL DJ001. At right, mean percentages of KSL cells in G_0 ($Ki67^{-}7AAD^{-}$), G_1 ($Ki67^{+}7AAD^{-}$) and G_2/S/M ($Ki67^{+}7AAD^{+}$) phases are shown. ** $P < 0.01$, *** $P < 0.001$.

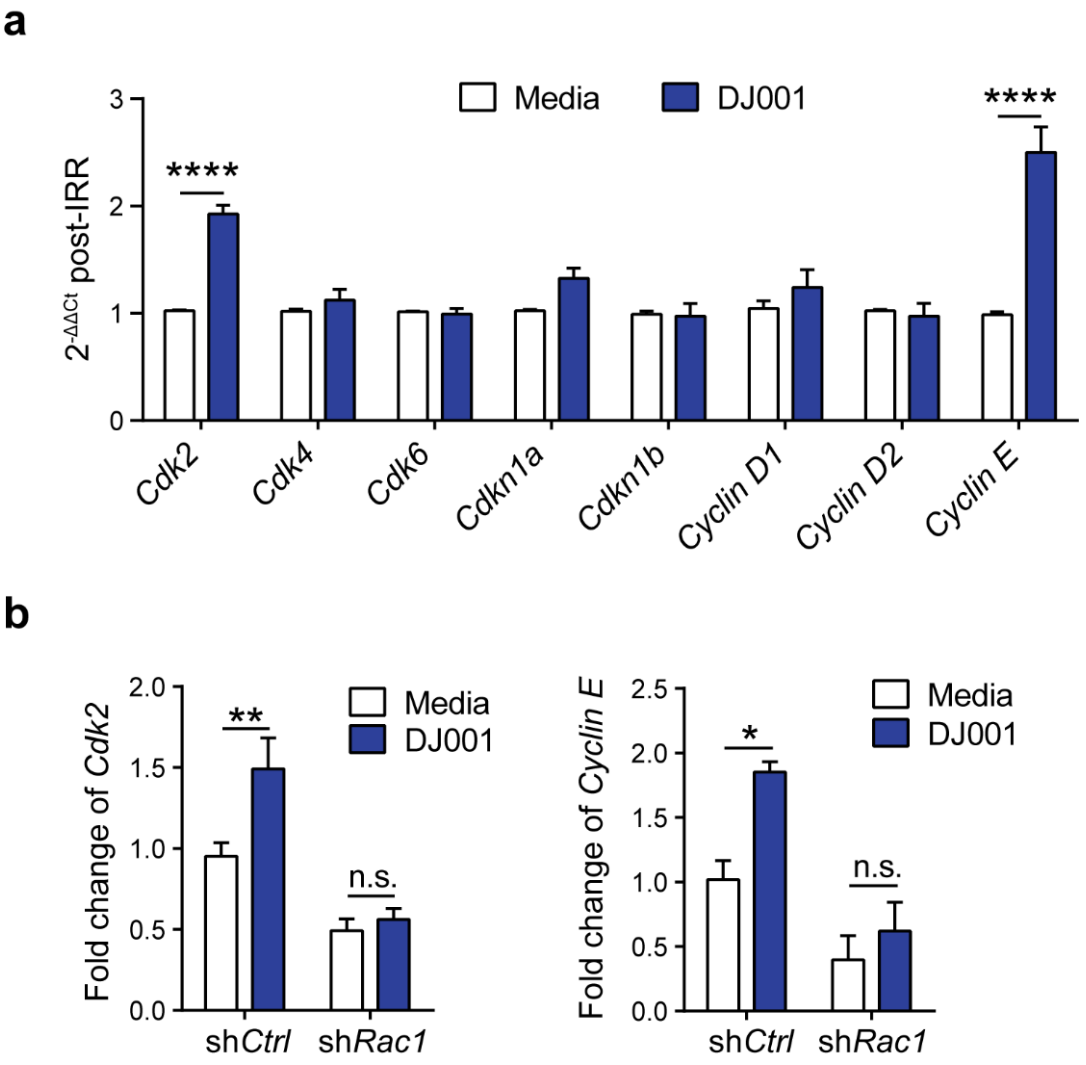

Figure 29 DJ001 promotes HSC cell cycling via upregulations of *Cdk2* and *Cyclin E*.

a Fold changes ($2^{-\Delta\Delta Ct}$) of cell cycle regulatory gene expression in BM KSL cells at 36 h following 300 cGy and treatment with or without DJ001 in culturing media ($n = 3$). Gene transcript changes are normalized to *Gapdh* in media treatment. Two-way ANOVA with Sidak's multiple comparison test. **b** Fold changes ($2^{-\Delta\Delta Ct}$) of Cdk2 and Cyclin E expressions in BM lin^- cells in response to DJ001 at 48 h post 300 cGy, with and without sh*Rac1* treatment (n = 3-5/group). Two-way ANOVA with Sidak's multiple comparison test. Error bars represent S.E.M. * $P < 0.05$, ** $P < 0.01$, **** $P < 0.0001$.

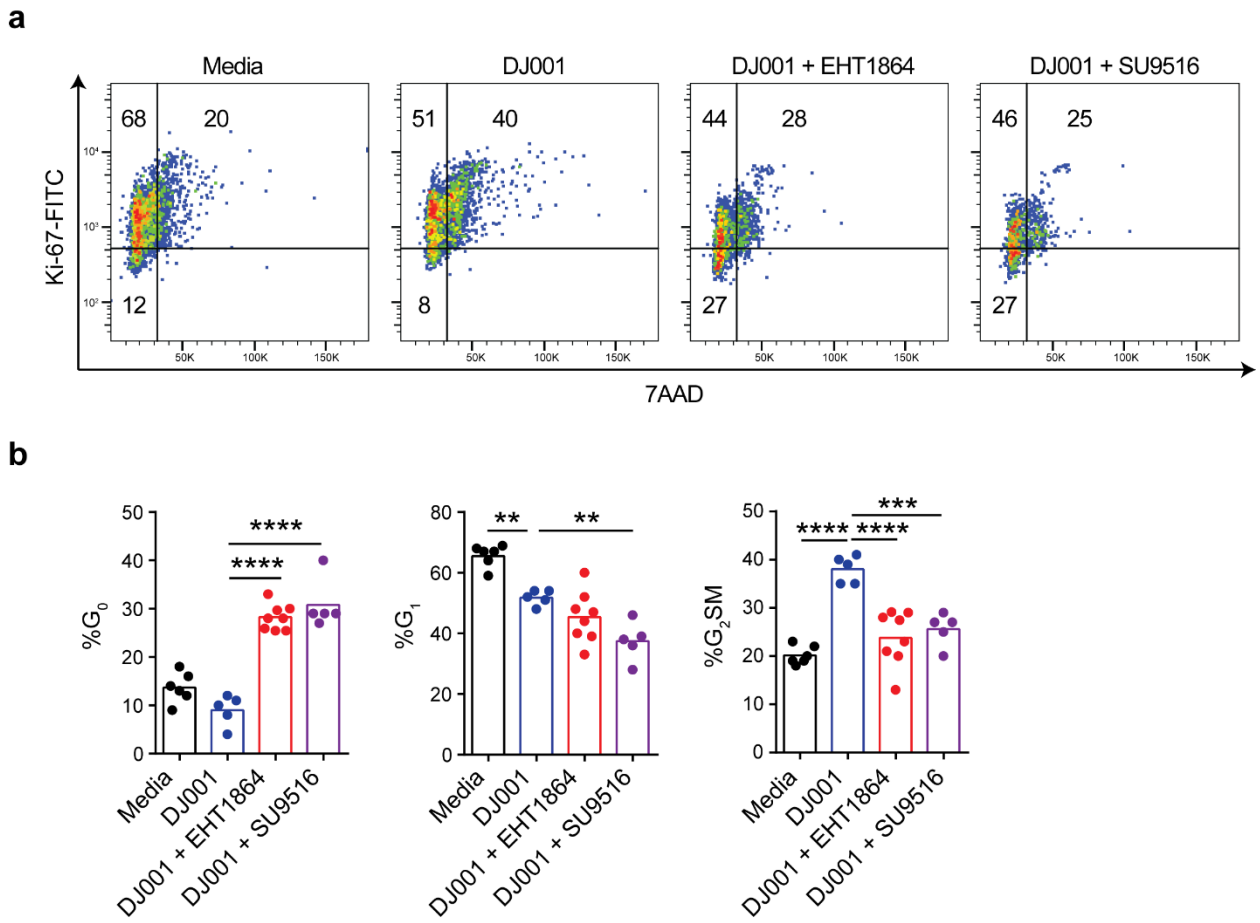

Figure 30 DJ001-mediated cell cycling effect is RAC1 and CDK2 dependent.

a Representative cell cycle analysis of KSL cells at 36 h following 300 cGy and culture with media ± 1 μg/mL DJ001, DJ001 + 6 μg/mL EHT1864, and DJ001 + 240 ng/mL CDK2 inhibitor SU9516.

b Percentages of BM KSL cells in G0, G1, G2/S/M phases for each condition (media, $n = 6$; DJ001 and DJ001 + SU9516 groups, $n = 5$; DJ001 + EHT1864, $n = 8$). One-way ANOVA with Tukey's multiple comparison test. ** $P < 0.01$, *** $P < 0.001$, **** $P < 0.0001$.

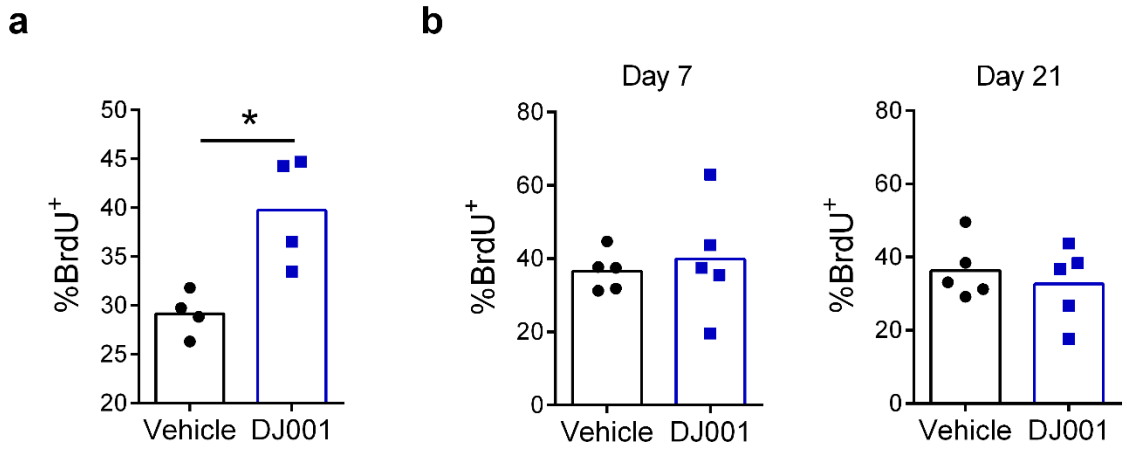

Figure 31 Effect of systemic DJ001 administration on HSC proliferation in vivo.

a %BrdU$^+$KSL cells at day +12 in mice following 750 cGy TBI and treated daily with 5 mg/kg DJ001 or vehicle (n = 4). **b** %BrdU$^+$CD45.2$^+$ donor cells at day +7 and day +21 following competitive transplantation into CD45.1$^+$ recipient mice, as described in Figure 2 (n = 5). * $P <$ 0.05

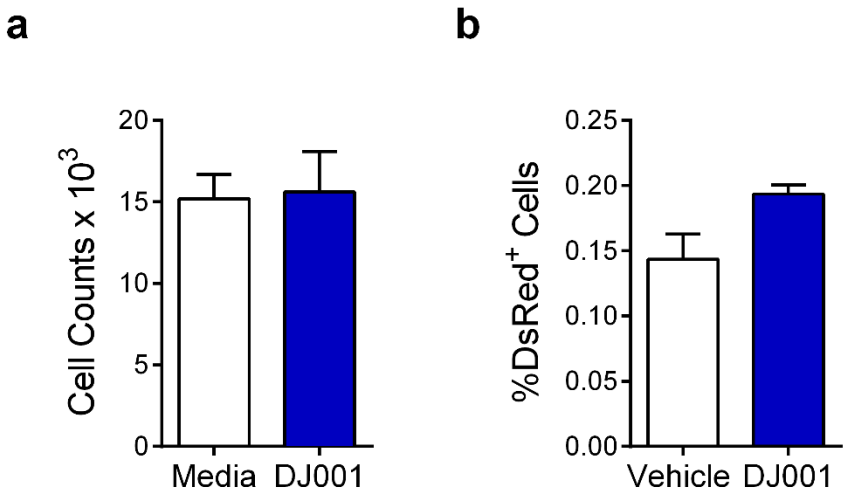

Figure 32 Effect of DJ001 treatment on BM HSPC migration and homing.

a Mean number of cells within the lower chambers of a trans-endothelial migration assay at 18 hours following culture of BM KSL cells in the upper chambers coated with mouse spleen ECs and treatment with and without 1 μg/ml DJ001 (*n* = 5/group). **b** Mean percentage of donor $DsRed^+$ cells in the BM of mice at 18 hours following intravenous injection of 1 x 10^5 $DsRed^+Sca1^+lin^-$ cells and treatment with 5 mg/kg DJ001 or vehicle subcutaneously (*n* = 3/group).

CHAPTER 4: Concluding Remarks

4.1 Conclusions

Chapter 1 of this dissertation outlines the most important concepts in HSC self-renewal, differentiation, intrinsic and extrinsic regulations, and post-injury regeneration. The first chapter also discusses the regulatory roles of PTPs and RhoGTPases in different physiological processes and their therapeutic potentials based on recent research advancements. Chapter 2 describes a small molecule inhibitor DJ001 that specifically inhibits PTPσ's phosphatase activity via allosteric binding to the intracellular active domain. DJ001 also displayed no inhibitory effect against twenty other phosphatases through a phosphatase profiler screening, with only modest inhibitory effect against Protein Phosphatase 5. Systemic administration of DJ001 to sub-lethally irradiated mice significantly accelerated hematologic and hematopoietic recovery in mice, which leads to improved survival rates compared to vehicle-treated controls. Importantly, donor BM cells from DJ001 treated mice when transplanted competitively into lethally irradiated recipients, displayed increased donor cell engraftment and multi-lineage reconstitution compared to vehicle-treated control mice, suggesting enhanced long-term repopulation capacity post DJ001 inhibition. Furthermore, in 5-FU treated chemotherapy model, DJ001 administration also increased the recovery of peripheral blood WBCs and neutrophils compared to control group. However, we did not observe any hematologic or hematopoietic effect in non-irradiated mice after 4-week of DJ001 treatment, suggesting the molecular alterations in BM HSCs post radiation or chemotherapy induced myelosuppression.

In Chapter 3, based on the regenerative effects of DJ001 administration *in* vivo, I delineate the intracellular mechanism of how DJ001-mediated inhibition of PTPσ contributed to HSC recovery following radiation injury. Mechanistically, DJ001-mediated inhibition of PTPσ led to increased

activation level of RAC1-GTP which further phosphorylated downstream effector proteins PAK1 and ERK. Furthermore, we observed that DJ001 treatment in mice decreased the percentages of apoptotic BM KSL cells post irradiation via increased expressions of anti-apoptotic protein BCL-X_L. Administration of RAC1 inhibitor in addition to DJ001 abrogated the anti-apoptotic effect in HSCs, suggesting DJ001-mediated suppression of apoptosis was RAC1 dependent. DJ001 treatment also promoted early HSPC proliferation post radiation by accelerating cell cycling transitions from G_1 to G_2/S/M phase. On a molecular level, DJ001 induced HSC cell cycle progression was dependent on RAC1 pathway activation which led to further upregulations of *Cdk2* and *Cyclin E*.

Since DJ001 promoted murine hematopoietic regeneration via RAC1 activation following myelosuppressive irradiation or chemotherapy, we sought to determine its effect in human HSC regeneration and results are presented in both Chapter 2 and 3. Treatment with DJ001 increased the recovery of live human BM HSPCs and CFCs post irradiation. Mechanistically, DJ001-mediated inhibition of PTPσ decreased radiation induced apoptosis in human HSPCs via upregulation of anti-apoptotic genes *BCL2L1* and *MCL1*. Most importantly, the progeny of DJ001 treated human BM HSPCs displayed long-term engraftment capacity in irradiated NSG mice, with improved capacity to reconstitute mature lineage cells including B cells, myeloid cells and T cells. Taken together, DJ001-mediated PTPσ inhibition presents significant translational values by promoting human HSC recovery following myelosuppressive irradiation.

The research interests of the Chute Laboratory are 1) to identify novel growth factors and membrane bound receptors that regulate HSC regeneration following BM myelosuppression of

myeloablative hematopoietic stem cell transplant and 2) to develop therapeutics that either antagonizes or activates newly discovered secreted factors or signaling pathways as a means to promote hematopoiesis. To achieve the first aim, we previously identified receptor PTPσ as a negative regulator of HSC self-renewal in hematopoiesis. Deletion or negative selection of PTPσ in BM cells significantly augmented the functional capacity of HSCs both in mouse and human. Our discovery revealed an unknown function of PTPσ in hematopoiesis and suggested its therapeutic potential as an approach to increase HSC self-renewal *in vivo*. Contents discussed in preceding chapters of this dissertation serve as an answer to the second goal of our lab, as well as a sequel to the previous PTPσ study. By identifying DJ001 as our lead compound, we potentially revealed a novel class of specific and non-competitive PTPσ inhibitors with significant therapeutic potential.

In summary, we identified small molecule DJ001 as a highly selective inhibitor of PTPσ via allosteric binding in BM HSCs (Figure 35). Systemic administration of PTPσ inhibitor promoted HSC regeneration, accelerated hematologic recovery, and improved survival in sub-lethally irradiated mice. Translationally, DJ001-mediated inhibition of PTPσ promoted the regeneration of human HSCs capable of multi-lineage reconstitution in NSG mice. Our results present a novel class of PTPσ inhibitor with therapeutic potential for human hematopoietic regeneration in patients receiving myelosuppressive chemotherapy, radiotherapy, and those undergoing myeloablative hematopoietic stem cell transplant.

4.2 Future Studies

4.2.1 PTPσ regulation: cell autonomous vs. niche dependent

Previously, we have been using constitutive PTPσ knockout mice in BALB/c background to study the role of PTPσ in hematopoietic system at homeostasis. However, constitutive deletion of PTPσ in mice displays severe neuronal defects leading to increased neonatal mortality of up to 50%. The remaining pups that survive through adulthood are significantly smaller in body sizes than the wildtype[87,164]. The deficiency in number and differences in body size make constitutive PTPσ knockout mice difficult to manipulate under a radiation setting. We recently obtained mice in C57BL/6 background with floxed alleles of PTPσ from the Jackson Laboratory. We are currently crossing *Ptprs*$^{flox/flox}$ mice with a *Vav*-Cre transgenic line to generate PTPσ deletion specific to adult BM hematopoietic cells[165,166]. After obtaining the first generation of *Vav*Cre;*Ptprs*$^{flox/flox}$ and Cre^{-};*Ptprs*$^{flox/flox}$ mice, we plan to evaluate their hematologic and hematopoietic profiles both at homeostasis and post radiation-induced stress.

If results do not indicate altered hematopoietic or hematologic profiles between *Vav*Cre;*Ptprs*$^{flox/flox}$ and Cre^{-};*Ptprs*$^{flox/flox}$ mice, we will further investigate the involvement of PTPσ in BM niche cells by crossing *Ptprs*$^{flox/flox}$ mice with *VeCad*-Cre and *Lepr*-Cre transgenic lines. We recently demonstrated that PTPσ is differentially expressed in BM HSCs and BM niche cells (Figure 33). We found that PTPσ is expressed in BM ECs and perivascular cells, but to a lower percentage compared to BM HSCs or HSPCs. Therefore, it seems necessary to examine the hematologic and hematopoietic profiles of the *VeCad*Cre;*Ptprs*$^{flox/flox}$ and *Lepr*Cre;*Ptprs*$^{flox/flox}$ mice both pre- and post- irradiation compared to the Cre^{-};*Ptprs*$^{flox/flox}$ controls. The results from this proposed study will help us better understand the whether PTPσ regulation occurs in a cell-autonomous or niche-

dependent manner, as well as whether DJ001 binds to one or multiple BM cellular players in promoting regeneration.

4.2.2 Development of a novel composition of matter

Our preliminary results indicate DJ001 as our lead PTPσ inhibitor. However, DJ001 is currently available in the public domain and we realized that there are a lot to be done to optimize the chemical structure of DJ001. Our collaboration with Dr. Michael Jung's lab at UCLA resulted in 110 novel compositions of matter that are analogues of the DJ001 compound. New analogues of DJ001 have been designed to vary the three important areas of the molecule: the left-hand aromatic ring (A), the central part of the molecule (B), and the right-hand aromatic ring (C) by substituting with other functional groups (Figure 34). Out of the 110 DJ001 analogues, we have so far tested the first 98 of the compounds using a NIH3T3 cell line based RAC1-GLISA assay, which measures the level of activated RAC1-GTP in a colorimetric ELISA format. From this study, we were able to select a total of 43 analogues that were able to increase the RAC1-GTP activation level in NIH3T3 cell lines. Furthermore, we also performed direct phosphatase assays to measure the inhibitory activities of the selected 43 analogues, followed by in vivo efficacy test in sub-lethally irradiated mice. So far, we have identified compound DJ009 as our candidates for future pre-IND studies.

4.3 Figures

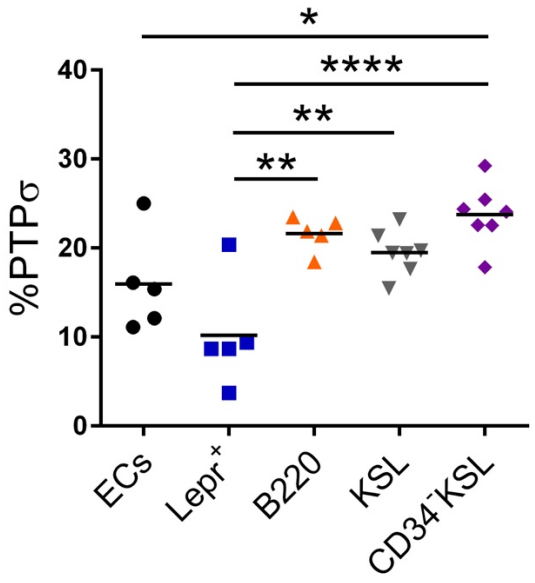

Figure 33 Expressions of PTPσ in bone marrow niche and hematopoietic cells.

Mean percentages of PTPσ protein expressions in bone marrow endothelial cells (ECs), $Lepr^+$ perivascular cells, $B220^+$ B cells, hematopoietic stem and progenitor KSL cells, and $CD34^-KSL$ hematopoietic stem cells. One-way ANOVA with Tukey's multiple comparison test for all comparisons. * $P < 0.05$, ** $P < 0.01$, **** $P < 0.0001$.

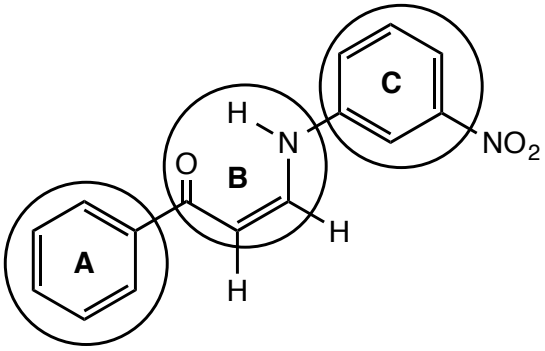

Figure 34 Schematics of designing novel compositions of matter based on chemical structures of DJ001.

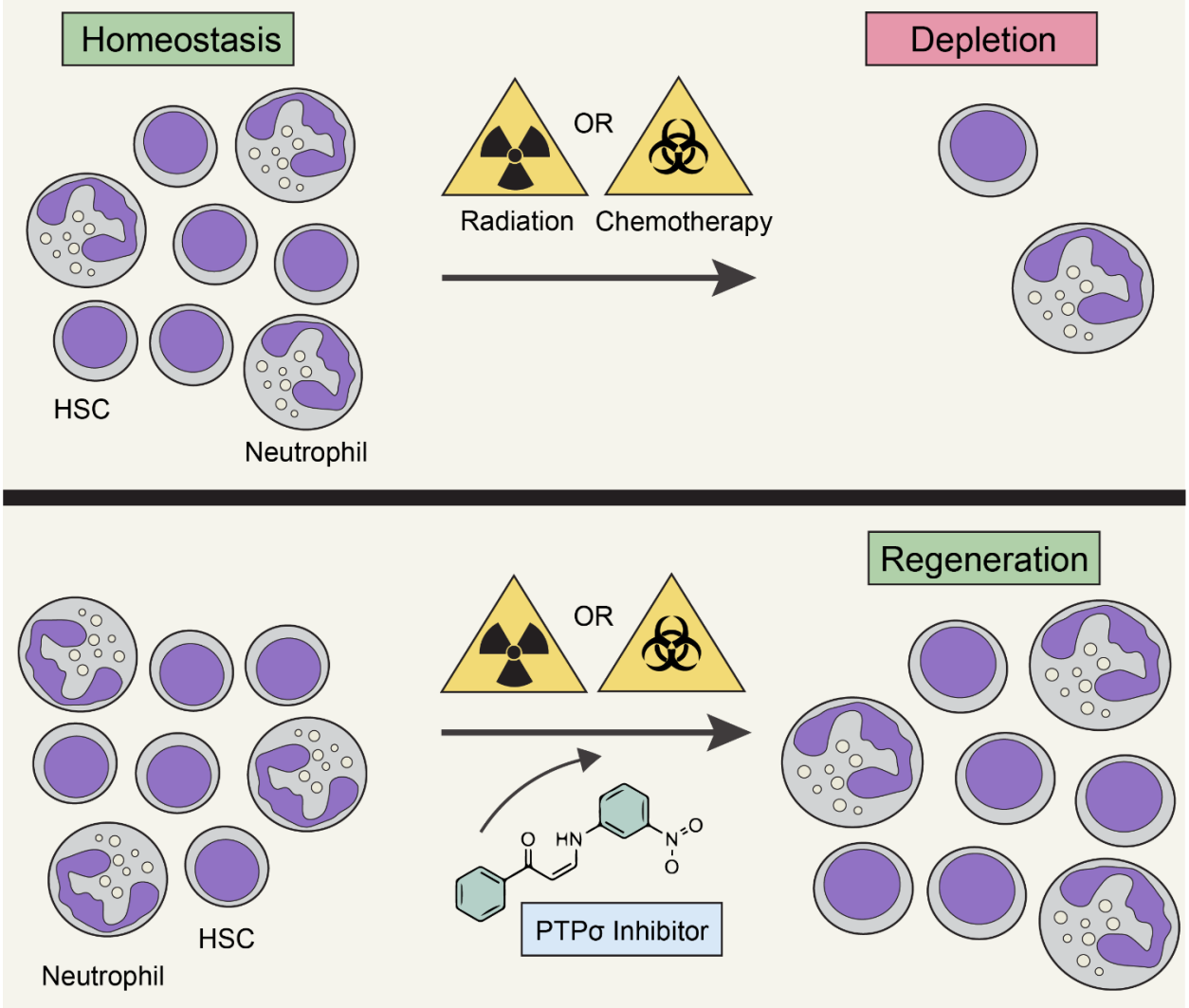

Figure 35 Summary of PTPσ inhibition in HSC regeneration.

Summary of DJ001-mediated inhibition of PTPσ in promoting hematopoietic regeneration following myelosuppressive irradiation or chemotherapy.

REFERENCES

1. Mendelson, A. & Frenette, P. S. Hematopoietic stem cell niche maintenance during homeostasis and regeneration. *Nat. Med.* **20**, 833–846 (2014).

2. Upadhaya, S. *et al.* Kinetics of adult hematopoietic stem cell differentiation in vivo. *J. Exp. Med.* **215**, 2815–2832 (2018).

3. Eaves, C. J. Review Series Hematopoietic stem cells: concepts, definitions, and the new reality. (2015). doi:10.1182/blood-2014

4. Pinho, S. & Frenette, P. S. Haematopoietic stem cell activity and interactions with the niche. *Nat. Rev. Mol. Cell Biol.* **20**, 303–320 (2019).

5. Rossmann, M. P., Orkin, S. H. & Chute, J. P. *Hematopoietic Stem Cell Biology*. *Hematology: Basic Principles and Practice* (2017). doi:10.1016/B978-0-323-35762-3.00009-3

6. Mauch, P. *et al.* Hematopoietic stem cell compartment: acute and late effects of radiation therapy and chemotherapy. *Int. J. Radiat. Oncol. Biol. Phys.* **31**, 1319–39 (1995).

7. Costa, G., Kouskoff, V. & Lacaud, G. Origin of blood cells and HSC production in the embryo. *Trends Immunol.* **33**, 215–223 (2012).

8. Medvinsky, A., Rybtsov, S. & Taoudi, S. Embryonic origin of the adult hematopoietic system: advances and questions. *Development* **138**, 1017–1031 (2011).

9. Dzierzak, E. & Bigas, A. Blood Development: Hematopoietic Stem Cell Dependence and Independence. *Cell Stem Cell* **22**, 639–651 (2018).

10. Golub, R. & Cumano, A. Embryonic hematopoiesis. (2013). doi:10.1016/j.bcmd.2013.08.004

11. Julien, E., El Omar, R. & Tavian, M. Origin of the hematopoietic system in the human embryo. *FEBS Lett.* **590**, 3987–4001 (2016).

12. Zhang, Y., Gao, S., Xia, J. & Liu, F. Hematopoietic Hierarchy – An Updated Roadmap.

Trends Cell Biol. **28**, 976–986 (2018).

13. Ema, H. *et al.* Adult mouse hematopoietic stem cells: purification and single-cell assays. *Nat. Protoc.* **1**, 2979–2987 (2006).

14. Mayle, A., Luo, M., Jeong, M. & Goodell, M. A. Mouse Hematopoietic Stem Cell Identification And Analysis. doi:10.1002/cyto.a.22093

15. Morrison, S. J., Wandycz, A. M., Hemmati, H. D., Wright, D. E. & Weissman, I. L. Identification of a lineage of multipotent hematopoietic progenitors. *Development* **124**, 1929–39 (1997).

16. Cimato, T. R., Furlage, R. L., Conway, A. & Wallace, P. K. Simultaneous Measurement of Human Hematopoietic Stem and Progenitor Cells In Blood Using Multi-color Flow Cytometry. doi:10.1002/cyto.b.21354

17. Benveniste, P. *et al.* Intermediate-Term Hematopoietic Stem Cells with Extended but Time-Limited Reconstitution Potential. *Cell Stem Cell* **6**, 48–58 (2010).

18. Pietras, E. M. *et al.* Functionally Distinct Subsets of Lineage-Biased Multipotent Progenitors Control Blood Production in Normal and Regenerative Conditions. *Cell Stem Cell* **17**, 35–46 (2015).

19. Velten, L. *et al.* Human haematopoietic stem cell lineage commitment is a continuous process. *Nat. Cell Biol.* **19**, 271–281 (2017).

20. Rodriguez-Fraticelli, A. E. *et al.* Clonal analysis of lineage fate in native haematopoiesis. *Nature* **553**, 212–216 (2018).

21. Carrelha, J. *et al.* Hierarchically related lineage-restricted fates of multipotent haematopoietic stem cells. *Nature* **554**, 106–111 (2018).

22. Wei, Q. & Frenette, P. S. Niches for Hematopoietic Stem Cells and Their Progeny. *Immunity* **48**, 632–648 (2018).

23. Decker, M., Leslie, J., Liu, Q. & Ding, L. *Hepatic thrombopoietin is required for bone marrow hematopoietic stem cell maintenance*.

24. Morrison, S. J. & Scadden, D. T. The bone marrow niche for haematopoietic stem cells. *Nature* **505**, 327–334 (2014).

25. Shao, L., Luo, Y. & Zhou, D. Hematopoietic Stem Cell Injury Induced by Ionizing Radiation. *Antioxid. Redox Signal.* **20**, 1447–1462 (2014).

26. Visnjic, D. *et al.* Hematopoiesis is severely altered in mice with an induced osteoblast deficiency. *Blood* **103**, 3258–3264 (2004).

27. Calvi, L. M. *et al.* Osteoblastic cells regulate the haematopoietic stem cell niche. *Nature* **425**, 841–846 (2003).

28. Zhang, J. *et al.* Identification of the haematopoietic stem cell niche and control of the niche size. *Nature* **425**, 836–841 (2003).

29. Ding, L., Saunders, T. L., Enikolopov, G. & Morrison, S. J. Endothelial and perivascular cells maintain haematopoietic stem cells. (2012). doi:10.1038/nature10783

30. Ding, L. & Morrison, S. J. Haematopoietic stem cells and early lymphoid progenitors occupy distinct bone marrow niches. (2013). doi:10.1038/nature11885

31. Greenbaum, A. *et al.* CXCL12 in early mesenchymal progenitors is required for haematopoietic stem-cell maintenance. (2013). doi:10.1038/nature11926

32. Kfoury, Y. & Scadden, D. T. Mesenchymal Cell Contributions to the Stem Cell Niche. *Cell Stem Cell* **16**, 239–253 (2015).

33. Méndez-Ferrer, S. *et al.* Mesenchymal and haematopoietic stem cells form a unique bone marrow niche. (2010). doi:10.1038/nature09262

34. Sugiyama, T., Kohara, H., Noda, M. & Nagasawa, T. Maintenance of the Hematopoietic Stem Cell Pool by CXCL12-CXCR4 Chemokine Signaling in Bone Marrow Stromal Cell Niches. *Immunity* **25**, 977–988 (2006).

35. Omatsu, Y. *et al.* The Essential Functions of Adipo-osteogenic Progenitors as the Hematopoietic Stem and Progenitor Cell Niche. *Immunity* **33**, 387–399 (2010).

36. Sacchetti, B. *et al.* Self-Renewing Osteoprogenitors in Bone Marrow Sinusoids Can Organize a Hematopoietic Microenvironment. *Cell* **131**, 324–336 (2007).

37. Shahrabi, S., Rezaeeyan, H., Ahmadzadeh, A., Shahjahani, M. & Saki, N. Bone Marrow Blood Vessels: Normal and Neoplastic Niche. *Oncol. Rev.* **10**, 306 (2016).

38. Kiel, M. J. *et al.* SLAM family receptors distinguish hematopoietic stem and progenitor cells and reveal endothelial niches for stem cells. *Cell* **121**, 1109–21 (2005).

39. Arai, F. *et al.* Tie2/angiopoietin-1 signaling regulates hematopoietic stem cell quiescence in the bone marrow niche. *Cell* **118**, 149–61 (2004).

40. Himburg, H. A. *et al.* Pleiotrophin regulates the expansion and regeneration of hematopoietic stem cells. *Nat. Med.* **16**, 475–482 (2010).

41. Himburg, H. A. *et al.* Distinct Bone Marrow Sources of Pleiotrophin Control Hematopoietic Stem Cell Maintenance and Regeneration. *Cell Stem Cell* **23**, 370-381.e5 (2018).

42. Winkler, I. G. *et al.* Vascular niche E-selectin regulates hematopoietic stem cell dormancy, self renewal and chemoresistance. *Nat. Med.* **18**, 1651–1657 (2012).

43. Doan, P. L. *et al.* Epidermal growth factor regulates hematopoietic regeneration after radiation injury. *Nat. Med.* **19**, 295–304 (2013).

44. Boulais, P. E. & Frenette, P. S. *Making sense of hematopoietic stem cell niches*. *Blood* **125**, (2015).

45. Wang, Y., Probin, V. & Zhou, D. *Cancer therapy-induced residual bone marrow injury-Mechanisms of induction and implication for therapy NIH Public Access*. *Curr Cancer Ther Rev* **2**, (2006).

46. Miller, K. D. *et al.* Cancer treatment and survivorship statistics, 2019. *CA. Cancer J. Clin.* **69**, 363–385 (2019).

47. Lijian Shao1, Yingying Wang1, 2, Jianhui Chang1, Yi Luo1, Aimin Meng2, and D. & Zhou. Hematopoietic stem cell senescence and cancer therapy- induced long-term bone

marrow injury Lijian. *Transl. Cancer Res.* **4**, 397–411 (2013).

48. Singh, V. K., Romaine, P. L. P. & Seed, T. M. Medical Countermeasures for Radiation Exposure and Related Injuries. *Health Phys.* **108**, 607–630 (2015).

49. Hachiya, M., Tominaga, T., Tatsuzaki, H. & Akashi, M. Medical Management of the Consequences of the Fukushima Nuclear Power Plant Incident. *Drug Dev. Res.* **75**, 3–9 (2014).

50. López, M. & Martín, M. Medical management of the acute radiation syndrome. *Reports Pract. Oncol. Radiother.* **16**, 138–146 (2011).

51. Donnelly, E. H. *et al.* Acute radiation syndrome: assessment and management. *South. Med. J.* **103**, 541–6 (2010).

52. Lomax, M. E., Folkes, L. K. & O'Neill, P. Biological Consequences of Radiation-induced DNA Damage: Relevance to Radiotherapy. *Clin. Oncol.* **25**, 578–585 (2013).

53. Wang, J. *et al.* A Differentiation Checkpoint Limits Hematopoietic Stem Cell Self-Renewal in Response to DNA Damage. *Cell* **148**, 1001–1014 (2012).

54. Spangrude, G. J., Heimfeld, S. & Weissman, I. L. *Purification and Characterization of Mouse Hematopoietic Stem Cells*. *Source: Science, New Series* **241**, (1988).

55. Okada, S. *et al. In Vivo and In Vitro Stem Cell Function of c-kit-and Sca-1-Positive Murine Hematopoietic Cells*.

56. Purton, L. E. & Scadden, D. T. Cell Stem Cell Protocol Review Limiting Factors in Murine Hematopoietic Stem Cell Assays. doi:10.1016/j.stem.2007.08.016

57. Frisch, B. J. & Calvi, L. M. Hematopoietic Stem Cell Cultures and Assays. doi:10.1007/978-1-62703-989-5_24

58. Ploemacher, R. E., van der Sluijs, J. P., Voerman, J. S. & Brons, N. H. An in vitro limiting-dilution assay of long-term repopulating hematopoietic stem cells in the mouse. *Blood* **74**, 2755–63 (1989).

59. van Os, R., Kamminga, L. M. & de Haan, G. Stem Cell Assays: Something Old, Something New, Something Borrowed. *Stem Cells* **22**, 1181–1190 (2004).

60. Denning-Kendall, P., Singha, S., Bradley, B. & Hows, J. Cobblestone Area-Forming Cells in Human Cord Blood Are Heterogeneous and Differ from Long-Term Culture-Initiating Cells. *Stem Cells* **21**, 694–701 (2003).

61. Cancelas, J. A. *et al.* Rac GTPases differentially integrate signals regulating hematopoietic stem cell localization. *Nat. Med.* **11**, 886–891 (2005).

62. Taswell, C. Limiting dilution assays for the determination of immunocompetent cell frequencies. I. Data analysis. *J. Immunol.* **126**, 1614–9 (1981).

63. Szilvassy, S. J., Humphries, R. K., Lansdorp, P. M., Eaves, A. C. & Eaves, C. J. Quantitative assay for totipotent reconstituting hematopoietic stem cells by a competitive repopulation strategy. *Proc. Natl. Acad. Sci. U. S. A.* **87**, 8736–40 (1990).

64. Tautz, L., Critton, D. A. & Grotegut, S. Protein Tyrosine Phosphatases: Structure, Function, and Implication in Human Disease. in 179–221 (Humana Press, Totowa, NJ, 2013). doi:10.1007/978-1-62703-562-0_13

65. Tiganis, T. & Bennett, A. M. Protein tyrosine phosphatase function: the substrate perspective. *Biochem. J.* **402**, 1–15 (2007).

66. Gurzov, E. N., Stanley, W. J., Brodnicki, T. C. & Thomas, H. E. Protein tyrosine phosphatases: molecular switches in metabolism and diabetes. *Trends Endocrinol. Metab.* **26**, 30–39 (2015).

67. Tonks, N. K. Protein tyrosine phosphatases: from genes, to function, to disease. *Nat. Rev. | Mol. CELL Biol.* **7**, 833 (2006).

68. He, R.-J., Yu, Z.-H., Zhang, R.-Y. & Zhang, Z.-Y. Protein tyrosine phosphatases as potential therapeutic targets. *Nat. Publ. Gr.* **35**, 1227–1246 (2014).

69. Tonks, N. K. & Neel, B. G. Combinatorial control of the specificity of protein tyrosine phosphatases. *Curr. Opin. Cell Biol.* **13**, 182–195 (2001).

70. Rheinländer, A., Schraven, B. & Bommhardt, U. CD45 in human physiology and clinical medicine. *Immunol. Lett.* **196**, 22–32 (2018).

71. Thomas, M. L. & Brown, E. J. Positive and negative regulation of Src-family membrane kinases by CD45. *Immunol. Today* **20**, 406–411 (1999).

72. Tchilian, E. Z. & Beverley, P. C. L. Altered CD45 expression and disease. *Trends Immunol.* **27**, 146–153 (2006).

73. Huntington, N. D., Xu, Y., Nutt, S. L. & Tarlinton, D. M. A requirement for CD45 distinguishes Ly49D-mediated cytokine and chemokine production from killing in primary natural killer cells. *J. Exp. Med.* **201**, 1421–1433 (2005).

74. Berger, S. A., Mak, T. W. & Paige, C. J. Leukocyte common antigen (CD45) is required for immunoglobulin E- mediated degranulation of mast cells. *J. Exp. Med.* **180**, 471–476 (1994).

75. Gao, H., Henderson, A., Flynn, D. C., Landreth, K. S. & Ericson, S. G. Effects of the protein tyrosine phosphatase CD45 on FcgammaRIIa signaling and neutrophil function. *Exp. Hematol.* **28**, 1062–70 (2000).

76. Chan, G. *et al.* Essential role for Ptpn11 in survival of hematopoietic stem and progenitor cells. *Blood* **117**, 4253–61 (2011).

77. Pandey, R., Saxena, M. & Kapur, R. Role of SHP2 in hematopoiesis and leukemogenesis. *Curr. Opin. Hematol.* **24**, 307–313 (2017).

78. Hale, A. J., ter Steege, E. & den Hertog, J. Recent advances in understanding the role of protein-tyrosine phosphatases in development and disease. *Dev. Biol.* **428**, 283–292 (2017).

79. Chan, G., Kalaitzidis, D. & Neel, B. G. The tyrosine phosphatase Shp2 (PTPN11) in cancer. *Cancer Metastasis Rev.* **27**, 179–192 (2008).

80. Quarmyne, M. *et al.* Protein tyrosine phosphatase–σ regulates hematopoietic stem cell–repopulating capacity. *J. Clin. Invest.* **125**, 177–182 (2015).

81. Zhang, Y. *et al.* PTPσ inhibitors promote hematopoietic stem cell regeneration. *Nat. Commun.* **10**, 3667 (2019).

82. Ni, F. *et al.* Ptpn21 Controls Hematopoietic Stem Cell Homeostasis and Biomechanics. *Stem Cell* **24**, 608-620.e6 (2019).

83. Gilden, J. K., Peck, S., Chen, Y.-C. M. & Krummel, M. F. The septin cytoskeleton facilitates membrane retraction during motility and blebbing. *J. Cell Biol.* **196**, 103–14 (2012).

84. Xu, Y. & Fisher, G. J. Receptor type protein tyrosine phosphatases (RPTPs)-roles in signal transduction and human disease. doi:10.1007/s12079-012-0171-5

85. Ohtake, Y., Saito, A. & Li, S. Diverse functions of protein tyrosine phosphatase σ in the nervous and immune systems. *Exp. Neurol.* **302**, 196–204 (2018).

86. Coles, C. H. *et al.* Proteoglycan-specific molecular switch for RPTPσ clustering and neuronal extension. *Science* **332**, 484–8 (2011).

87. Elchebly, M. *et al.* Neuroendocrine dysplasia in mice lacking protein tyrosine phosphatase σ. *Nat. Genet.* **21**, 330–333 (1999).

88. Horn, K. E. *et al.* Receptor protein tyrosine phosphatase sigma regulates synapse structure, function and plasticity. *J. Neurochem.* **122**, 147–161 (2012).

89. Thompson, K. M. *et al.* Receptor protein tyrosine phosphatase sigma inhibits axonal regeneration and the rate of axon extension. *Mol. Cell. Neurosci.* **23**, 681–92 (2003).

90. Lang, B. T. *et al.* Modulation of the proteoglycan receptor PTPs promotes recovery after spinal cord injury. *Nature* **518**, (2015).

91. Bunin, A. *et al.* Protein Tyrosine Phosphatase PTPRS Is an Inhibitory Receptor on Human and Murine Plasmacytoid Dendritic Cells. *Immunity* **43**, 277–288 (2015).

92. Zhang, Z.-Y. Drugging the Undruggable: Therapeutic Potential of Targeting Protein Tyrosine Phosphatases. *Acc. Chem. Res* **50**, 59 (2017).

93. Stanford, S. M. & Bottini, N. Targeting Tyrosine Phosphatases: Time to End the Stigma. *Trends Pharmacol. Sci.* **38**, (2017).

94. Frye, M. *et al.* Interfering with VE-PTP stabilizes endothelial junctions in vivo via Tie-2 in the absence of VE-cadherin. *J. Exp. Med.* **212**, 2267–87 (2015).

95. Campochiaro, P. A. *et al.* Treatment of Diabetic Macular Edema with an Inhibitor of Vascular Endothelial-Protein Tyrosine Phosphatase That Activates Tie2. *Ophthalmology* **122**, 545–554 (2015).

96. Krishnan, N. *et al.* Targeting the disordered C terminus of PTP1B with an allosteric inhibitor. *Nat. Chem. Biol.* **10**, 558–566 (2014).

97. Gardner, R. T. *et al.* Targeting protein tyrosine phosphatase σ after myocardial infarction restores cardiac sympathetic innervation and prevents arrhythmias. *Nat. Commun.* **6**, 6235 (2015).

98. Doody, K. M. *et al.* Targeting phosphatase-dependent proteoglycan switch for rheumatoid arthritis therapy. *Sci. Transl. Med.* **7**, 288ra76 (2015).

99. Martin, K. R. *et al.* Identification of Small Molecule Inhibitors of PTPσ through an Integrative Virtual and Biochemical Approach. *PLoS One* **7**, e50217 (2012).

100. Lee, H. S. *et al.* Identification of novel protein tyrosine phosphatase sigma inhibitors promoting neurite extension. *Bioorg. Med. Chem. Lett.* **26**, 87–93 (2016).

101. Muise, A. M. *et al.* Protein-Tyrosine Phosphatase Sigma Is Associated with Ulcerative Colitis. *Curr. Biol.* **17**, 1212–1218 (2007).

102. Murchie, R., Guo, C.-H., Persaud, A., Muise, A. & Rotin, D. Protein tyrosine phosphatase σ targets apical junction complex proteins in the intestine and regulates epithelial permeability. doi:10.1073/pnas.1315017111

103. Chagnon, M. J. *et al.* Receptor tyrosine phosphatase sigma (RPTPσ) regulates, p250GAP, a novel substrate that attenuates Rac signaling. *Cell. Signal.* **22**, 1626–1633 (2010).

104. Lawson, C. D. & Ridley, A. J. Rho GTPase signaling complexes in cell migration and

invasion. *J. Cell Biol.* **217**, 447–457 (2018).

105. Yang, F. *et al. Rac and Cdc42 GTPases control hematopoietic stem cell shape, adhesion, migration, and mobilization*.

106. Kazanietz, M. G. & Caloca, M. J. The Rac GTPase in Cancer: From Old Concepts to New Paradigms. *Cancer Res* **77**, (2017).

107. Cancelas, J. A. & Williams, D. A. Rho GTPases in hematopoietic stem cell functions. *Curr. Opin. Hematol.* **16**, 249–54 (2009).

108. Bustelo, X. R., Sauzeau, V. & Berenjeno, I. M. *GTP-binding proteins of the Rho/Rac family: regulation, effectors and functions in vivo*.

109. Gu Y *et al.* Hematopoietic cell regulation by Rac1 and Rac2 guanosine triphosphatases. *Science (80-.).* **302**, 445–449 (2003).

110. Mulloy, J. C. *et al.* Rho GTPases in hematopoiesis and hemopathies. (2010). doi:10.1182/blood-2009-09

111. Wang, Z. *et al.* Rac1 is crucial for Ras-dependent skin tumor formation by controlling Pak1-Mek-Erk hyperactivation and hyperproliferation in vivo. *Oncogene* **29**, 3362–3373 (2010).

112. Yang, F.-C. *et al.* Rac2 Stimulates Akt Activation Affecting BAD/Bcl-XL Expression while Mediating Survival and Actin Function in Primary Mast Cells. *Immunity* **12**, 557–568 (2000).

113. Wu, X. *et al.* Rac1 Activation Controls Nuclear Localization of β-catenin during Canonical Wnt Signaling. *Cell* **133**, 340–353 (2008).

114. Haga, R. B. & Ridley, A. J. Small GTPases Rho GTPases: Regulation and roles in cancer cell biology. (2016). doi:10.1080/21541248.2016.1232583

115. Li, X. *et al.* The Hematopoiesis-Specific GTP-Binding Protein RhoH Is GTPase Deficient and Modulates Activities of Other Rho GTPases by an Inhibitory Function. *Mol. Cell. Biol.* **22**, 1158–1171 (2002).

116. Xing, Z. *et al.* Increased hematopoietic stem cell mobilization in aged mice. *Blood* **108**, 2190–2197 (2006).

117. Wu, C.-Y. C. *et al.* PI3K Regulation of RAC1 Is Required for KRAS-Induced Pancreatic Tumorigenesis in Mice. *Gastroenterology* **147**, 1405-1416.e7 (2014).

118. Kissil, J. L. *et al.* Requirement for Rac1 in a K-ras–Induced Lung Cancer in the Mouse. *Cancer Res.* **67**, 8089–8094 (2007).

119. Müller, L. W. *et al.* Rac Guanosine Triphosphatases represent a potential target in AML. *Leukemia* **22**, 1803 (2008).

120. Cho, Y. J. *et al.* Generation of rac3 Null Mutant Mice: Role of Rac3 in Bcr/Abl-Caused Lymphoblastic Leukemia. *Mol. Cell. Biol.* **25**, 5777–5785 (2005).

121. Thomas, E. K. *et al.* Article Rac Guanosine Triphosphatases Represent Integrating Molecular Therapeutic Targets for BCR-ABL-Induced Myeloproliferative Disease. doi:10.1016/j.ccr.2007.10.015

122. Spiekermann, K., Roesler, J., Emmendoerffer, A., Elsner, J. & Welte, K. *REVIEW Functional features of neutrophils induced by G-CSF and GM-CSF treatment: differential effects and clinical implications*. *Leukemia* **11**, (1997).

123. Bendall, L. J. & Bradstock, K. F. G-CSF: From granulopoietic stimulant to bone marrow stem cell mobilizing agent. (2014). doi:10.1016/j.cytogfr.2014.07.011

124. Singh, A. K. & Mcguirk, J. P. Allogeneic Stem Cell Transplantation: A Historical and Scientific Overview. (2016). doi:10.1158/0008-5472.CAN-16-1311

125. Hatzimichael, E. & Tuthill, M. Hematopoietic stem cell transplantation. *Stem Cells Cloning* **3**, 105–17 (2010).

126. Ballen, K. K., Gluckman, E. & Broxmeyer, H. E. Umbilical cord blood transplantation: the first 25 years and beyond. *Blood* **122**, 491–8 (2013).

127. Himburg, H. A. *et al.* Dickkopf-1 promotes hematopoietic regeneration via direct and niche-mediated mechanisms. *Nat. Med.* **23**, 91–99 (2017).

128. Goncalves, K. A. *et al.* Angiogenin Promotes Hematopoietic Regeneration by Dichotomously Regulating Quiescence of Stem and Progenitor Cells. *Cell* **166**, 894–906 (2016).

129. Orkin, S. H. & Zon, L. I. Hematopoiesis: An Evolving Paradigm for Stem Cell Biology. *Cell* **132**, 631–644 (2008).

130. Zon, L. I. Intrinsic and extrinsic control of haematopoietic stem-cell self-renewal. *Nature* **453**, 306–313 (2008).

131. Wang, B. *et al.* Sodium orthovanadate (vanadate), a potent mitigator of radiation-induced damage to the hematopoietic system in mice. *J. Radiat. Res.* **54**, 620–9 (2013).

132. Himburg, H. A. *et al.* Article Pleiotrophin Regulates the Retention and Self-Renewal of Hematopoietic Stem Cells in the Bone Marrow Vascular Niche. *CellReports* **2**, 964–975 (2012).

133. Barr, A. J. Protein tyrosine phosphatases as drug targets: Strategies and challenges of inhibitor development. *Future Medicinal Chemistry* **2**, 1563–1576 (2010).

134. Reilly, J. T. Receptor tyrosine kinases in normal and malignant haematopoiesis. *Blood Rev.* **17**, 241–248 (2003).

135. McDonell, L. M., Kernohan, K. D., Boycott, K. M. & Sawyer, S. L. Receptor tyrosine kinase mutations in developmental syndromes and cancer: two sides of the same coin. *Hum. Mol. Genet.* **24**, R60-6 (2015).

136. Mirshafiey, A., Ghalamfarsa, G., Asghari, B. & Azizi, G. Receptor Tyrosine Kinase and Tyrosine Kinase Inhibitors: New Hope for Success in Multiple Sclerosis Therapy. *Innov. Clin. Neurosci.* **11**, 23–36 (2014).

137. Liao, S. *et al.* Bifunctional Ligand Enables Efficient Gold-Catalyzed Hydroalkenylation of Propargylic Alcohol. *Angew. Chemie Int. Ed.* **57**, 8250–8254 (2018).

138. Jeon, T. J., Chien, P. N., Chun, H.-J. & Ryu, S. E. Structure of the catalytic domain of protein tyrosine phosphatase sigma in the sulfenic acid form. *Mol. Cells* **36**, 55–61 (2013).

139. Van Veldhoven, P. P. & Mannaerts, G. P. Inorganic and organic phosphate measurements in the nanomolar range. *Anal. Biochem.* **161**, 45–8 (1987).

140. Trott, O. & Olson, A. J. AutoDock Vina: improving the speed and accuracy of docking with a new scoring function, efficient optimization, and multithreading. *J. Comput. Chem.* **31**, 455–61 (2010).

141. Yan, X. *et al.* Deletion of the Imprinted Gene Grb10 Promotes Hematopoietic Stem Cell Self-Renewal and Regeneration. *Cell Rep.* **17**, 1584–1594 (2016).

142. Himburg, H. A. *et al.* Distinct Bone Marrow Sources of Pleiotrophin Control Hematopoietic Stem Cell Maintenance and Regeneration. *Cell Stem Cell* **23**, 370-381.e5 (2018).

143. Longley, D. B., Harkin, D. P. & Johnston, P. G. 5-Fluorouracil: mechanisms of action and clinical strategies. *Nat. Rev. Cancer* **3**, 330–338 (2003).

144. Shen, Y. *et al.* PTPsigma is a receptor for chondroitin sulfate proteoglycan, an inhibitor of neural regeneration. *Science* **326**, 592–6 (2009).

145. Tonnessen-Murray, C. A., Lozano, G. & Jackson, J. G. The Regulation of Cellular Functions by the p53 Protein: Cellular Senescence. *Cold Spring Harb. Perspect. Med.* **7**, a026112 (2017).

146. Domen, J., Gandy, K. L. & Weissman, I. L. Systemic overexpression of BCL-2 in the hematopoietic system protects transgenic mice from the consequences of lethal irradiation. *Blood* **91**, 2272–82 (1998).

147. Cui, Y. F. *et al.* Apoptosis in bone marrow cells of mice with different p53 genotypes after gamma-rays irradiation in vitro. *J. Environ. Pathol. Toxicol. Oncol.* **14**, 159–63 (1995).

148. Lee, J. M. & Bernstein, A. p53 mutations increase resistance to ionizing radiation. *Proc. Natl. Acad. Sci.* **90**, 5742–5746 (1993).

149. Komarov, P. G. *et al.* A Chemical Inhibitor of p53 That Protects Mice from the Side Effects of Cancer Therapy. *Science (80-.).* **285**, 1733–1737 (1999).

150. Hellman, S. & Botnick, L. E. Stem cell depletion: An explanation of the late effects of cytotoxins. *Int. J. Radiat. Oncol.* **2**, 181–184 (1977).

151. Inomata, K. *et al.* Genotoxic Stress Abrogates Renewal of Melanocyte Stem Cells by Triggering Their Differentiation. *Cell* **137**, 1088–1099 (2009).

152. Carbonneau, C. L. *et al.* Ionizing radiation-induced expression of INK4a/ARF in murine bone marrow-derived stromal cell populations interferes with bone marrow homeostasis. *Blood* **119**, 717–26 (2012).

153. Dominici, M. *et al.* Restoration and reversible expansion of the osteoblastic hematopoietic stem cell niche after marrow radioablation. *Blood* **114**, 2333–2343 (2009).

154. Hooper, A. T. *et al.* Engraftment and reconstitution of hematopoiesis is dependent on VEGFR2-mediated regeneration of sinusoidal endothelial cells. *Cell Stem Cell* **4**, 263–74 (2009).

155. Murga, C., Zohar, M., Teramoto, H. & Gutkind, J. S. Rac1 and RhoG promote cell survival by the activation of PI3K and Akt, independently of their ability to stimulate JNK and NF-κB. *Oncogene* **21**, 207–216 (2002).

156. Hein, A. L. *et al.* RAC1 GTPase promotes the survival of breast cancer cells in response to hyper-fractionated radiation treatment. *Oncogene* **35**, 6319–6329 (2016).

157. Sapieha, P. S. *et al.* Receptor protein tyrosine phosphatase sigma inhibits axon regrowth in the adult injured CNS. *Mol. Cell. Neurosci.* **28**, 625–635 (2005).

158. Livak, K. J. & Schmittgen, T. D. Analysis of Relative Gene Expression Data Using Real-Time Quantitative PCR and the 2−ΔΔCT Method. *Methods* **25**, 402–408 (2001).

159. Yang, F. C. *et al.* Rac2 stimulates Akt activation affecting BAD/Bcl-XL expression while mediating survival and actin function in primary mast cells. *Immunity* **12**, 557–68 (2000).

160. Eblen, S. T., Slack, J. K., Weber, M. J. & Catling, A. D. Rac-PAK signaling stimulates extracellular signal-regulated kinase (ERK) activation by regulating formation of MEK1-ERK complexes. *Mol. Cell. Biol.* **22**, 6023–33 (2002).

161. Tisi, M. A., Xie, Y., Yeo, T. T. & Longo, F. M. Downregulation of LAR tyrosine phosphatase prevents apoptosis and augments NGF-induced neurite outgrowth. *J. Neurobiol.* **42**, 477–86 (2000).

162. Fiorentini, C. *et al.* Toxin-Induced Activation of Rho GTP-Binding Protein Increases Bcl-2 Expression and Influences Mitochondrial Homeostasis. *Exp. Cell Res.* **242**, 341–350 (1998).

163. Gómez, J., Martínez-A., C., Giry, M., García, A. & Rebollo, A. Rho prevents apoptosis through Bcl-2 expression: Implications for interleukin-2 receptor signal transduction. *Eur. J. Immunol.* **27**, 2793–2799 (1997).

164. Wallace, M. J. *et al.* Neuronal defects and posterior pituitary hypoplasia in mice lacking the receptor tyrosine phosphatase PTPσ. *Nat. Genet.* **21**, 334–338 (1999).

165. Joseph, C. *et al.* Deciphering hematopoietic stem cells in their niches: a critical appraisal of genetic models, lineage tracing, and imaging strategies. *Cell Stem Cell* **13**, 520–33 (2013).

166. Georgiades, P. *et al.* vavCre Transgenic mice: A tool for mutagenesis in hematopoietic and endothelial lineages. *genesis* **34**, 251–256 (2002).